HIGH-RESOLUTION MOLECULAR BEAM SPECTROSCOPY AT MICROWAVE AND OPTICAL FREQUENCIES

J. P. BEKOOIJ

HIGH-RESOLUTION MOLECULAR BEAM SPECTROSCOPY
AT MICROWAVE AND OPTICAL FREQUENCIES

HIGH-RESOLUTION MOLECULAR BEAM SPECTROSCOPY AT MICROWAVE AND OPTICAL FREQUENCIES

PROEFSCHRIFT

door

JOHAN PIETER BEKOOIJ

geboren te Leiden

Aan mijn ouders
Aan Sien

CONTENTS

CHAPTER I

INTRODUCTION

1. BACKGROUND AND GOAL

Molecular spectroscopy is by far the most important source of information on
structures and properties of molecules   Generally, molecular spectra provide
information on the energy levels of a molecule, on the lifetimes in excited
states, on the transition probabilities and on population distributions. The
spectra can be described in terms of certain parameters, often called molecular
constants, which are related to electronic and geometrical structures, to vi-
brations and rotations of the molecular frame, to electronic and nuclear proper-
ties and to electric and magnetic molecular properties. These constants are of
interest for understanding the physical and chemical properties of substances
and for testing the adequacy of *ab initio* calculations. Molecular spectra them-
selves are useful for identification and determination of the concentration of
molecules and to characterize the physical conditions in a given (remote) sys-
tem.

Studies by high-resolution molecular beam spectroscopy have been undertaken
on the hydroxyl (OH) radical, the potassium-cyanide (KCN) molecule and the iod-
ine-oxide (IO) radical. The hyperfine Λ-doubling spectrum in the ground vibra-
tional $X^2\Pi$ states of OH has been subject of extensive theoretical and
experimental investigations. Experimental data for excited vibrational states,
however, were restricted to the $X^2\Pi_{3/2}$ state (CHU 70, CLO 71, LEE 71, LEE 74),
which seriously limited the determination of molecular constants. No precise in-
formation on the hyperfine Λ-doubling spectrum and constants in excited vibra-
tional levels of both the $X^2\Pi_{1/2}$ and $X^2\Pi_{3/2}$ states was available.

Of all group I cyanides only the structure of hydrogen-cyanide was well es-
tablished as linear cyanide (HCN) or isocyanide (HNC). The alkali cyanides were
generally assumed to be linear, too, although experimental and theoretical evi-
dence was scarce and contradictory. *Ab initio* calculations (BAK 70) for lithi-
um-cyanide indicated a linear isocyanide structure with only a very small energy
difference (about 0.4 eV) between LiNC and LiCN. The energy surface between the
two configurations was calculated (CLE 73) and it was found that the linear LiNC
molecule undergoes large amplitude bending vibrations and that moderate excita-

tion (0.3-0.4 eV) will permit orbiting of the Li^+ ion around the CN^- group. No calculations for the heavier alkali cyanides were performed. The rotational spectrum of KCN was first studied by microwave absorption spectroscopy in the frequency region 85 to 107 GHz (KUI 76). Although no assignment of individual spectral lines was possible, the spectrum excluded a linear structure.

The possible intermediate role of the halogen monoxides in stratospheric (ClO and BrO) and tropospheric (IO) (CHA 80) photochemistry, which limits the atmospheric abundance of ozone, has raised interest in the past years. Spectroscopy on the ground and first excited electronic states is hindered by instability of these radicals and extensive predissociation in the $A^2\Pi$ states. The spectra of ClO and BrO have been studied most extensively and the spectrum of FO in the gas phase has been observed only recently by laser magnetic resonance (MCK 79). The $A^2\Pi_{3/2}$-$X^2\Pi_{3/2}$ system of IO has been subject of several investigations at moderate resolutions. The vibrational and rotational spectrum of the electronic transition was studied from flame emission (DUR 60). The ground vibrational $X^2\Pi_{3/2}$ state was studied by electron resonance (CAR 70, BRO 72) and microwave absorption (SAI 73) spectroscopy. Information on hyperfine interactions and predissociation in the excited state and on hyperfine interactions in the ground state was either restricted or completely lacking.

The finer details in molecular spectra, like hyperfine structures, are normally obscured by Doppler and collision broadening of spectral lines when observed from a gaseous sample. Molecular beam spectroscopy is one of the most powerful methods developed to reduce these broadening effects. Doppler broadening is reduced by irradiating a collimated beam of molecules at right angles, while collision broadening is negligible at the low pressure conditions in a beam apparatus. Application of molecular beams offers the important possibility to achieve cooling of internal degrees of freedom of a molecule by supersonic expansion of gas or seeded gas mixtures from a nozzle source. This internal cooling reduces complexity of molecular spectra by enhancing intensities of transitions originating in lower energy levels. Besides, these conditions favour formation of weakly-bound van der Waals complexes. Furthermore, molecular beams can be produced of unstable species, like radicals, molecules in metastable states and molecular ions.

Narrow-band and tunable radiation sources are required to benefit from the high resolution of molecular beam spectroscopy. These sources are readily available at microwave and radio-frequencies. At optical frequencies the development of lasers has led to a break-through. Particularly dye lasers are suit-

able, because these sources can produce a low-divergence beam of nearly monochromatic, tunable, coherent and polarized radiation of high intensities.

2. PRINCIPLES OF EXPERIMENTAL METHODS

Experimental methods for molecular beam spectroscopy, which combine one or more of the following techniques: state selection by inhomogeneous external fields, excitation by microwave radiation, laser-induced fluorescence and double resonance, can be divided into four categories:

(a) molecular-beam electric-resonance (MBER),

(b) molecular-beam laser-excitation (MBLE),

(c) microwave optical double-resonance on an electrically state-selected beam (MODRES),

(d) molecular-beam laser-induced fluorescence resonance (MBLIFR).

The experimental configurations for these spectroscopic methods are presented in Fig. 1, (a) through (d).

The molecular-beam electric-resonance (MBER) method (Fig. 1 (a)) is well established (for a review see e.g. ZOR 73). The molecular beam, produced by the source, is passed to the detector, which yields a signal proportional to the number of striking molecules. The molecular beam is state selected by the A-field (state polarizer) and B-field (state analyzer). These inhomogeneous electric fields deflect molecules according to their quantum states, towards the molecular beam axis (positive Stark effect, trajectories indicated by solid lines in Fig. 1 (a)) or away from it (negative Stark effect, dashed line trajectories). If a transition is induced in the C-field by microwave (MW) or radio frequency (RF) radiation from a state transmitted by the A- and B-fields to a state rejected by the B-field, a decrease in the detector signal will occur. In the transition region (C-field) static and homogeneous electric and/or magnetic fields can be applied. The MBER method furnishes high sensitivity in a large spectral range at very high resolution (in the order of 1-10 kHz). The linewidths are generally only limited by the transit time of the molecules through the transition region. Its drawback is the restriction to transitions between states complying with certain, rather strict, state-selection rules.

The molecular-beam laser-excitation (MBLE) method (Fig. 1 (b)) is also well established nowadays (e.g. DEM 81). With this method transitions to excited electronic states can be studied by means of detection of the subsequently emitted laser-induced fluorescence (LIF). The spectral resolution is usually limit-
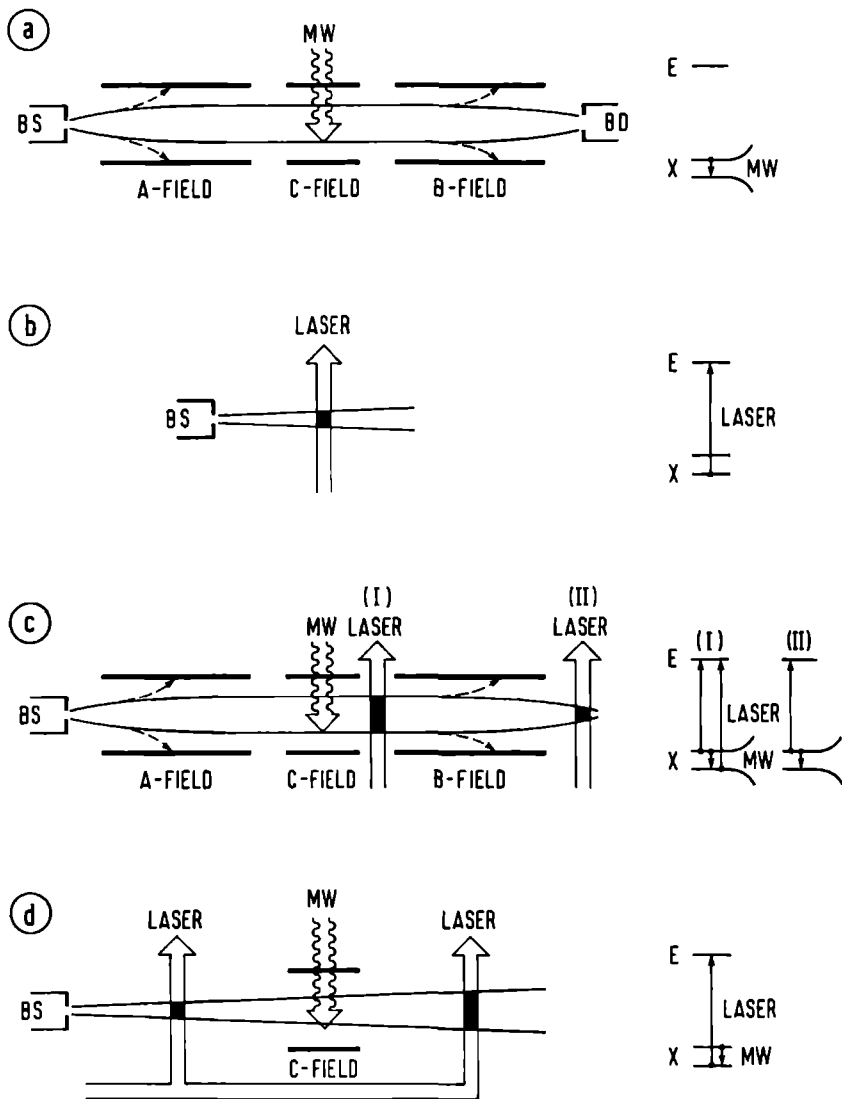
Fig. 1. Configurations of the spectrometer in case of the MBER (a), MBLE (b), MODRES (c) and MBLIFR (d) methods (see text). Transitions are indicated in energy level diagrams at the right-hand side, in which Stark effects are drawn if relevant; X and E represents the ground and excited electronic state, respectively. In the MODRES method (c) the laser beam intersects the molecular beam either at position (I) or at position (II). Shaded beam intersections indicate LIF detection. BS: beam source and BD: beam detector.

12

ed (apart from the natural linewidth) by the residual Doppler broadening (in the order of 10 MHz) determined by the degree of molecular beam collimation. The MBLE method requires sufficient laser-induced excitation and fluorescence yields. However, the feasible sensitivities of the state-resolved LIF detection are several orders of magnitude higher than obtained by total beam detection. Because the noise and the LIF detection signals originate only from the molecular states of interest, aside from spurious background due to straylight and photodetector noise.

The microwave optical double-resonance on an electrically state-selected beam (MODRES) method developed in this work (Fig. 1 (c)) is a new and powerful technique, that combines the high-resolution spectroscopy of the MBER method with the high sensitivity of the state-resolved detection in the MBLE method. The laser frequency is kept fixed at a specific optical excitation transition and the LIF intensity is monitored. The laser thus provides detection of the number of molecules in a specific energy level of the ground electronic state. At first, the configuration in which the laser beam intersects the molecular beam at position (I) in Fig. 1 (c) is considered. If a transition is induced in the C-field by microwave radiation from a state transmitted to a state rejected by the A-field, a decrease (flop-out) in the LIF intensity will occur if the initial state is probed by the laser (double-resonance condition). Alternatively, an increase (flop-in) in the LIF intensity will occur if the final state is probed by the laser. In the configuration with LIF detection at position (II) in Fig. 1 (c) only one of the two states connected by the microwave radiation is transmitted by the additional state-analysing B-field. This configuration has the advantage that it can be applied in the (rare) case the laser detection at position (I) cannot accomplish full state analysis because the two states fall within its spectral resolution. Disadvantage is the lower intensity as a consequence of the larger distance from the source. The magnetic variant of the MODRES (II) method, employing inhomogeneous magnetic A- and B-fields, has been developed by Grundevik *et al.* (GRU 79). This technique can be applied to atoms or molecules with magnetic dipole moments. It should be noted that the linewidths in the double-resonance MW spectra do not depend on the much broader linewidths of the LIF transitions. The spectral resolutions are (like in case of MBER) normally only determined by the transit time of the molecules through the C-field transition region, as the natural lifetimes in electronic ground states are comparatively large. The configuration with intersection at position (I) will hereafter be referred to by MODRES without further specification.

The molecular-beam laser-induced fluorescence resonance (MBLIFR) method (Fig.1 (d)) was introduced by Rosner *et al.* (ROS 75) and resembles the MODRES method. The A-field is replaced by the intersection with another beam from the same laser. The first laser beam produces state labeling by depleting the population of a specific energy level in the ground electronic state by means of optical pumping. If transitions are induced in the C-field by microwave radiation, terminating in the state probed by the second laser beam (double-resonance condition), an increase in the LIF intensity will occur. This MBLIFR method is not restricted to polar molecules; however, it is only applicable if sufficient optical pumping can be achieved.

Not considered above are methods employing photoionization and photodissociation detection, multiple-resonances by application of more than one microwave and/or optical frequency, transitions induced by separated fields and spectral analysis of LIF.

3. OUTLINE OF THESIS

In Ch. III (A) and (B) the results of the experiments on the hydroxyl (OH) radical are given. These experiments have been performed using the MBER method. The molecular beam of OH radicals was produced by a reaction source, by means of the reaction $H+NO_2 \rightarrow OH+NO$. It was detected by a universal mass spectrometer. The hyperfine Λ-doubling transitions of OH in the $X^2\Pi_{1/2}$, J=1/2 and 3/2 and in the $X^2\Pi_{3/2}$, J=3/2 and 5/2 levels of the v=1 and v=2 excited vibrational states have been measured. All Λ-doubling and hyperfine constants could be determined independently. Predictions for molecular constants and transition frequencies in the v=3 and 4 vibrational states are given. The results have been compared with *ab initio* calculations, yielding satisfactory agreement. The transition frequencies may be helpful for astronomical observation of emission from interstellar OH in excited vibrational states.

In Ch. IV the results of the experiments on the potassium-cyanide (KCN) molecule are given. These experiments have been performed by MBER as well. A supersonic beam of KCN seeded in Ar was produced by a two-chamber oven source and cooling of the internal rotational temperature to about 40 K was achieved. The KCN beam was detected by a surface-ionization detector, which offers detection efficiency of nearly 100% for alkaline compounds. The rotational spectrum of KCN has been measured at frequencies below 31 GHz. These results have been combined with rotational transitions from microwave absorption experiments, an in-

dependent study at the Freie Universität Berlin in the frequency regions 27 to 29 GHz and 36 to 39 GHz and the earlier study at our laboratory (KUI 76). Altogether 64 transitions have been assigned to the ground vibrational state. From the rotational constants determined, the geometrical structure of the KCN molecule has been evaluated. It was found to have an unexpected T-shape.

In Ch. V the results of the experiments on the iodine-oxide (IO) radical are presented. The molecular beam of IO radicals was produced by a reaction source, via the reaction $I_2 + O \rightarrow IO + I$. The rotational spectra of the vibrational bands 2-0, 2-1 and 2-2 of the $A^2\Pi_{3/2} - X^2\Pi_{3/2}$ transition have been studied using the MBLE method. The tunable optical radiation was produced by a c.w. dye laser. Hyperfine structures could be resolved for the lowest rotational levels. Rotational and hyperfine constants have been determined for both the excited and ground $X^2\Pi_{3/2}$ states. For the ground state, vibrational constants and vibrational series expansion coefficients for the rotational constants have been derived. Hyperfine splittings within rotational levels of the ground vibrational $X^2\Pi_{3/2}$ state have been measured with the MODRES method. From these splittings hyperfine constants, including non-axial coupling constants, have been determined as well. These results have been combined by a merging procedure with data from flame emission (DUR 60) and microwave absorption (SAI 73) spectroscopy. The widths of rotational levels in the excited v=2, $X^2\Pi_{3/2}$ state have been measured. Apart from vibrationally-dependent predissociation, a rotationally-dependent predissociation has been observed.

A description of the spectrometer in the MBLE and MODRES configurations, used to study the IO spectra, is given in Ch. II.

CHAPTER II

DESCRIPTION OF THE SPECTROMETER FOR THE IO EXPERIMENTS

1 INTRODUCTION

This chapter gives a description of the spectrometer in the configuration of molecular-beam laser-excitation (MBLE) and microwave optical double-resonance on an electrically state-selected beam (MODRES) These configurations have been used to study spectra of the iodine-oxide (IO) radical, of which the results are presented in Ch V The principles have been described in Ch I

The spectrometer is a modified version of the molecular-beam electric-resonance apparatus described elsewhere (LEE 73, MEE 75, MEE 79) For the present experiments the most essential modification is the extension of the frequency range of the spectrometer to the optical frequency region For this purpose the equipment has been extented with a dye laser set-up and the molecular beam apparatus has been equipped with windows and light baffles to allow the laser beam to intersect the molecular beam orthogonally at two different positions The laser-induced fluorescence (LIF) from molecules in the beam is collected and transmitted by optical systems and detected by photomultipliers connected to a photon-counting system

The topics that successively will be discussed in the following sections, are the molecular beam apparatus in the MBLE and MODRES configurations, the spectral resolution, the dye laser with peripheral equipment and the digital wavelength meter

2 MOLECULAR BEAM APPARATUS

An outline of the spectrometer is presented in Fig 1 The IO radical was produced by the reaction of atomic oxygen with iodine molecules,

$$O+I_2 \rightarrow IO+I. \tag{1}$$

The molecular beam of IO radicals was produced in a reaction source (see Ch V) This reaction source is located in the source chamber (typical pressure 4×10^{-2}
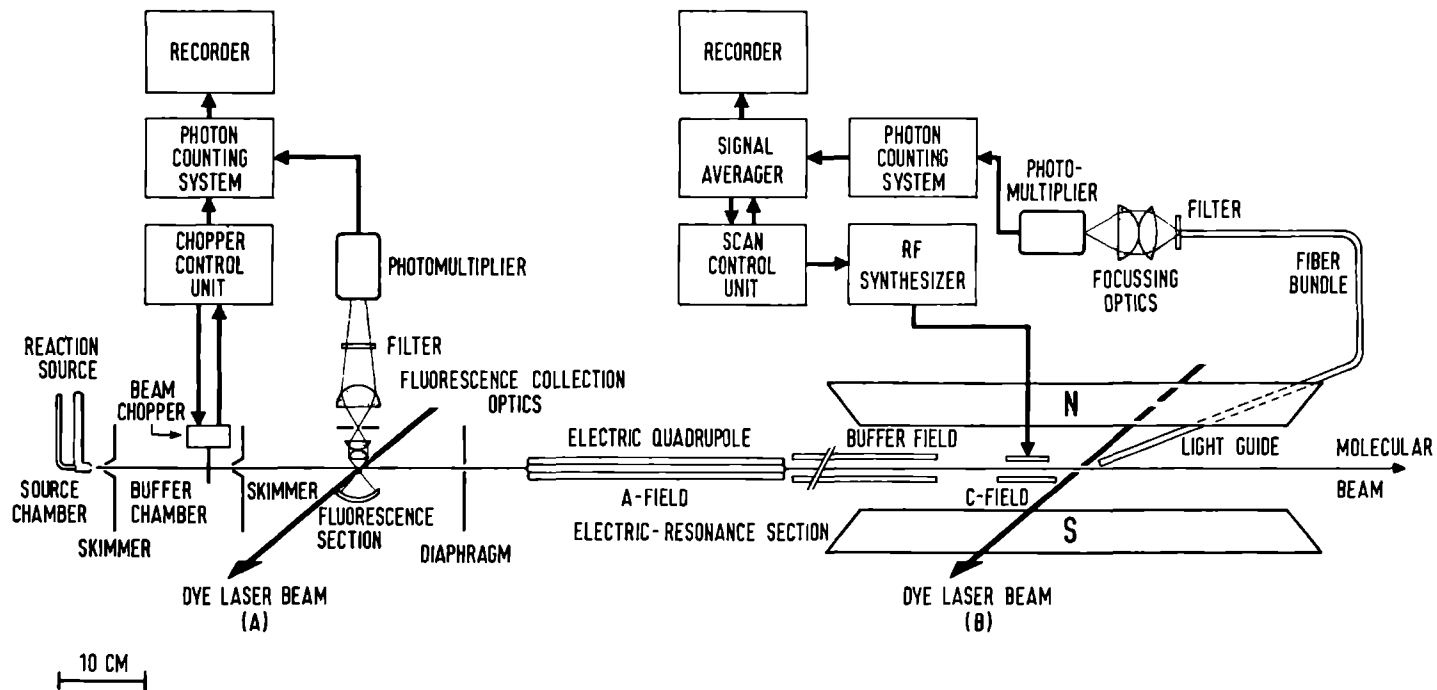
Fig. 1. Outline of the spectrometer. The direction of the laser beams is perpen-
dicular to the plane of drawing, the light guide is in the plane of the molecular
and laser beam at an angle of 45° with both beams. Intersections at position
(A) and (B) correspond to the MBLE and MODRES configurations, respectively.
The actual length of the buffer field is 47 cm.

mbar) and the molecular beam is formed by a conical skimmer with an aperture of 2 mm The IO beam traverses a buffer chamber (pressure of 3×10^{-5} mbar) and passes a second skimmer with an aperture of 3 mm, before it enters the fluorescence section (pressure of 4×10^{-6} mbar)

2 1 MBLE configuration

In the fluorescence section the dye laser beam intersects the molecular beam (at position (A) in Fig 1) in case of the MBLE configuration, at a distance from the source of 30 cm A schematic cross-section of this fluorescence section is shown in Fig 2   The LIF from the interaction region is collected in a direction perpendicular to both the laser and molecular beam by a system consisting of three aspherical lenses and a concave spherical mirror Aspherical lenses with broadband anti-reflection (AR) coating are used because of their low f-numbers The fluorescence collection efficiency is 20-25% A diaphragm situated in the intermediate focus of the lens system provides spatial filtering, to screen off stray light not originating from the interaction volume The collected fluores- cence is transmitted to the photocathode of a photomultiplier (EMI 9635, bialka- line response) through an AR-coated vacuum seal window and a spectral filter This filter (Schott CG 495, thickness 3 mm) has a cut-off wavelength at 495 nm and absorbs scattered laser light The observed vibrational bands of the optical IO spectra are located at 445 nm (2-0 band), 459 nm (2-1) and 473 nm (2-2) The IO fluorescence from the excited, v=2 state at longer wavelengths (above 495 nm) is transmitted This fraction amounts about 75% of the total LIF as estimated from the Franck-Condon factors (RAO 74) However, due to fluorescence in the filter, the extinction efficiency of scattered laser light was only 99% For general prevention against stray light the optical collection system is enclosed in a tube and the complete inside of the fluorescence section has been coated black The laser beam passes through AR coated windows The exit window has been mounted at an angle of 45° to prevent backscatter Light baffles are placed in both side arms to screen off scattered laser light from the windows and stray light from outside the vacuum

In the MBLE experiments the IO beam is modulated by a mechanical chopper at a frequency of 24 Hz The LIF signal from the photomultiplier is monitored by a photon-counting system (ORTEC-Brookdeal 5C1) The in-phase part of pulses from the photomultiplier is extracted during a preset counting time, in order to eliminate all off-phase background contributions The LIF intensity is recorded as a function of the frequency of the dye laser The diameter of the laser beam
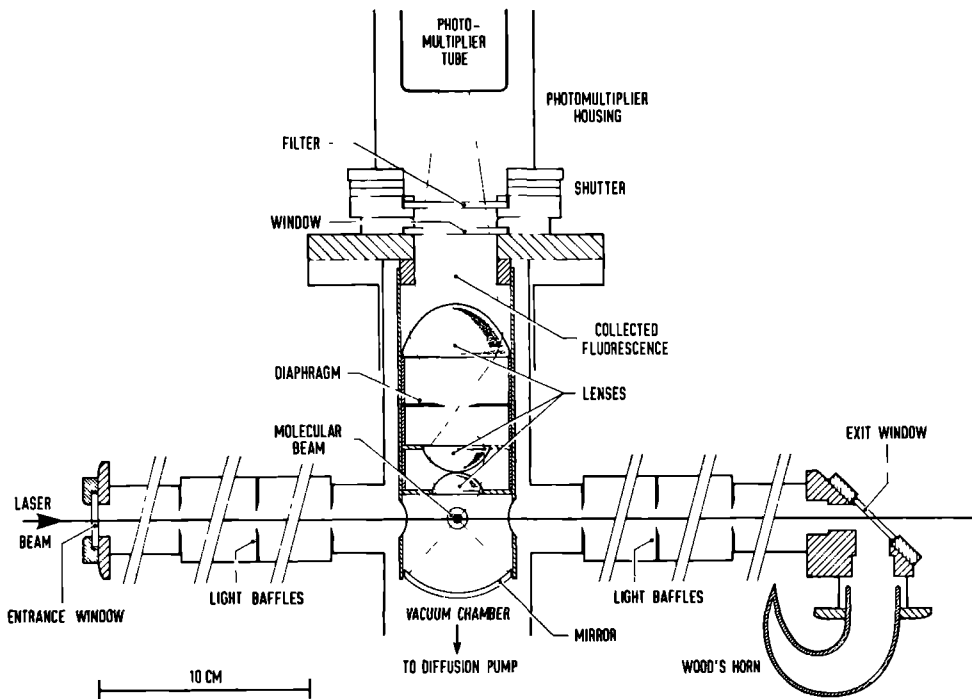
Fig. 2. Schematic cross-section of the fluorescence section. The direction of the molecular beam is perpendicular to the plane of drawing. The actual length of each side arm with light baffles is about 40 cm.

was about 5 mm and the typical laser power was 30 mW, resulting in an intensity of 1.5 mW/mm². The background signal from scattered laser light was 300 counts per second (c/s), from stray light from outside the vacuum 15 c/s and from dark current of the photomultiplier 35 c/s. The reaction source contributed 150 c/s in-phase, presumably from stray light from the discharge, chemiluminescence and metastable oxygen. The main contribution to the background was a continuous (only weakly dependent on laser frequency) off-phase signal of about 1500 c/s. This unidentified signal appeared when the laser and molecular beam crossed each other while the reaction source was in operation. So the total off-phase background signal amounted to about 2000 c/s and caused a noise of 90 counts at a counting time of 1 s. The strongest lines in the IO spectra had an intensity of about 8000 c/s, so the best signal to noise ratio was about 40 at a counting time of 1 s.

In the MODRES configuration the electric-resonance section (pressure about 1×10^{-7} mbar) of the molecular beam apparatus is used The dye laser beam inter-sects the molecular beam at position (B) in Fig 1, at a distance from the source of 145 cm

The molecular beam is state selected by the inhomogeneous electric A-field In this electric quadrupole field polar molecules experience a radial force giv-en by

$$\underline{F} = -gradW = -(\partial W/\partial E)gradE = -\mu^{eff}(2V_0/r_0{}^2)\underline{e}_r \tag{2}$$

Herein, W is the Stark energy, E is the electric field strength, $\mu^{eff}=\partial W/\partial E$ is the effective dipole moment, $2V_0$ is the potential difference between adjacent electrodes, r_0 is the distance (3mm) of an electrode to the quadrupole axis and $\underline{e}_r$ is the radial unit vector The cylindrical electrodes have a diameter of 7 mm and the length is 30 cm The effective dipole moment μ^{eff} depends on the quantum state of the molecule and on the electric field strength Molecular states with positive Stark effect ($\mu^{eff}>0$) are deflected towards the beam axis and those with negative Stark effect ($\mu^{eff}<0$) are deflected away from it The IO radical has a $^2\Pi$ electronic ground state Each hyperfine component of a rotational state is split into two closely spaced Λ-doublet states with different symmetry These upper and lower Λ-doublet states exhibit mainly positive and negative linear Stark effects, respectively, at higher field strengths This offers the possi-bility to observe transitions induced in the C-field, between hyperfine levels within a rotational state The large dipole moment of 2 5 D (BYF 71) allows state selection for the lower rotational levels at moderate voltages In the buffer field an electric field can be applied to conserve the space quantization of molecular states

The C-field consists of a travelling wave system It is a scaled-up version of the electronic micro-strip device and serves as a 50 Ω transmission line The upper plate has a width of 5 cm and the distance between upper and ground plate is 10 mm The microwave radiation propagates between these plates in a direction perpendicular to the molecular beam axis The transmission line is terminated by an absorber This C-field can be used at frequencies from RF up to a few GHz The RF has been generated by a programmable RF synthesizer (Hewlett-Packard 8660 B)

Directly after the C-field the dye laser beam intersects the molecular beam to detect molecules in specific quantum states by LIF A construction of win-

dows and light baffles similar to those in the fluorescence section is used to reduce background signal from stray light. The fluorescence is collected by a light guide with a diameter of 6 mm (Schott LST) at an angle of 45° with both beams. A flexible fiber bundle (Schott) transmits the collected fluorescence to a photomultiplier. The exit of the fiber bundle is imaged through a spectral filter onto the photocathode of the photomultiplier (EMI 9863/350, S20 response) by two AR-coated aspherical lenses mounted inside the photomultiplier housing. The fluorescence collection efficiency is about 2%, which is one tenth of the efficiency obtained by the optical system in the fluorescence section. However, a similar system could not be applied in this region because of the limited available space. Advantage of the light guide system is the possibility to apply electric and/or magnetic fields in the laser interaction volume and the unobstructed passage of the molecular beam.

In the MODRES experiments the LIF intensity is monitored by a photon-counting system as a function of the microwave frequency. Because the signals in the IO experiments were very weak, a signal averager (Hewlett-Packard 5480 B), interfaced with the RF scan control unit, has been employed. The diameter of the laser beam was about 4 mm and the typical laser power was 45 mW, resulting in an intensity of 3.5 mW/mm^2. The background signal from scattered laser light was about 110 c/s, stray light from the reaction source contributed 60 c/s and dark current of the cooled photomultiplier was 15 c/s. The line intensities of the laser detection transitions were about 50 c/s with state selection, which corresponds to a signal to noise ratio of about two at a counting time of 1 s. The signals of the double-resonance RF transitions were about 15 c/s. In most cases 32 RF scans (each scan took one minute at 1 s time constant) were averaged, yielding a final signal to noise ratio in the order of two.

3. SPECTRAL RESOLUTION

In principle the spectral resolution in the MBLE experiments is determined by the natural lifetime of the excited molecular state. Apart from this natural linewidth instrumental limitations are imposed by residual Doppler broadening, laser frequency jitter, transit time broadening and wavefront curvature broadening (SHI 76, DEM 81).

In the experimental set-up the main instrumental contribution to the observed linewidths arises from the residual Doppler broadening. The full angular divergence ε of the molecular beam is determined by the collimation affected by

the skimmer configuration; $tg\varepsilon=\phi/1$, where ϕ is the aperture of the second skim-
mer and 1 is the skimmer to source distance (see Fig. 1). Because of finite di-
vergence the molecules will have a velocity component along the direction of the
laser beam and accordingly their absorption frequency will be slightly shifted
by first-order Doppler effect. Assuming thermal equilibrium in the source re-
gion, the velocity distribution in the molecular beam is Maxwellian with the
most probable velocity $v_p=(2kT/m)^{\frac{1}{2}}$, where k is the Boltzmann constant, T is the
source temperature and m is the molecular mass. Integration of these shifts in
the absorption frequency over the molecular beam cross-section and velocity dis-
tribution yields a Gaussian absorption profile with full width at half maximum
(FWHM)

$$\Delta\nu_D = 2\nu_0(v_p/c)(\ln 2)^{\frac{1}{2}}\sin(\varepsilon/2), \tag{3}$$

where ν_0 is the unshifted absorption frequency and c is the speed of light. The
experimental conditions; $\varepsilon=20$ mrad, $T\sim 500$ K, $v_p\sim 240$ m/s and $\nu_0/c=2.17\times 10^4$ cm^{-1},
result in $\Delta\nu_D\sim 8.7$ MHz. It should be noted that in the reaction source the ther-
mal equilibrium assumption may not be valid and for instance a velocity slip
with the much lighter oxygen may result in a higher molecular beam velocity and
therefore larger Doppler broadening. The laser frequency jitter causes an effec-
tive radiation bandwidth $\Delta\nu_J\sim 3$ MHz. The transit time broadening arises from the
finite interaction time of molecules with the laser light. Its profile is Gauss-
ian with a width

$$\Delta\nu_T = (2/\pi)(2\ln 2)^{\frac{1}{2}}v_p/d, \tag{4}$$

where d is the diameter of the laser beam between $1/e^2$ intensity points of the
fundamental mode (TEM$_{00}$). The contribution $\Delta\nu_T$ of the transit time broadening to
the linewidth is about 0.04 MHz, for d=5 mm. The broadening due to wavefront
curvature arises from the spatial phase shift $\Delta\psi$ experienced by the molecules
while passing the low-divergent laser beam; $\Delta\psi=(d/2)^2\pi\nu_0/Rc$, with R the radius
of curvature of the wavefronts. This broadening contributes by the width

$$\Delta\nu_C = (\Delta\psi/\pi)v_p/d. \tag{5}$$

As in the experiments R is about 10 m and so the phase shift $\Delta\psi\sim\pi$, $\Delta\nu_C$ is compar-
able in magnitude to $\Delta\nu_T$. The total instrumental resolution is given by the con-
volution of all the contributions discussed above. Convolution yields a Gauss-

ian profile with a width given by the composition rule $\Delta\nu=[\Sigma(\Delta\nu_i)^2]^{\frac{1}{2}}$, where i labels the individual contributions to the profile. For the IO experiments this width has been estimated as 10-20 MHz.

The observed spectral line profile is a convolution of a Lorentzian (natural linewidth, homogeneous line broadening) and a Gaussian profile (instrumental resolution, inhomogeneous line broadening), which is a Voigt profile. This profile, normalized to unity, is given by

$$I(\nu) =$$

$$(\Delta\nu_L/\Delta\nu_G)(\ln2)^{\frac{1}{2}}\pi^{-3/2}\int_{-\infty}^{\infty}\exp[-4\ln2(\nu_G-\nu_0)^2/(\Delta\nu_G)^2]/[(\nu-\nu_G)^2+(\Delta\nu_L/2)^2]d\nu_G, \quad (6)$$

where $\Delta\nu_L$ and $\Delta\nu_G$ is the linewidth of the Lorentzian and Gaussian profile, respectively, ν_0 is the frequency at the line centre and ν_G is the shifted radiation frequency as experienced in the molecular frame. The Lorentzian contribution originates from the natural absorption profile of the molecular transition. Its width is determined by the finite lifetime of the excited state. This lifetime is a combination of a radiative and a predissociative decay time. The excited state of the IO radical exhibits extensive predissociation. Predissociation decreases the fluorescence yield and increases the natural linewidth. The observed transitions terminate in the less predissociative vibrational level (v=2) of the excited state, where the predissociation rate exceeds the radiation rate by more than two orders of magnitude. The observed natural linewidths vary from 150 MHz up to about 2 GHz.

The spectral resolution in the MODRES experiments is normally only limited by the transit time of the molecules through the C-field transition region. Because the other instrumental contributions discussed above are negligible at microwave frequencies and the natural lifetimes in electronic ground states are comparatively large. The transition region has a width of 5 cm and so the transit time broadening contributes about 10 kHz to the linewidth.

The observed microwave spectra belong to the $X^2\Pi_{3/2}$ ground state of the IO radical. As this state is paramagnetic, with a magnetic moment in the order of one Bohr magneton, the Earth's magnetic field gives rise to considerable Zeeman splitting of hyperfine levels. The magnitude of these splittings decreases with increasing rotational quantum number and is in the order of 1 MHz for the lowest rotational state (J=3/2). The Earth's magnetic field has been compensated to avoid broadening due to this Zeeman splitting. The compensating field was produced by a magnet that surrounds the double-resonance region (see Fig 1). Be-

fore each run of experiments on IO, careful compensation was achieved on a field-sensitive hyperfine Λ-doubling transition in the $X^2\Pi_{3/2}$ state of NO (J=3/2, F_+=3/2←F_-=5/2 (MEE 72)) For this purpose an NO beam was produced by passing NO gas through the reaction source and the transition was observed using the MBER method The linewidth of transitions in the J=3/2 state could be reduced to less than 100 kHz, which corresponds to a residual magnetic field of less than 35 mG

4 LASER SET-UP

A diagram of the arrangement of the laser set-up is shown in Fig 3 The dye laser and interferometers have been rigidly mounted to a granite plate, that rests in a container filled with sand to damp its resonances This is placed on top of a column of styropor blocks, which stands on a rubber layer The Ar-ion laser and the digital wavelength meter are rigidly mounted to separate tables

4 1 Dye laser

The tunable optical radiation for the experiments has been generated by a single-frequency c w dye laser (Coherent Radiation 599-21) Since principles of dye laser operation are well known, only a brief description of features relevant to the present study is given The standing-wave dye laser has a dye jet-stream located in the intracavity focus of an astigmatically compensated folded three-mirror resonator The gain medium is a solution of Stilbene 3 (420) dye in ethylene glycol (0 75 g/l) The dye laser is pumped by the UV lines (351-364 nm) from an Ar-ion laser (Spectra Physics 171-UV) An intracavity hierarchy consisting of a three-plate birefringent filter, a thin etalon and a thick etalon, accomplishes passive selection of and locking to one single longitudinal mode (TEM_{00q}) of the dye laser resonator Part of the output power (10%) is used for active frequency stabilization Two partial beams are split off from the output beam, one of them passes directly to a photodiode and the other beam passes to another photodiode via a confocal Fabry-Perot interferometer This interferometer has a low finesse and serves as reference cavity It is enclosed in a pressure-tight and temperature-stabilized housing to minimize drift of the transmission frequencies The dye laser frequency is locked to the frequency corresponding to the position half-way the slope of a reference cavity transmission peak The difference signal from the two photodiodes is used to generate
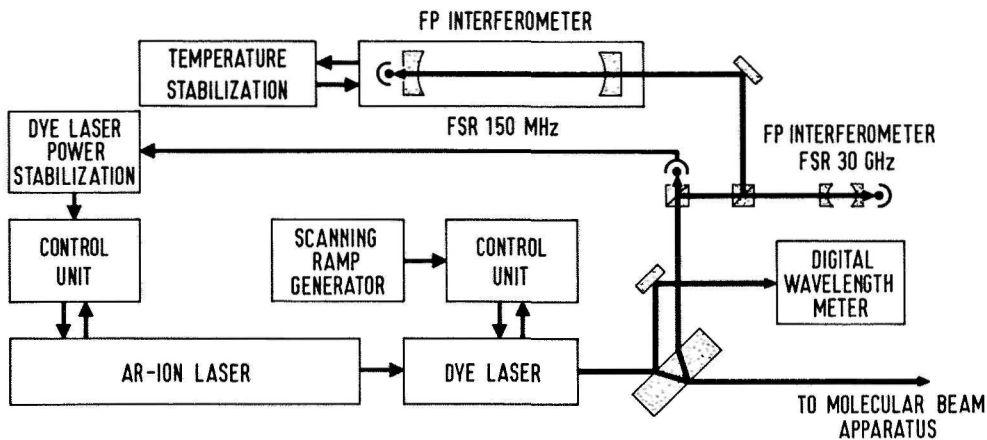
Fig. 3. Diagram of the arrangement of the laser set-up.

the error signal, that is minimized by a servo loop system. The laser frequency is controlled by adjustment of the length of the dye laser cavity. This is accomplished by means of translation of the fold mirror (piezo-electric driven, fast response) and tilting of an intracavity plate mounted at Brewster's angle (galvo driven, slow response). Scanning of the stabilized laser frequency is achieved by tuning the transmission frequency of the reference cavity, by means of tilting of a similar Brewster plate inside this reference cavity. The dye laser can be continuously scanned over a range of 30 GHz. An external scanning ramp generator provides an up or down going ramp (linearity is better than 0.2%, maximum sweep time is 55 minutes) to drive the scan controls of the dye laser.

The effective spectral bandwidth due to residual jitter of the laser frequency is 3 MHz and the drift in the laser frequency is less than 50 MHz/h. As the IO excitation spectrum is located in the blue-green wing of the broad Stilbene tuning curve, the dye laser has been equipped with mirrors coated for operation with Coumarin 102 (480) dye. The following single-frequency output powers were obtained: 95 mW at 445 nm (1.5 W UV TEM_{00} pumping power), 60 mW at 459 nm (1.7 W UV) and 35 mW at 473 nm (1.7 W UV). At higher pumping powers instabilities in the dye jet appear.

4.2 Peripheral equipment

A beam splitter at the exit of the dye laser (see Fig. 3) samples off two weak beams (each ~8% of the output intensity) for monitoring purposes, the re-

maining part is transmitted to the molecular beam apparatus One beam feeds the digital wavelength meter and the other beam is sent to a photodiode and two interferometers.

The photodiode (EG&G HAV-1000A) monitors the laser power and provides reference for an external power stabilization system This system counteracts variations in the dye laser power by regulating the Ar-ion laser power The stability obtained is better than 0 5% in the response range from DC to 100 Hz

The interferometer with a free spectral range (FSR) of 30 GHz, is used in the scanning mode of operation It is interfaced with an oscilloscope, which displays the mode properties of the dye laser

The interferometer with a FSR of 150 MHz (Burleigh CF T-500), is used to monitor the frequency of the dye laser It consists of a confocal Fabry-Perot etalon with a mirror spacing of 50 cm and with highly reflective mirror coatings to obtain a high finesse (>125) (HER 68) A sealed etalon construction of super-invar in a thermally stabilized housing, accomplishes passive stabilization of its transmission frequencies (stability better than 5 MHz/h) While scanning optical spectra with the MBLE method, the transmission peaks in the fixed mode of operation are recorded simultaneously with the LIF intensity on a dual-channel chart recorder These transmission peaks furnish relative frequency marking Between each pair of markers a linear frequency interpolation has been performed As no systematic nonlinearity in the scans could be noticed within the experimental accuracy, the main contribution to any irregularities occurring in the scans arose from random drift of the laser frequency During the LIF detection in the MODRES method, the interferometer is used in the scanning mode It is interfaced to an oscilloscope, which displays shifts of the transmission peak pattern due to eventual drift of the dye laser frequency These frequency shifts are subsequently compensated by manual adjustment of the scan controls of the dye laser

Calibration of the free spectral range of the reference interferometer has been performed against known splittings in the IO ground state In the calibration experiments the MBLE configuration was used to observe the optical excitation spectum of IO, in the 2-0 vibrational band (at 445 nm) The dye laser was scanned across transitions terminating in the same hyperfine level of a rotational state in the excited state, but originating from different hyperfine sub-levels in rotational states of the ground state whose energy separation is known from microwave absorption data (SAI 73) The calibration scans covered intervals of 50 GHz, hyperfine structures of the rotational transitions Q(1 5) to P(2 5), and of 70 GHz, Q(2 5) to P(3 5) Within each interval about five pairs

of hyperfine components were suitable for calibration The results manifest good internal consistency and the FSR has been determined to be 149 605(15) MHz

5 DIGITAL WAVELENGTH METER

Determination of the absolute frequency of the dye laser is accomplished by the digital wavelength meter, which compares the dye laser wavelength with the accurately kwown wavelength of a reference laser Its principle is based on a Michelson interferometer with electronic counting of interference fringes (HAL 76, KOW 76, KOW 78) The digital wavelength meter that has been constructed incorporates variation of the optical path length inside a vacuum chamber (evacuated to 10^{-2} mbar), which eliminates the need of elaborate and inadequatly known dispersion corrections (EDL 66, OWE 67) The electronic counting system includes phase-locked 100-fold multiplication of the fringe frequencies to allow for interpolation to 1/100 part of a fringe A stabilized single-frequency He\e laser serves as reference

An outline of the digital wavelength meter is shown in Fig 4 At the beam splitter an incident laser beam is split into two parts of equal intensity These two partial beams traverse the two arms of the Michelson interferometer before they recombine at the beam splitter One of the beams passes through the arm of variable optical path length and is reflected by a moving corner cube located inside the vacuum chamber The other beam passes through the arm of fixed length and is reflected by the combination of a mirror and a corner cube These reflected beams are each split again at the beam splitter into two parts of equal intensity, that are sent to the two photodiodes Recombination of beams from the two different arms results in an interference dependent on the difference in traversed optical path length Variation of the length in one arm by the moving corner cube yields a sinusoidal beat signal from the photodiodes Corner cube prisms (Spindler & Hoyer 330009) are used to ensure that beams are reflected parrallel to their incident directions, independent of slight angular motion

The beams from the dye laser and the reference HeNe laser are aligned coincident to ensure that both beams traverse identical paths As the incident laser beams are polarized orthogonally to each other, they can be separated at the photodiodes by means of polarization filters (or by spectral filters if the wavelengths are sufficiently distinct)

FROM DYE LASER

CYLINDER CONTROL

P   HeNe LASER FRINGES

// MODE PBS   PLASMA TUBE $\frac{\lambda}{2}$ P

CC

⊥ MODE

HEATING

BEAM SPLITTER   VACUUM CHAMBER   HYDRAULIC CYLINDER

THERMAL FREQUENCY STABILIZATION

P

DYE LASER FRINGES

CC

GAIN CURVE

//   ⊥

MODE SPACING

x100 PHASE LOCK   GATE   COUNTER N

x100 PHASE LOCK   PRESET SCALER C
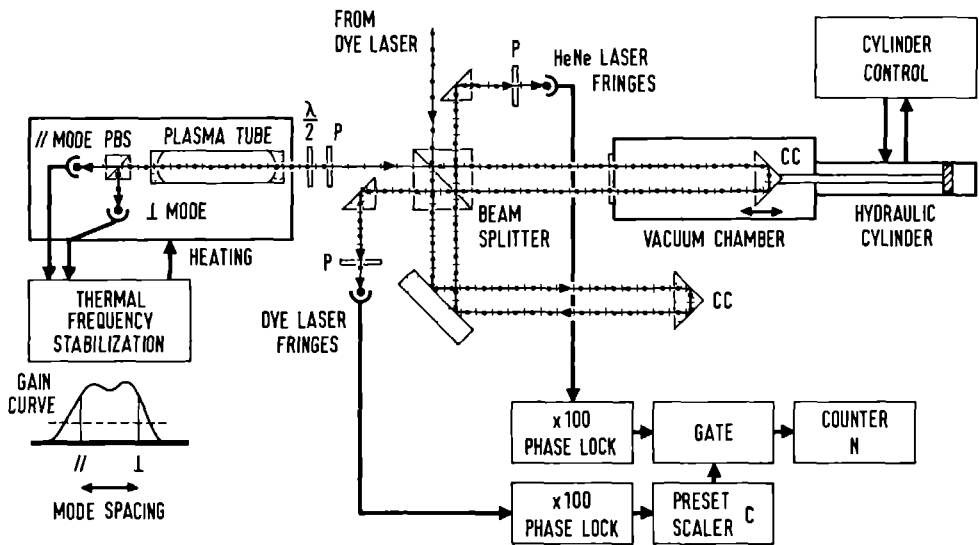
Fig. 4. Outline of the digital wavelength meter. Polarization of laser beams is indicated by dots for polarization perpendicular to the plane of drawing and by stripes for polarization in the plane of drawing. CC: corner cube prism, P: polarization filter, PBS: polarizing beam splitter and $\lambda/2$: half-wave plate.

The output signals from the PIN-photodiodes (Hewlett-Packard 5082-4207) are fed into a counting system. The phase-locked 100-fold multiplication of the fringe frequencies requires a nearly constant velocity of the moving corner cube This has been accomplished by mounting it to the piston rod of a hydrau- lically driven cylinder. Its speed of about 1 cm/s is uniform within ±5% The corresponding frequency at the photodiode for HeNe laser (633 nm) fringes is 32 kHz Furthermore, care has to be taken to avoid bubble formation in the dye jet system These bubbles, when passing the cavity focus, cause spike-shaped drops in the output power, that may offset the phase lock.

A measurement is started by a photosensor, after an initial travel of 5 cm, that triggers simultaneous opening of the gates to the counters As soon as the preset scaler has reached the value C, the gate to the counter, which then dis- plays the value N, is closed The ratio of the number of interference fringes at the two photodiodes for a given displacement of the moving corner cube is pro- portional to the inverse ratio of the wavelengths of the two lasers The vacuum wavelength of the dye laser is given by

$$\lambda_{dye}^{vac} = \lambda_{ref}^{vac} N/(C-\tfrac{1}{2}), \qquad\qquad (7)$$

where λ_{ref}^{vac} is the vacuum wavelength of the reference HeNe laser. The value C has been preset to 63299145 and can be truncated to 6 or 7 digits for quick but less accurate wavelength determinations. A measurement cycle at full accuracy takes 14 s at 450 nm.

The counting accuracy of the value N is limited by the resolution. For each wavelength determination a set of repeated measurements needs to be performed. The resulting N values follow a statistical distribution with standard deviation of 1.5 counts (4×10^{-8} at 450 nm). The electronic counting system has been checked by feeding the reference laser fringes to both photodiodes. Since the beams from dye laser and reference laser coincide and the interferometer arms are of nearly equal length, the main source of systematic deviation arises from any residual angle α between the laser beams. The consequent difference in optical path length for the two beams is proportional to $\cos^2\alpha$. The beams have been aligned to within 0.2 mrad, corresponding to deviations smaller than 4×10^{-8}. For absolute wavelength measurements, however, the uncertainty of 1×10^{-7} in the wavelength of the reference HeNe laser is dominating; λ_{ref}^{vac}=632.99125(6) nm. Consequently the absolute accuracy of the digital wavelength meter is 1.2×10^{-7} throughout the visible region. For the IO spectrum around 450 nm it corresponds, expressed in frequency, to 0.0025 cm^{-1} or 70 MHz.

The reference laser is a commercial HeNe laser (Hughes 3222 H-C) modified to obtain stabilized single-frequency operation (BAL 72, BEN 73). A schematic view is shown in the left-hand part of Fig. 4. Cavity modes of this HeNe laser are alternately polarized orthogonally to each other. The mode spacing is about 685 MHz and generally the laser oscillates in two modes. A polarizing beam splitter (Melles-Griot 04LPB001) mounted behind the plasma tube (with internal mirrors) feeds these modes to different photodiodes (EG&G HAV-1000A). The intensities of the two modes are equalized by a servo loop system. The cavity length is thermally adjusted by regulation of the power applied to heating elements. By means of a half-wave plate and a polarization filter one of the modes can be selected. The short term stability obtained is about 12 MHz and the long term stability, with emphasis on the reproducibility, is better than 45 MHz (1×10^{-7}). Stability characteristics are comparable to those obtained by stabilization on the Lamb-dip (MIE 68). This is not unexpected because both methods are sensitive to changes in the gain curve (especially in the asymmetry). Stabilization on the Lamb-dip of a molecular iodine transition improves obtainable stability by several orders of magnitude, but is much more elaborate. Besides, the present

counting accuracy allows only for improvement in the measurement accuracy by a factor two

The wavelength of the reference HeNe laser has been determined regularly during experiments, by measuring the wavelength of the dye laser tuned to the Lamb-dip of a transition $(6p^3P_1-7s^3S_1)$ of the ^{198}Hg secondary standard The absolute wavelength of this transition has been determined accurately (435 95625(1) nm) relative to the ^{86}Kr primary standard (KAU 62) The mercury lamp consists of a pyrex tube, with a length of 15 cm and an inner diameter of 10 mm, terminated with Brewster windows It contains argon at a pressure of 4 mbar and a drop of mercury A microwave discharge at 2 45 GHz was applied to the lamp Dissipated power was about 50 W and forced air cooling has been used The absorption spectrum has been recorded first by passing the dye laser beam through the mercury lamp to a photodiode detector The spectrum shows a hyperfine pattern spread over a region of 55 GHz, arising from the different isotopes (see e g RAN 60) The highest absorption strength was about 50% The observed linewidths were Doppler broadened to about 0 7 GHz and the separation between the ^{198}Hg and ^{200}Hg components is only 0 9 GHz To improve resolution the calibration measurements have been performed by Doppler-free saturation spectroscopy (LET 77) on the selected ^{198}Hg transition For this purpose the laser beam is reflected back through the mercury lamp by a mirror, at a small angle with the incident beam The Lamb-dip in the absorption spectrum occurs at the centre of the transition and has a Lorentzian line shape Its linewidth is determined by the natural linewidth with homogeneous broadening due to collisions and saturation The observed linewidth was about 100 MHz The accuracy of the wavelength determination of the line centre is set by the counting accuracy (4×10^{-8}) By this intrinsic method of calibration any eventual systematic errors are eliminated

Vibrational effects in the hydroxyl radical by molecular beam electric resonance spectroscopy

by W. L. MEERTS, J. P. BEKOOY and A. DYMANUS

Fysisch Laboratorium, Katholieke Universiteit,
Nijmegen, The Netherlands

The hyperfine Λ-doubling transitions of OH in the $^2\Pi_{1/2}$, $J=1/2$ and $3/2$ and in the $^2\Pi_{3/2}$, $J=3/2$ and $5/2$ levels of the $v=1$ and $v=2$ excited vibrational states have been measured in a molecular beam electric resonance spectrometer. Vibrational effects in the deduced Λ-doubling and hyperfine structure constants have been determined. A comparison is made with *ab initio* calculations.

1. INTRODUCTION

The hyperfine Λ-doubling spectrum in the ground vibrational state of the hydroxyl radical has been the subject of extensive theoretical and experimental studies. A summary of the results can be found in several papers [1, 2, 3]. Many less experimental data are available for the excited vibrational states of OH. The paramagnetic resonance spectra were investigated up to $v=9$ [4, 5, 6, 7]. However, these measurements were restricted to the $J=3/2$ and $5/2$ (for $v \leqslant 4$) levels in the $^2\Pi_{3/2}$ electronic state. This limits seriously the possibility of deducing the Λ-doubling and the hyperfine structure constants in the vibrationally excited states and their dependence on the internuclear distance in the OH molecule.

This paper reports a molecular beam electric resonance (MBER) study of the hyperfine Λ-doubling spectra originating in the $v=1$ and $v=2$ vibrational states. The complete set of microwave transitions has been obtained for the $J=1/2$ and $3/2$ rotational levels of the $X^2\Pi_{1/2}$ electronic state and for the $J=3/2$ and $5/2$ levels of the $X^2\Pi_{3/2}$ state. The electric resonance data are interpreted in terms of the theory for a $^2\Pi$ state, developed previously [1, 8]. All Λ-doubling and hyperfine structure constants could independently be determined for the $v=1$ and $v=2$ vibrational states. Together with the results for the $v=0$ state, accurate and rather complete experimental information about the variation of these constants with the internuclear distance has become available. The experimental results are compared with *ab initio* calculations performed by Hinkley *et al.* [9] and Coxon and Hammersley [10] for the Λ-doubling constants p and q and by Kayama [11] for the hyperfine constants. The overall agreement is satisfactory.

2. EXPERIMENT

The experiments were performed using a molecular beam electric resonance spectrometer described in detail elsewhere [8, 12]. Only some features relevant to the present work are discussed here.

Previous investigators have produced the vibrationally excited OH radical by the reaction of atomic hydrogen with ozone [5, 6] or with F_2O [4]. Although the techniques of producing beams of ozone were well developed in our laboratory [13], the reaction between atomic hydrogen and NO_2 was preferred for reasons of convenience and safety. The expected low signal-to-noise ratio for the transitions in excited vibrational states, and consequently integration times up to a few hours (see below) for a single transition, would require production and storage of large quantities of ozone. The reaction

$$H + NO_2 \rightarrow OH + NO$$
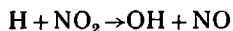
[14] was found to be quite effective in producing vibrationally excited OH radicals under optimized experimental conditions. Two different types of reaction sources were used. The type (a) source (figure 1 (a)) consisted of a quartz tube (inner diameter 9 mm) in which the NO_2 gas is injected through a ring of small holes 10 mm from the end. The type (b) source (figure 1 (b)), similar to the one used by ter Meulen in a beam maser [15], is made of a Pyrex tube (inner diameter 17 mm) in which the NO_2 gas is injected in the direction of the molecular flow via a fine glass capillary array 10 mm from the end of the tube. In both sources the beam was formed by a conical diaphragm (skimmer)
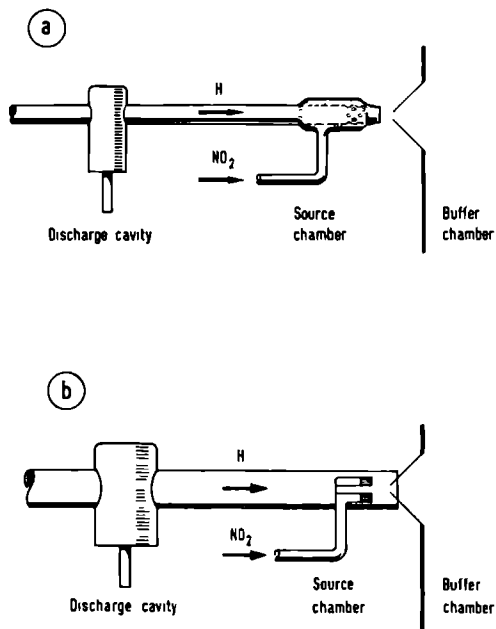
Figure 1. The two types of reaction sources for OH.
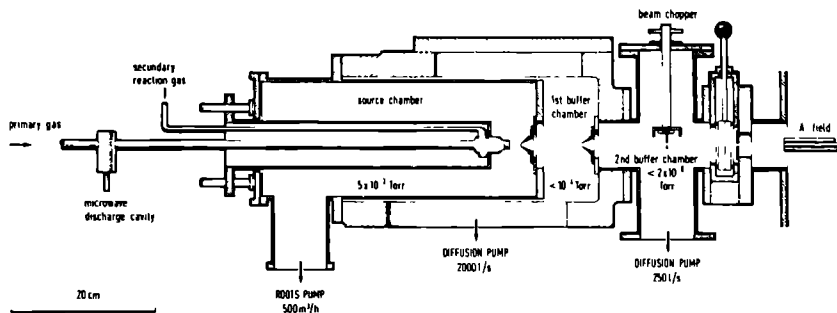
Figure 2. Schematic view of the reaction source section of the spectrometer.

2 mm in diameter. The hydrogen atoms were produced by a 2·45 GHz microwave discharge in water vapour ; the typical microwave power dissipated was 175 W. The source chamber was separated from the high vacuum of the electric resonance machine by two buffer chambers pumped by oil diffusion pumps, shown schematically in figure 2. The distance between the skimmer and the end of the source tube could be varied, which turned out to be of utmost importance for the production of a beam of vibrationally excited OH radicals. Under optimum flow conditions, typically $1·5 \times 10^{19}$ mol/s water and 1×10^{19} mol/s NO_2 through the reaction tube, the intensity of the $v = 0$ spectrum was found to be almost equal for the two sources. However, the optimum intensity ratio between the $v = 1$ and $v = 0$ spectra was 1·5 per cent and 6 per cent for the type (a) and type (b) sources, respectively. The maximum intensities were obtained for both sources when the distance between the end of the source tube and the skimmer was as short as possible, sometimes the skimmer was even inside the tube. Since the tube diameter of the type (b) source is larger the beam could be skimmed in the region where the reaction between atomic hydrogen and NO_2 took place. A displacement of a few millimeters of the skimmer downstream from the reaction zone reduced the intensity of the $v = 1$ spectrum considerably, while the intensity of the $v = 0$ spectrum was almost unchanged. This phenomenon can be understood by assuming that a large fraction of the OH radicals formed in the reaction is produced in excited vibrational states. The OH molecules cascade down the vibrational ladder by collisions with the gas molecules and the walls inside the reaction tube. Since the ratio of the number of OH radicals in the $v = 1$ and $v = 0$ state depends so strongly on the geometry of the source and skimmer it is not very sensible to define a vibrational temperature for the OH molecules in the beam. The $v = 2$ state of OH has only been investigated with the type (b) source and its spectrum was approximately 2·4 times weaker than the $v = 1$ spectrum. These results show that a beam of vibrationally excited OH radicals can be produced quite efficiently using the reaction between H and NO_2, while it is even competitive with the production by ozone reactions used by other investigators [5, 7] or by reaction with F_2O [4].

The microwave power for inducing the transitions was obtained from two Varian backward wave oscillators (BWO) type VA-183GA and VA-185M for

the region 1–2 GHz and 4–8 GHz, respectively. The most prominent features of these BWO's are the flat power response as a function of the frequency and the helix voltage as the only tuning element which completely determines the frequency. These features enabled searches for lines over wide frequency regions, 100 MHz or more. Since the instrumental linewidth of the electric resonance spectrometer varies between 8 and 25 kHz such a large frequency region can not normally be covered in a single scan. The reason is that the lines are wiped out by a fast scan (e.g. 20 kHz is scanned in about 10^{-2} s). A way out is line broadening by a random frequency modulation of the microwave power from the BWO, for example by superimposing a white noise voltage upon the helix voltage. This method of line broadening does not affect its peak intensity. The linewidth is controlled by the RMS value of the voltage from the noise generator. We were able to broaden the spectral lines up to 20 MHz allowing a scan over 150 MHz in 50 s when the RC-time of the lock-in amplifier was 1 s. Once a line was located roughly from a wide scan an accurate frequency measurement was performed with the normal linewidth. For this measurement the BWO frequency was stabilized by phase locking the 30 MHz beat signal between the BWO frequency and that of a Hewlett-Packard 8660B synthesizer to a 30 MHz reference signal by means of a Schomandl FDS 30 syncriminator.

The signal-to-noise of the transitions originating in the excited vibrational states of OH was smaller than unity at an RC time of 1 s, which forced us to use signal averaging techniques. For this purpose a Hewlett–Packard 5480B signal analyser has been interfaced either directly with the power supply of the helix voltage for wide scans or with the HP synthesizer for narrow scans. The typical time for a single scan over a spectral region was 50 s with RC of the lock-in set at 1 s, while usually 0·5 and 1·5 hour of signal averaging was required for the spectra from the $v = 1$ and $v = 2$ states, respectively. Figure 3 shows the strongest transitions observed in the $v = 0$, 1 and 2 states of OH. The search for the spectra originating in the excited vibrational states of OH was only possible by using the combination of the wide frequency region scan facility and the averaging techniques.
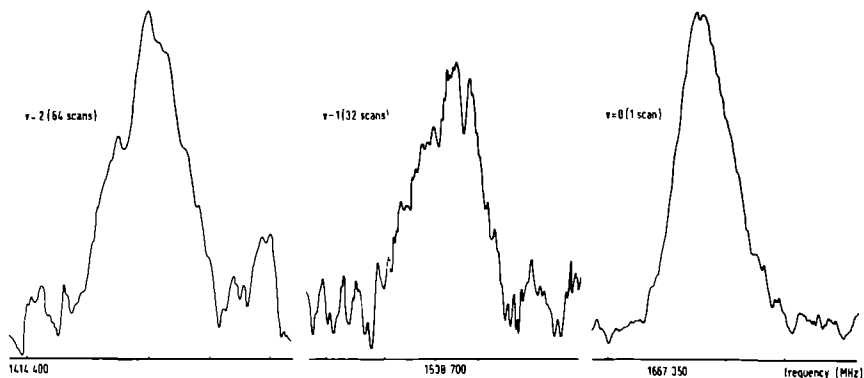
Figure 3.   Spectral lines of the $^2\Pi_{3/2}$, $J = 3/2$, $F = 2 \to 2$ transition in the $v = 0$, 1 and 2 vibrational states of OH. Separation between markers is 10 kHz.

3. THEORY

Since the theory used for the interpretation of the high resolution microwave spectrum of OH has been discussed in detail previously [1, 8, 16], only a short summary is given here. The hamiltonian for the microwave spectra of open shell molecules can be written formally as

$$H = H_F + H_{hf}, \qquad (1)$$

where H_F contains the spin-orbit, rotational and gyroscopic terms which give rise to the Λ-splitting; H_{hf} describes the hyperfine contributions induced by the interactions between the magnetic moments associated with the nuclear spin (**I**) and the orbital (**L**) and spin (**S**) angular momenta of the electrons. The explicit form of H_F and H_{hf} can be found in a previous paper [8]. The coupling scheme for the electronic and rotational part of the wavefunctions used here is Hund's case (a). The basis wavefunctions symmetrized with respect to a reflection (σ_{xz}) of the coordinates and spins of all particles in a plane containing the nuclei can be expressed as

$$|^2\Pi_\Omega{}^\pm \, J\rangle = \frac{1}{\sqrt{2}} \left[|J\Lambda\Sigma\Omega\rangle \pm (-1)^{J-1/2} |J - \Lambda - \Sigma - \Omega\rangle \right], \qquad (2)$$

where $\Omega = \Lambda + \Sigma$ is taken to be positive; Λ, Σ, Ω is the projection on the molecular axis of **L**, **S** and **J**, respectively, with **J** as the total angular momentum excluding nuclear spin. The Kronig symmetry of the functions of equation (2) is ± 1, the eigenvalues of the operator $\sigma_{xz}(\sigma_{xz}|^2\Pi_\Omega{}^\pm \, J\rangle = \pm |^2\Pi_\Omega{}^\pm \, J\rangle)$. The total wavefunction $|^2\Pi_\Omega{}^\pm \, JIF\rangle$ including the nuclear part is constructed as a product of the functions $|^2\Pi_\Omega{}^\pm \, J\rangle$ and the nuclear spin functions $|IM_I\rangle$ according to the coupling scheme $\mathbf{F} = \mathbf{J} + \mathbf{I}$, where **F** is the total angular momentum.

The OH molecule can be described by a coupling which is intermediate between Hund's case (a) and (b). The proper energies are obtained automatically by solving the secular equation. This equation can be set up using a degenerate perturbation calculation [17, 18]. The dimension of the secular equation is two in the absence of hyperfine effects and $2(2I+1)$ if hyperfine contributions diagonal and off-diagonal in J are included. The relevant equations discussed in earlier studies [1, 8, 16, 17] are summarized below. In these equations the generally accepted notation for the Λ-doubling constants p and q [19] and for the hyperfine structure constants a, b, c and d [20] is used. This is felt necessary to achieve a more uniform notation. However, while Mulliken and Christy [19] and Frosch and Foley [20] define the parameters in terms of expressions from second and first order perturbation theory, respectively, our definitions contain also contributions from higher order perturbations. The matrix elements for the hamiltonian of equation (1) containing contributions up to fourth order take the form:

$$\langle {}^2\Pi_{1/2}{}^\pm \, JIF | H | {}^2\Pi_{1/2}{}^\pm \, J'IF \rangle$$
$$= \delta_{JJ'}[-1/2 A_{n_v} + B_{n_v}(J+1/2)^2 \pm (-1)^{J-1/2}(J+1/2)\{(1/2 p_v + q_v)$$
$$+ D_{p_v}(J+1/2)^2 + \delta_{p_v}(J+1/2)^4\}] + G(J, J', I, F)$$
$$\times \left[(-1)^{J'-1/2} \begin{pmatrix} J & 1 & J' \\ -1/2 & 0 & 1/2 \end{pmatrix} \{(a_v - 1/2(b_v + c_v)) + \delta_{JJ'}.2C_{I_v}z^2\} \right.$$
$$\left. \pm \frac{(-1)}{\sqrt{2}} \begin{pmatrix} J & 1 & J' \\ -1/2 & 1 & -1/2 \end{pmatrix} (d_v + \delta_{JJ'}.D_{d_v}z^2) \right], \qquad (3)$$

$$\langle {}^2\Pi_{3/2}{}^\pm\ JIF|H|{}^2\Pi_{3/2}{}^\pm\ J'IF\rangle = \delta_{JJ'}\ [1/2A_{\Pi_v} + B_{\Pi_v}((J+1/2)^2 - 2)$$

$$\pm(-1)^{J-1/2}\ z^2(J+1/2)D_{q_v}] + G(J, J', I, F)(-1)^{J'-1/2}$$

$$\times \begin{pmatrix} J & 1 & J' \\ -3/2 & 0 & 3/2 \end{pmatrix} \{(a_v + 1/2(b_v + c_v)) + \delta_{JJ'}\cdot 2/3C_{I_v}z^2\}, \qquad (4)$$

$$\langle {}^2\Pi_{3/2}{}^\pm\ JIF|H|{}^2\Pi_{1/2}{}^\pm\ J'IF\rangle$$

$$= \delta_{JJ'}\cdot z[B_{\Pi_v} \pm (-1)^{J-1/2}(J+1/2)\{1/2q_v + D_{q_v}(J+1/2)^2 + \delta_{q_v}$$

$$\times (J+1/2)^4\}] + G(J, J', I, F)(-1)^{J'+1/2} \begin{pmatrix} J & 1 & J' \\ -3/2 & 1 & 1/2 \end{pmatrix}$$

$$\times \frac{1}{\sqrt{2}} \{b_v \pm \delta_{JJ'}\cdot(-1)^{J-1/2}(J+1/2)C'_{I_v}\}, \qquad (5)$$

where

$$G(J, J', I, F) = [(2J+1)(2J'+1)I(I+1)(2I+1)]^{1/2}(-1)^{J+I+F} \begin{Bmatrix} F & J & I \\ 1 & I & J' \end{Bmatrix}$$

and $z = \sqrt{(J-1/2)(J+3/2)}$. In these expressions the third-order hyperfine constants C_{I_v}, D_{d_v} and C'_{I_v} replace the constants $X_5 + X_7$, X_8 and X_9 defined in the original work [17] similar to recent work of Coxon *et al.* [29] ; A_{Π_v} represents the spin-orbit coupling constant, B_{Π_v} is the rotational constant while the other coupling constants D_{p_v}, δ_{p_v}, D_{q_v} and δ_{q_v} are third- and fourth-order Λ-doubling parameters discussed by Meerts [1]. The centrifugal distortion contributions were included by taking the square of the pure rotational matrix and multiplying the result by $-D_{\Pi_v}$ [21].

It was shown by Meerts [1] that this model discussed is capable of explaining all the available high precision microwave data of the vibrational ground state of OH. In the present study we shall use the model to deduce the molecular constants in the excited vibrational states of OH from the corresponding experimental spectra.

4. EXPERIMENTAL RESULTS

All the transitions observed are electric dipole transitions between hyperfine sublevels in zero electric and magnetic fields from a $(+)$ Kronig symmetry level to a $(-)$ Kronig symmetry level within one rotational state. The spectra of the $v = 1$ and $v = 2$ vibrational states of OH were investigated in the rotational levels $J = 1/2$ and $3/2$ of the ${}^2\Pi_{1/2}$ state and in the rotational levels $J = 3/2$ and $5/2$ of the ${}^2\Pi_{3/2}$ state. The observed transition frequencies are reproduced in table 1. The molecular constants for each vibrational state were adjusted in a least squares fit of the observed spectra to the spectra calculated using the theory outlined in the previous section. However, not all the necessary constants could be determined from only Λ-doubling spectra. We have taken the B_{Π_v} and D_{Π_v} constants from Veseth's [22] analysis of the U.V. spectra measured by Dieke and Crosswhite [23]. Our rotational hamiltonian including distortional effects is equivalent to that of Veseth [22].

Table 1. Observed and calculated hyperfine Λ-doubling transitions of OH in the $v = 1$ and $v = 2$ vibrational states.

Electronic state	J	F_+†	F_-	$v = 1$ Observed frequency (MHz)	$v = 1$ Observed − calculated frequency (kHz)	$v = 2$ Observed frequency (MHz)	$v = 2$ Observed − calculated frequency (kHz)
$^2\Pi_{1/2}$	1/2	1	1	4537·381 (5)	−0·1	4319·938 (5)	−0·2
		0	1	4449·064 (5)	0·1	4233·346 (5)	0·1
		1	0	4553·998 (5)	0·1	4338·543 (6)	0·1
$^2\Pi_{1/2}$	3/2	1	1	7467·323 (8)	3·9	7160·046 (7)	0·7
		2	2	7522·842 (6)	2·5	7212·791 (6)	0·8
		2	1	7454·592 (6)	−2·3	7146·208 (6)	−0·6
		1	2	7535·563 (5)	−1·6	7226·627 (5)	−0·4
$^2\Pi_{3/2}$	3/2	1	1	1536·944 (3)	−2·0	1412·850 (3)	−0·9
		2	2	1538·702 (3)	−0·4	1414·424 (3)	0·9
		2	1	1489·438 (3)	1·2	1371·377 (3)	0·0
		1	2	1586·213 (3)	1·2	1455·896 (3)	0·0
$^2\Pi_{3/2}$	5/2	2	2	5594·246 (5)	1·4	5168·657 (6)	−1·8
		3	3	5598·168 (5)	−0·3	5172·192 (6)	−4·6
		2	3	5583·476 (7)	−1·1	5161·489 (7)	4·4
		3	2	5608·935 (6)	−0·8	5179·376 (8)	5·7

† The subscript $+(-)$ refers to the even (odd) Kronig symmetry.

The OH molecule is described properly in a Hund's case intermediate between (a) and (b) resulting in a strong mixing between the $^2\Pi_{1/2}$ and $^2\Pi_{3/2}$ states determined by the value of the parameter $\lambda_v (\equiv A_{\Pi_v}/B_{\Pi_v})$ and the rotational quantum number. For the $v = 0$ state it was possible [1] to determine an effective value for λ_0 because data from many rotational levels were available. This was not possible for the $v = 1$ and $v = 2$ states as only a limited number of rotational levels have been investigated. The value of λ_v for these states has been fixed in the least squares fit at the values obtained by extrapolation from the $v = 0$ value [1] using the vibrational effects in A_{Π_v} and B_{Π_v} as deduced by Veseth [22].

Because transitions in only a few low J levels have been observed in the $v = 1$ and $v = 2$ states the fourth order Λ-doubling parameters δ_{p_v} and δ_{q_v} were assumed to be zero. All other molecular parameters for $v = 1$ and $v = 2$ could be determined from the observed spectra. The results are given in table 2 together with the values used for B_{Π_v}, D_{Π_v} and λ_v. In this table we list the value for $(b_v + \frac{1}{3}c_v)$ rather than b_v because $(b_v + \frac{1}{3}c_v)$ is proportional to the Fermi contact term [8] and has consequently a more direct physical significance than b_v itself. The differences between the calculated spectra using the best fit constants from table 2 and the observed frequencies are given for both the $v = 1$ and $v = 2$ states in table 1. The differences lie within the quoted experimental accuracy. For comparison the coupling constants for the $v = 0$ state are also reproduced in table 2.

Table 2 Molecular constants of OH in the $v=0$, 1 and 2 vibrational states and the vibrational dependences derived from the present investigation (all values in MHz)

Quantity	$v=0$†	$v=1$†	$v=2$†	O_e	$O^{(1)}$	$O^{(2)}$
B_{Π_v}‡	556100 0	534827 0	513664 0			
D_{Π_v}‡	57 1	56 0	54 9			
λ_v§	−7 4794	−7 7893	−8 1230			
p_v	7052 600 (4)	6734 080 (9)	6411 516 (9)	7210 344	−314 48	−2 02
q_v	−1160 298 (1)	−1107 200 (2)	−1054 166 (2)	−1186 871	53 162	−0 032
D_{p_v}	−0 1122 (6)	−0 112 (1)	−0 123 (1)			
D_{q_v}	0 2206 (1)	0 2080 (2)	0 2027 (3)			
a_v	86 011 (6)	81 976 (9)	78 035 (9)	88 064	−4 129	0 047
$b_v + \frac{1}{2}c_v$	−73 746 (43)	−77 679 (43)	−82 518 (57)	−72 119	−3 03	−0 45
c_v	131 681 (42)	126 346 (42)	121 194 (56)	134 417	−5 518	0 092
d_v	56 632 (8)	53 774 (14)	50 990 (16)	58 089	−2 932	0 037
C_{I_v}	−0 100 (3)	−0 099 (3)	−0 097 (4)			
C'_{I_v}	0 0166 (4)	0 010 (6)	0 008 (6)			
D_{a_v}	−0 0226 (6)	−0 026 (6)	−0 022 (6)			

† The uncertainties in the molecular constants represent one standard deviation, based on a confidence level of the fit of 95 per cent
‡ Parameter held fixed at this value [22]
§ See text

Table 3 Experimental Λ-splittings (ν_Λ) in the $J=3/2$ and $J=5/2$ rotational levels of the $^2\Pi_{3/2}$ state

		$v=0$	$v=1$	$v=2$	$v=3$†	$v=4$†
$J=3/2$	present work	1666 625 (10)	1538 044 (10)	1413 833 (10)	1294 12 (10)	1178 80 (30)
	Clough et al [5]	1666 20 (20)	1537 84 (30)	1413 46 (30)	1293 23 (30)	1176 37 (30)
	Lee et al [6]	1666 5 (1 3)	1537 1 (1 5)	1413 5 (1 5)	1293 1 (1 5)	1176 2 (1 5)
$J=5/2$	present work	6033 282 (30)	5596 533 (30)	5170 723 (30)	4756 75 (30)	4354 59 (90)
	Clough et al [5]	6032 0 (1 5)	5593 3 (1 5)		4751 3 (2 0)	4346 3 (2 0)

† The values from the present investigation for $v=3$ and $v=4$ are obtained using extrapolated values of the Λ-doubling constants from table 2.

5. DISCUSSION

In the Born–Oppenheimer approximation it is assumed that the average value for an arbitrary operator $\mathbf{O}$ of a diatomic molecule in a given electronic state is a function of the internuclear distance (R) only. Expanding $\mathbf{O}$ in a Taylor series about R_e yields

$$\langle \mathbf{O} \rangle = O_e + O_e{}' \, R_e \langle \xi \rangle + \tfrac{1}{2} O_e{}'' \, R_e{}^2 \langle \xi^2 \rangle + \dots \tag{6}$$

The primed quantities are the successive derivatives of the operator $\mathbf{O}$ with respect to R at the equilibrium internuclear distance R_e, $\xi = (R - R_e)/R_e$, and O_e is the expectation value at $R = R_e$. Using Dunham's rotation-vibration theory [24] and restricting the problem to the vibrational dependence equation (6) can be approximated by

$$\langle O \rangle_v \simeq O_e + O^{(1)}(v + \tfrac{1}{2}) + O^{(2)}(v + \tfrac{1}{2})^2. \tag{7}$$

Generally $O^{(2)}$ is much smaller than $O^{(1)}$. Consequently for the discussion of the vibrational effects, that is the dependence of the molecular constants on the internuclear distance, we will consider only O_e and $O^{(1)}$. This restriction is legitimate because, as will be shown later, the theoretical predictions for the vibrational behaviour of both the Λ-doubling and the hyperfine structure constants are only in agreement with the experimental results to first order and are yet far from capable of explaining higher order effects described by $O^{(2)}$. However, for an accurate calculation of the molecular constants relevant, for example for prediction of transitions in higher vibrational states, the effect of $O^{(2)}$ cannot be neglected. In table 2 are listed O_e, $O^{(1)}$ and $O^{(2)}$ determined from a fit of the $v = 0$, 1 and 2 constants to equation (7) for p_v, q_v, a_v, $(b_v + \tfrac{1}{3}c_v)$, c_v and d_v. Only for the first-order Λ-doubling and hyperfine coupling constants is the experimental error small enough to extract significant vibrational effects. It is interesting to note that the relative vibrational effect $(O^{(1)}/O_e)$ is almost the same for both the Λ-doubling and the hyperfine structure constants. Predictions of the frequencies of the hyperfine Λ-doubling transitions in the ${}^2\Pi_{3/2}$, $J = 3/2$, $v = 3$ and $v = 4$ states based on the constants of table 2 have been given in a separate paper [25].

5.1. *The lambda doubling constants p and q*

Previous investigations of the E.P.R. spectrum of vibrationally excited OH in the $J = 3/2$ and $J = 5/2$ rotational levels of the ${}^2\Pi_{3/2}$ state [5, 6] yielded the experimental values for the zero field Λ-doublet splittings in these states. The results, together with the values deduced from the present investigation, are given in table 3. The agreement is reasonable although the E.P.R. values tend to be somewhat lower than the electric resonance data. Rather than expressing the Λ-splitting in p_v and q_v Clough *et al.* [5] deduced this splitting by solving a 3×3 secular matrix involving the lowest electronically excited $A^2\Sigma^+$ state [26, 27] and the $X^2\Pi_{1/2}$ and $X^2\Pi_{3/2}$ states. In this solution the matrix elements $\langle \Pi v | AL_+ + 2BL_+ | \Sigma v \rangle$ and $\langle \Pi v | BL_+ | \Sigma v \rangle$ were considered as fit parameters for each vibrational state and were varied until the best agreement was obtained with the observed splittings. The best fit parameters in this procedure may be considered as effective matrix elements. Since separate values for those matrix elements cannot be obtained from Λ-splitting in the

Table 4. Lambda-doubling constants p_v, p_e and q_v, q_e (all in MHz), the value for $O^{(1)}/O_e$ (dimensionless), and the average internuclear distance R (in Å)

Quantity	$v=0$	$v=1$	$v=2$	$v=3$	$v=4$	O_e‖	$O^{(1)}/O_e$ (per cent)‖
R†	0·9791	0·9984	1·0187	1·0385	1·0583		
p_v Present work	7025·600	6734 080	6411·516	6084·91‡	5762·85‡	7216·36	−4·47
Observed [5]	7045	6895	6775	6625	6476	7115	−2·0
Calculated [9]	7255	6985	6835	6625	6296	7369	−3·1
Calculated § [10]	6922	6673	6455			7034	−3·3
q_v Present work	−1160·298	−1107·200	−1054·166	−1001·20‡	−948·15‡	−1186·78	−4 47
Observed [5]	−1160	−1097	−1034	−974	−908	−1191	−5·3
Calculated [9]	−1172	−1118	−1085	−1046	−995	−1190	−3·6
Calculated § [10]	−1141	−1084	−1035			−1166	−4·5

† Calculated from the rotational constants quoted by Veseth [22] for $v=0$ through $v=2$ and extrapolated from these results to $v=3$ and 4.
‡ Values predicted by extrapolation from results of table 2 and equation (7).
§ Deduced from the *ab initio* calculations for OD [10] by isotopic substitution.
‖ The values for O_e and $O^{(1)}/O_e$ have been determined from a least squares fit of the data for $v=0$ through $v=4$ to a straight line.
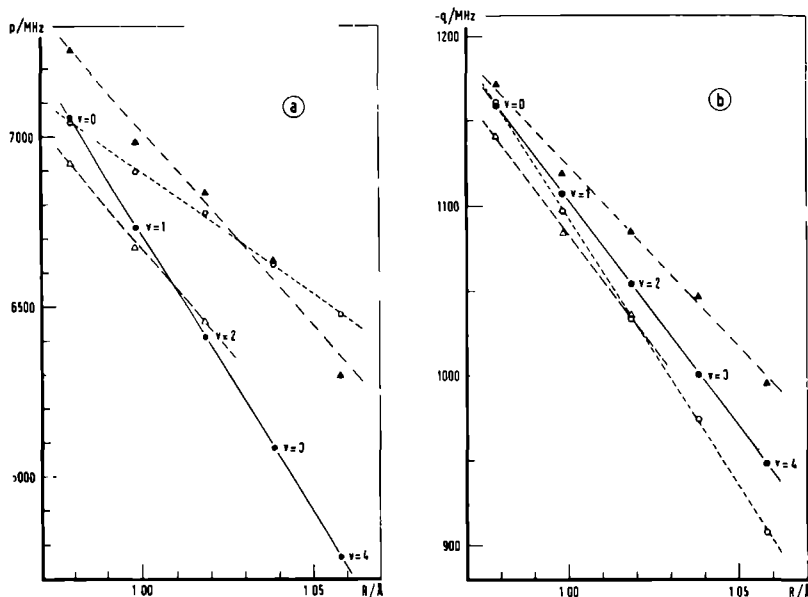
Figure 4. The Λ-doubling constants p (a) and q (b) as a function of the average internuclear distance R with ● for : observed in the present investigation, the values for $v = 3$ and $v = 4$ are obtained by extrapolation from table 2 ; ○ for : results of Clough *et al.* [5] ; ▲ for : *ab initio* calculations of Hinkley *et al.* [9] ; △ for : values obtained by isotopic substitution from the *ab initio* calculations for OD by Coxon and Hammersley [10].

$^2\Pi_{3/2}$ state alone Clough *et al.* assumed the vibrational dependence of $\langle \Pi v | AL_+ + 2BL_+ | \Sigma v \rangle$ to be the same as that of the diagonal matrix element $(A_\Pi + 2B_\Pi)_v$. Only the value of $\langle \Pi v | BL_+ | \Sigma v \rangle$ was then varied in the fit. Values for p_v and q_v can be deduced from these matrix elements and the results [9] are shown in table 4 and also in figure 4 which displays clearly their v-dependence. It is seen from this figure that p_v and q_v deduced from the results of Clough *et al.* deviate systematically from the values obtained in the present investigation. The most likely explanation of these deviations is an unsatisfactory vibrational dependence of $\langle \Pi v | AL_+ + 2BL_+ | \Sigma v \rangle$ adopted by Clough *et al.* [5].

Ab initio calculations of p_v and q_v defined as

$$p_r = 2 \sum_{v'} \frac{\langle \Pi v | AL_+ | \Sigma v' \rangle \langle \Pi v | BL_+ | \Sigma v' \rangle}{E_{\Pi v} - E_{\Sigma v'}}, \qquad (8)$$

$$q_v = 2 \sum_{v'} \frac{|\langle \Pi v | BL_+ | \Sigma v' \rangle|^2}{E_{\Pi v} - E_{\Sigma v'}}, \qquad (9)$$

have been performed by Hinkley *et al.* [9, 28]. In these definitions $(E_{\Pi v} - E_{\Sigma v'})$ is the energy separation between the $X^2\Pi v$ and the $A^2\Sigma^+ v'$ states, the only states taken into account. Hinkley *et al.* assumed that the electronic and nuclear

motions are completely separable and the expressions (8) and (9) reduce to

$$p_v = 2\langle AL_{,}\rangle\langle L_+\rangle \sum_v \frac{\langle v|v'\rangle\langle v|B|v'\rangle}{E_{vv}} \tag{10}$$

and

$$q_v = 2\langle L_+\rangle^2 \sum_v \frac{\langle v|B|v'\rangle^2}{E_{vv}}, \tag{11}$$

where $\langle AL_+\rangle$, $\langle L_+\rangle$ and E_{vv} are abbreviations for $\langle\Pi|AL_+|\Sigma\rangle$, $\langle\Pi|L_+|\Sigma\rangle$ and $(E_{\Pi v} - E_{\Sigma v})$, respectively   The off-diagonal electronic matrix elements $\langle AL_+\rangle$ and $\langle L_+\rangle$ were calculated at R_e only and all two-centre integrals were neglected Restricted Hartree–Fock (RHF) orbitals computed for the electronic ground state were employed in constructing the wavefunctions for the $A^2\Sigma^+$ state (invariant orbital approximation)   The Franck–Condon factors $\langle v|v'\rangle$, the expectation values of $\langle v|B|v'\rangle$ and E_{vv} were computed using numerical vibrational wavefunctions obtained from Rydberg–Klein–Rees (RKR) potential curves   The calculated values for p_v and q_v are given in table 4 and plotted in figure 4 assuming that the electronic matrix elements were independent of R

Coxon and Hammersley [10] performed more accurate *ab initio* calculations for p_v and q_v for the OD radical defined as (see equations (8) and (9))

$$p_v = 2\sum_v \frac{\langle AL_+\rangle_{R_{vv}}\langle v|v'\rangle\langle L_+\rangle_{R_{eff}}\langle v|B|v'\rangle}{E_{vv}} \tag{12}$$

and

$$q_v = 2\sum_v \frac{\langle L_+\rangle_{R_{eff}}^2\langle v|B|v'\rangle^2}{E_{vv}} \tag{13}$$

Herein $\langle L_+\rangle_{R_{eff}}$ and $\langle AL_+\rangle_{R_{vv}}$ is the value of $\langle L_+\rangle$ at an effective internuclear distance $(R_{eff} = \langle v|1/R|v'\rangle/\langle v|1/R^2|v'\rangle)$ and of $\langle AL_+\rangle$ at the R-centroid $(\bar{R}_{vv})$, respectively, for each vibrational state v' Using a different set of RHF orbitals for each electronic state the off-diagonal matrix elements $\langle L_+\rangle$ and $\langle AL_+\rangle$ were calculated over a much larger range of internuclear distances than the region $R_{v=0}$ to $R_{v=4}$ to allow for an R-dependence   Two-centre integrals were taken into account for $\langle L_+\rangle$ but not for the spin–orbit integrals $\langle AL_+\rangle$ The former quantity was found to be nearly independent of R, while $\langle AL_+\rangle$ varied considerably and showed an almost linear dependence on R All expectation values over vibrational wavefunctions were obtained from RKR curves

To profit from the higher accuracy of the *ab initio* calculations by Coxon and Hammersley, their results for OD were converted to OH by isotopic substitution [8] and are shown in table 4 and figure 4   Only a small error in the absolute magnitudes is introduced in this way   However, the most interesting feature, the vibrational dependence is practically unaffected

From table 4 and figure 4 (*b*) it follows that the *ab initio* results of Coxon and Hammersley for q_v are somewhat lower than those of Hinkley *et al*   The dependence of q_v on the internuclear distance as found by Coxon and Hammersley agrees very well with the results of the present investigation (figure 4 (*b*))   This is most probably a consequence of the fact that Coxon and Hammersley allowed for the R-dependence and included two-centre integrals in their calculations of $\langle L_+\rangle$

It is seen from table 4 and figure 4 (*a*) that the *ab initio* results of Hinkley *et al.* for p_v are also somewhat too high. Coxon and Hammersley concluded that the invariant orbital approximation applied by Hinkley *et al.* is responsible for the value of p_v being too high, and also that of q_v. The *ab initio* calculations of both Hinkley *et al.* [9] and of Coxon and Hammersley [10] show a weaker *R*-dependence than observed experimentally. However, the vibrational dependence of p_v found by Coxon and Hammersley is in slightly better agreement with the experimental results than that found by Hinkley *et al.* as expected from the arguments given for q_v. The remaining difference between the *ab initio* calculations of Coxon and Hammersley and the experimentally observed *R*-dependence in p_r might be due to the neglect of two-centre spin-orbit integrals in the evaluation of $\langle AL_1 \rangle$. A similar argument was used by Coxon and Hammersley to explain discrepancy between their *ab initio* values for A_v of OD and the experimental results [10].

The overall agreement between the *ab initio* calculations of p_v and q_v and the experiment is satisfactory indicating that extended *ab initio* calculations can be used to predict Λ-splittings in various vibrational states with an accuracy of about 1 per cent.

5.2. *The hyperfine structure constants*

The magnetic hyperfine constants a_v, $(b_v + \frac{1}{3}c_v)$, c_v and d_v are proportional to $\langle 1/r^3 \rangle_v$, $\langle \psi^2(0) \rangle_v$, $\langle (3 \cos^2 \chi - 1)/r^3 \rangle_v$ and $\langle \sin^2 \chi/r^3 \rangle_v$, respectively [8]. The last four quantities are related to the properties of the unpaired π-electron. Their values deduced from the results of table 2 for the different vibrational states are given in table 5 together with the value at R_e and the relative vibrational changes $(O^{(1)}/O_e)$.

Table 5. Hyperfine structure constants (in units of 10^{24} cm^{-3}, except $O^{(1)}/O_e$ which is dimensionless).

Quantity		$v = 0$†	$v = 1$†	$v = 2$†	O_e	$O^{(1)}/O_e$ (per cent)
$\langle 1/r^3 \rangle_v$	obs	1·089	1·038	0·988	1·115	−4·7
	calc‡	0·993	0·945	0·896	1·015	−4·4
$\langle (3 \cos^2 \chi - 1)/r^3 \rangle_v$	obs	1·112	1·067	1·023	1·135	−4·1
	calc‡	1·022	0·990	0·957	1·038	−2·9
$\langle \sin^2 \chi/r^3 \rangle_v$	obs	0·478	0·454	0·431	0·490	−5·0
	calc‡	0·320	0·299	0·278	0·330	−6·0
$\langle \Psi^2(0) \rangle_v$	obs	−0·111	−0·117	−0·125	−0·109	+4·2
	calc‡	−0·105	−0·109	−0·113	−0·103	+3·7

† The corresponding internuclear distances are given in table 4.
‡ Kayama [11].

Kayama [11] has performed *ab initio* LCAO MO CI calculations in which he determined the magnetic hyperfine structure constants at two different internuclear distances R_e and $1 \cdot 0584$ Å ($\equiv R_1$). Table 5 summarizes the predicted values for the $v = 0$, 1 and 2 states obtained by interpolation between R_e and R_1 using the relation

$$O(R) = O(R_e) + (R - R_e) \frac{O(R_1) - O(R_e)}{R_1 - R_e}, \tag{14}$$

where $O(R_e) \equiv O_e$, while R in each vibrational state has been deduced from the corresponding rotational constants $B_{\Pi v}$. The calculated values for $\langle 1/r^3 \rangle_U$, $\langle (3 \cos^2 \chi - 1)/r^3 \rangle_U$ and $\langle \psi^2(0) \rangle_U$ at the equilibrium distance agree quite well with the experimental values. The calculated value of $\langle \sin^2 \chi/r^3 \rangle_U$ deviates, however, considerably from the experimental results for all vibrational states and for the equilibrium distance. The reason of this disagreement is not clear. The rather strong variation with the internuclear distance of these four quantities predicted by Kayama's calculations is very well confirmed experimentally. This can be clearly seen from the $(O^{(1)}/O_e)$ column of table 5.

In summary the present measurements show a gratifying agreement with the vibrational dependence of the Λ-doubling and hyperfine constants of OH predicted by the *ab initio* calculations.

REFERENCES

[1] MEERTS, W. L., 1977, *Chem. Phys. Lett.*, **46**, 24.
[2] DESTOMBES, J. L., MARLIERE, C., and ROHART, F., 1977, *J. molec. Spectrosc.*, **67**, 93.
[3] BROWN, J. M., KAISE, M., KERR, C. M. L., and MILTON, D. J., 1978, *Molec. Phys.*, **36**, 553.
[4] CHURG, A., and LEVY, D. H., 1970, *Astrophys. J.*, **162**, L161.
[5] CLOUGH, P. N., CURRAN, A. H., and THRUSH, B. A., 1971, *Proc. R. Soc.* A, **323**, 541.
[6] LEE, K. P., TAM, W. G., LAROUCHE, R., and WOONTON, G. A., 1971, *Can. J. Phys.*, **49**, 2207.
[7] LEE, K. P., and TAM, W. G., 1974, *Chem. Phys.*, **4**, 434.
[8] MEERTS, W. L., and DYMANUS, A., 1975, *Can. J. Phys.*, **53**, 2123.
[9] HINKLEY, R. K., WALKER, T. E. H., and RICHARDS, W. G., 1973, *Proc. R. Soc.* A, **331**, 553.
[10] COXON, J. A., and HAMMERSLEY, R. E., 1975, *J. molec. Spectrosc.*, **58**, 29.
[11] KAYAMA, K., 1963, *J. chem. Phys.*, **39**, 1507.
[12] DE LEEUW, F. H., and DYMANUS, A., 1973, *J. molec. Spectrosc.*, **48**, 427.
[13] MEERTS, W. L., STOLTE, S., and DYMANUS, A., 1977, *Chem. Phys.*, **19**, 467.
[14] DEL GRECO, F. P., and KAUFMAN, F., 1962, *Discuss. Faraday Soc.*, **33**, 128.
[15] TER MEULEN, J. J., MEERTS, W. L., VAN MIERLO, G. W. M., and DYMANUS, A., 1976, *Phys. Rev. Lett.*, **36**, 1031.
[16] MEERTS, W. L., 1976, *Chem. Phys.*, **14**, 421.
[17] MEERTS, W. L., and DYMANUS, A., 1972, *J. molec. Spectrosc.*, **44**, 320.
[18] FREED, K. F., 1966, *J. chem. Phys.*, **45**, 4214.
[19] MULLIKEN, R. S., and CHRISTY, A., 1931, *Phys. Rev.*, **38**, 87.
[20] FROSCH, R. A., and FOLEY, M. M., 1952, *Phys. Rev.*, **88**, 1337.
[21] ALMY, G. M., and HORSFALL, R. B., 1937, *Phys. Rev.*, **51**, 491.
[22] VESETH, L., 1971, *J. molec. Spectrosc.*, **38**, 228.

[23] DIEKE, G. H., and CROSSWHITE, H. M., 1962, *J. quant. Spectrosc. Radiat. Transfer*, **2**, 97.

[24] TOWNES, C. H., and SCHAWLOW, A. L., 1955, *Microwave Spectroscopy* (McGraw-Hill).

[25] BEKOOY, J. P., MEERTS, W. L., and DYMANUS, A., 1978, *Astrophys. J.*, **224**, L77.

[26] DOUSMANIS, G. C., SANDERS, T. M., JR., and TOWNES, C. H., 1955, *Phys. Rev.*, **100**, 1735.

[27] RADFORD, H. E., 1961, *Phys. Rev.*, **122**, 114.

[28] HINKLEY, R. K., HALL, J. A., WALKER, T. E. H., and RICHARDS, W. G., 1972, *J. Phys.* B, **5**, 204.

[29] COXON, J. A., SASTRY, K. V. L. N., AUSTIN, J. A., and LEVY, D. H., 1979, *Can. J. Phys.* (in the press). It should be noted that the definitions for d and C'_{I_v} in the present paper and in the here cited reference deviate slightly from those used by Brown *et al.* [3].

THE HIGH-RESOLUTION HYPERFINE LAMBDA-DOUBLING SPECTRUM OF VIBRATIONALLY EXCITED OH

J. P. BEKOOY, W. L. MEERTS, AND A. DYMANUS

Fysisch Laboratorium, Katholieke Universiteit, Nijmegen, The Netherlands

ABSTRACT

The hyperfine Λ-doubling transitions of OH originating in the $J = 3$ rotational, the $v = 1$ and $v = 2$ vibrational, and the $X\ ^2\Pi_{3/2}$ electronic ground state have been measured using the molecular beam electric resonance technique. Predictions for the frequencies of the transitions in the $X\ ^2\Pi_{3/2}$, $J = 3/2$, $v = 3$ and $v = 4$ states are given.

Subject heading: hyperfine structure — laboratory spectra

Astronomical observations of radio spectra from excited vibrational states of OH may provide important information about the near-infrared pumping model as proposed by Litvak (1969). It is expected that emission of interstellar OH in these states is very weak, and a successful observation would depend critically on laboratory measurements of the rest frequencies of the transitions in question. The magnetic resonance spectroscopy has been used by Churg and Levy (1970), by Clough, Curran, and Thrush (1971), and by Lee *et al.* (1971; Lee and Tam 1974) to investigate the $^2\Pi_{3/2}$, $J = 3/2$ state of vibrationally excited OH up to $v = 9$. The zero-field frequencies of lambda-doubling transitions in the $^2\Pi_{3/2}$, $J = 3/2$ level could be predicted from magnetic resonance data by Churg and Levy (1970) for the $v = 1$ state (uncertainty 0.1 MHz), and those for higher vibrational states can be deduced from the results of Clough, Curran, and Thrush (1971), Lee *et al.* (1971), and Lee and Tam (1974). Since these magnetic resonance data were obtained from the $J = 3/2$ and $J = 5/2$ (for $v \le 4$) levels in the $^2\Pi_{1/2}$ state only, the possibility of deducing the Λ-doubling and the hyperfine-structure constants in the vibrationally excited states is seriously limited. It was felt that the predictions may be subject to a much larger uncertainty than claimed. A direct measurement of the zero-field transitions was considered well justified. The molecular-beam electric resonance spectrometer has been used to investigate the $v = 1$ and $v = 2$ vibrational states of OH. The electric dipole allowed transitions originating in the $^2\Pi_{3/2}$, $J = 3/2$ state for both vibrational states are reported here. These are the first direct measurements of the hyperfine Λ-doubling transitions in excited vibrational states of OH.

The OH radicals have been produced by the reaction $H + NO_3 \rightarrow OH + NO$. Hydrogen atoms were generated by passing water vapor through a microwave discharge at 2.45 GHz. The experimental setup previously used to investigate the ground vibrational state of OH has been discussed in detail elsewhere (Meerts and Dymanus 1975). The observed intensity ratio between the $v = 1$ and $v = 0$ spectra and between the

$v = 2$ and $v = 0$ spectra was 6% and 2.5%, respectively. The maximum intensities of the transitions from the excited vibrational states were obtained when the beam-forming orifice was in the reaction zone. By moving it a few millimeters downstream from the reaction zone, the intensities of the $v = 1$ and $v = 2$ spectra were reduced considerably, while those of the $v = 0$ spectra were almost unaffected. This suggests the occurrence of strong vibrational relaxation induced by collisions. Since the signal-to-noise ratio of the $v = 1$ and $v = 2$ spectra was very low, signal-averaging techniques had to be used. Typical integration times for the spectra from the $v = 1$ and $v = 2$ states were 0.5 and 1.5 hours, respectively. A single scan took 50 s. The signal-to-noise ratio after the averaging process varied between 3 and 5.

The observed transition frequencies are given in Table 1. The experimental uncertainties were mainly determined by the signal-to-noise ratio. A full spectroscopic discussion including also observed transitions in the $^2\Pi_{3/2}$, $J = 5/2$ and the $^2\Pi_{1/2}$, $J = 1/2$ and $3/2$ states is given in a separate paper (Meerts, Bekooy, and Dymanus 1978). In that paper vibrational effects in the Λ-doubling and hyperfine structure constants are discussed. The theoretical framework used has been described (for the $v = 0$ state) by Meerts (1977). In this

TABLE 1

FREQUENCIES OF THE OBSERVED HYPERFINE Λ-DOUBLING TRANSITIONS OF OH IN THE $^2\Pi_{3/2}$, $J = 3/2$, $v = 1$ AND $v = 2$ STATES

F_+[*]	F_-	OBSERVED FREQUENCY (MHz)	
		$v = 1$	$v = 2$
1	1	1536 944(3)	1412 850(3)
2	2	1538 702(3)	1414 424(3)
2	1	1489 438(3)	1371 377(3)
1	2	1586 213(3)	1455 896(3)

[*] The subscript $+$ $(-)$ refers to the even (odd) Kronig symmetry (Meerts and Dymanus 1975).

framework, by incorporating up to third-order perturbation contributions in fine and hyperfine structure and the major part of the fourth-order Λ-splitting, a prediction could be made for transitions in higher vibrational states by extrapolation of the molecular constants of the $v = 0, 1$, and 2 states. The results are presented in Table 2 for the $v = 3$ and $v = 4$ states. In this extrapolation the vibrational dependence of the molecular constants is approximated by an expansion up to second order in v. The expansion is found to converge very rapidly; the second-order term contributes an order of magnitude less for the $v = 3$ and $v = 4$ states than the first-order term. For the transition frequencies in the $v = 3$ and in the $v = 4$ state this yields an estimated reliability of 100 kHz and 300 kHz, respectively.

The technical assistance of Mr. F. A. van Rijn is gratefully acknowledged.

TABLE 2

PREDICTED FREQUENCIES OF THE HYPERFINE Λ-DOUBLING
TRANSITIONS OF THE $^2\pi_{3/2}, J = 3/2, v = 3$
AND $v = 4$ STATES OF OH

		PREDICTED FREQUENCY (MHz)	
F_+	F_-	$v = 3$*	$v = 4$*
1	1	1293 245	1178 024
2	2	1294 650	1179 269
2	1	1258 169	1148 906
1	2	1329 726	1208 387

* Accuracy is estimated to be 100 kHz and 300 kHz for the frequencies in the $v = 3$ and $v = 4$ states, respectively

REFERENCES

Churg, A., and Levy, D. H. 1970, *Ap. J. (Letters)*, **162**, L161.
Clough, P. N., Curran, A H., and Thrush, B. A. 1971, *Proc Roy. Soc. London, A*, **323**, 541.
Lee, K. P., and Tam, W G 1974, *Chem. Phys.*, **4**, 434.
Lee, K P , Tam, W. G., Larouche, R , and Woonton, G. A. 1971, *Canadian J. Phys*, **49**, 2207.

Litvak, M. M. 1969, *Ap J* , **156**, 471.
Meerts, W. L 1977, *Chem. Phys Letters*, **46**, 24.
Meerts, W. L , Bekooy, J. P., and Dymanus, A. 1978, *Molec. Phys.*, in press.
Meerts, W L , and Dymanus, A. 1975, *Canadian J. Phys.*, **53**, 2123.

J. P. BEKOOY, A. DYMANUS, and W. L. MEERTS: Fysisch Laboratorium, Katholieke Universiteit, Nijmegen, The Netherlands

47

Rotational spectrum and structure of KCN

T Törring

Freie Universitat Berlin, Berlin Germany

J P Bekooy and W Leo Meerts

Fysisch Laboratorium Katholieke Universiteit Nijmegen The Netherlands

J Hoeft

Freie Universitat Berlin Berlin Germany

E Tiemann

Universitat Hannover Hannover Germany

A Dymanus

Fysisch Laboratorium Katholieke Universiteit Nijmegen The Netherlands
(Received 27 June 1980· accepted 5 August 1980)

The spectrum of gaseous KCN was measured in the frequency range between 2 and 39 GHz by microwave absorption and by molecular beam electric resonance spectroscopy Combination of the new results with earlier microwave data of KCN in the 100 GHz range made it possible to assign 64 transitions to the ground vibrational state and to fit them to the asymmetric rotor model The three rotational constants, the five quartic distortion constants, and two sextic distortion coefficients could be determined Assuming a CN distance of 1 162(10) A we find $r_{\kappa C} = 2\ 6(1)$ A and $\angle$ KCN = 76 °(10) The molecules thus have a nonlinear T shaped structure The inertial defect gives an estimated value of the lowest vibrational frequency of KCN $\omega_2 = 157$ cm^{-1} which is in reasonable agreement with $\omega_2 = 139$ cm^{-1} from matrix isolation studies

I. INTRODUCTION

From all group I cyanides only the structure of hydrogen cyanide is well established by microwave spectroscopy. The molecule is linear and the hydrogen may be attached either to the C atom (cyanide)[1] or to the N atom (isocyanide) [2] The alkali cyanides are generally assumed to be linear, too, although experimental and theoretical evidence is scarce and contradictory. Therefore in this paper, unless explicitly indicated, these molecules are denoted by LiCN, etc., whatever the structure may be.

Bak et al.[3] performed a detailed set of quantum mechanical calculations for LiCN. They showed that the equilibrium configuration is the linear isocyanide, with only a very small energy difference of about 0 4 eV between Li–NC and Li–CN. Clementi et al.[4] extended these calculations by mapping the energy surface for the Li⁺ ion around the CN⁻ anion They found that the lowest energy path from Li–NC to Li–CN will permit the Li⁺ to "orbit" the CN⁻ upon excitation of 0.3–0.4 eV In this situation there is no preferred structural formula and the bond has been called "polytopic " However, the barrier of 0 3–0.4 eV is high enough to allow many excited vibrational states below the barrier Another way of interpreting these results is to say that the linear Li–NC undergoes large amplitude bending vibrations In the limit of highly excited states this motion changes to an orbiting of the Li⁺ around CN⁻. Unfortunately, no calculations for the heavier alkali cyanides have been performed It may be assumed that the barrier will be lower than in LiCN.[5]

Vibrational frequencies of the alkali cyanides have been measured by Ismail et al.[6] using the matrix-isolation technique. Their results are listed in Table I.

From isotopic effects the isocyanide structure was confirmed for LiCN, but the cyanide structure was preferred for NaCN and KCN. A linear equilibrium configuration was assumed in all cases. The large increase of the bending vibrational frequency from LiCN to NaCN seems to contradict this interpretation and to indicate a more drastic structural change The matrix results are in complete disagreement with earlier infrared absorption work on KCN vapor by Leroi and Klemperer.[7] They studied the region above 200 cm^{-1} and reported two vibrational frequencies. One of them ($\omega = 2158$ cm^{-1}) clearly belongs to the C–N stretching mode, the other one ($\omega = 207$ cm^{-1}) does not agree with any of the values reported by Ismail et al.[6] The reason for this discrepancy is not clear.

The microwave rotational spectrum of KCN was measured by Kuijpers et al.[8] Altogether 165 lines were found in the frequency region between 85 and 107 GHz. No assignment of vibrational quantum numbers was possible from intensity ratios. This was due to the low signal to noise ratio of the spectrum and the small intensity variations expected from excitation of low frequency vibrations at a temperature of 870 K From a number of transitions effective rotational constants

TABLE 1. Vibrational frequencies in cm^{-1} for LiCN, NaCN, and KCN from matrix-isolation studies (Ref 6)

	LICN	NaCN	KCN
ω_1	681	368	288
ω_2	119	168	139
ω_3	2080	2047	2050

B_{eff} and distortion constants D_{eff} were tentatively fitted. The obtained constants showed clearly that the observed spectrum was inconsistent with that of a linear molecule. Assuming reasonable bond distances rotational constants $B = 3.0(5)$ and 3 4(5) GHz are expected for K–CN or K–NC, respectively. The discrepancy with the experimental value of $B_{eff} = 4.70(15)$ GHz is much larger than any possible errors in the bond length extrapolations. It was concluded that the structure was incompatible with that of a linear or slightly bent molecule.

In the polytopic model the CN^- behaves more or less like one ion (pseudo halogen). The rotational constant is therefore related to the atomic masses and to the average distance $\bar{r}$ between K^+ and the center of mass of the CN^- group. From $B_{eff} = 4.7$ GHz a value for $\bar{r} = 2.63$ Å was found which compares very well to the internuclear distance of KCl: $r_e = 2.67$ Å. Polytopic bonding was therefore assumed to give the most satisfactory explanation for the overall pattern of the observed spectrum in Ref. 8. In a more refined model one has to solve the rotation–vibration Hamiltonian that allows for large amplitude motions.[9–11] In such a model the KCN molecule is assumed to be composed of a diatomic rigid core (CN^-) and an ion (K^+) which can move in an angle dependent potential around this core. For a reasonably high potential barrier (> 500 cm^{-1}) the average position of the K^+ in the lowest vibrational state of the molecule will be near the minimum of that potential. Some preliminary calculations performed in Nijmegen on KCN using the model discussed by Zhilinskii *et al.*[11] with a proper choice for the angle dependent potential ($V \cos^2\theta$, θ being the angle between K^+ and the CN axis) yielded values for the effective rotational constant close to the experimental value Unfortunately, it was not possible to test if this model could explain the details of the 100 GHz spectrum without additional information. Assignment of lines was prevented not only by the presence of many lines from excited vibrational states but also by the high J levels involved and the large centrifugal effects expected for these lines.

Two independent studies were undertaken in order to obtain more experimental data on the KCN molecule. In Berlin the microwave absorption technique was used to study the lower rotational transitions around 28 and 38 GHz. The molecular-beam electric-resonance (MBER) spectrometer in Nijmegen was equipped with a supersonic source. This method reduced the internal rotational and vibrational temperatures of the KCN molecules in the beam drastically, thus simplifying the interpretation of the spectrum. The microwave and radiofrequency transitions below 31 GHz were investigated. The two groups were successful in observing many transitions and unraveled the spectrum from the ground vibrational state. The new and old[8] microwave data were combined with the MBER spectra and the transitions for the ground vibrational state could be selected. The identified ground state spectrum was unambiguously assigned to that of a near prolate asymmetric top molecule.

The derived rotational constants and a reasonable assumption for the CN distance lead to a T-shape structure for the KCN molecule, where the connecting line between the K nucleus and the center of mass of the C and N nuclei is approximately perpendicular to the CN axis.

II. MICROWAVE ABSORPTION EXPERIMENTS

Observation of low J transitions by microwave absorption was seriously impeded by the outstandingly low intensity of the spectrum. Even in the 100 GHz region most lines were near to the limit of sensitivity of the spectrometer. Fortunately, the reduced absorption coefficients at lower frequencies could be partly compensated by using larger absorption cells and by improving performance of detectors at lower frequencies A conventional Stark effect spectrometer was used in the present experiment. Several constructions of high temperature absorption cells have been given in Ref. 12. A cell of type III was used with an effective absorption length of about 80 cm at a temperature of 800–900 K. For intensity reasons our efforts were concentrated on the observation of $J = 4 \to 3$ and $J = 3 \to 2$ transitions. In the expected frequency range from 36 to 39 and from 27 to 29 GHz a total number of 109 lines was found. One line from a $J = 2 \to 1$ transition was detected at 19 GHz. The overall pattern of these transitions is very similar to the spectrum in the 100 GHz region The large number of observed transitions shows that many excited vibrational states contribute to the spectrum.

The measurements confirmed the average effective rotational constant of $B_{eff} = 4\ 7$ GHz derived from the measurements around 100 GHz.[8] Due to the poor signal to noise ratio it was not possible to obtain additional information from Stark effect measurements or to assign vibrational quantum numbers from intensity ratios. It was therefore necessary to use an estimated structural model as a guideline for the analysis of the spectrum. The general pattern of the spectrum with well defined groups of lines for the different rotational transitions clearly indicated that the asymmetry of the molecular rotor could only be very small Moreover the structure must be consistent with the measured B_{eff} and with reasonable bond distances. These conditions forced us to start our analysis based on a quite unusual T-shaped structure for the KCN molecule. The K nucleus was assumed to be located between the C and N nuclei at a distance of approximately 2.55 Å perpendicular to the C–N internuclear axis.

For this configuration the largest dipole moment component is expected to be μ_a, parallel to the a-axis of the molecule. The strongest rotational transitions of a slightly asymmetric top will then be a-type transitions with selection rules:

$$\Delta J = 1 ; \quad \Delta K_{-1} = 0 ; \quad \Delta(J - K_1) = 0 . \tag{1}$$

The frequencies of these transitions can be written as

$$\nu = 2B_{eff}(J+1) - 4D_{eff}(J+1)^3 , \tag{2}$$

where B_{eff} and D_{eff} depend only on K_{-1} and $(J - K_1)$ and on the vibrational state of the molecule.[13] Using this expression we were able to select series of lines from the spectrum with fixed quantum numbers v, K_{-1}, and $(J$

$-K_1$). The previous microwave data were included in that analysis. If only series including the transition $J = 3 \rightarrow 2$ are considered, $K_{-1} \lesssim 2$ This made it possible to determine the quantum numbers K_1 and $(J - K_1)$ from the characteristic variation of B_{eff} and D_{eff}, and a clear distinction could be made between series belonging to different vibrational states.

The transitions were then fitted to an asymmetric rotor spectrum using a computer program written by Kirchhoff.[14] Large centrifugal distortion effects were to be expected for lines with higher K_{-1} values. These transitions were therefore calculated step by step and after identification from the spectrum included in the calculation. In the last step 40 microwave transitions with K_{-1} quantum numbers up to 10 were fitted all well within the experimental uncertainties. All assigned lines were a-type transitions with the selection rules given in (1). No strict conclusion was possible about which vibrational state had been assigned. However, the overall intensity and the position of the fitted lines gave a very strong indication that these transitions belong to the ground vibrational state

III MOLECULAR BEAM ELECTRIC RESONANCE EXPERIMENTS

Several attempts both at Nijmegen[15] and elsewhere (see, e.g., Ref. 16) have been undertaken to observe and analyze MBER spectra of KCN using MBER spectrometers equipped with effusive sources. Weak, many MHz's wide features were observed if high rf powers were applied resulting in saturated and power broadened transitions. Reduction of the rf powers lead to unobservable weak signals. In order to obtain a drastic decrease of the internal temperatures of the KCN molecules we decided to use the seeded beam technique. With this technique a large gain in sensitivity for low J transitions has been realized thanks to rotational cooling ($T_r \sim 40$ K) and improved focusing of the seeded beam with its reduced velocity spread and angular divergence.

The electric resonance spectrometer is basically the one described by van Wachem[17] with a modification on the source chamber to handle the large gas load[18] necessary for the production of the seeded beam. The KCN beam intensity was monitored by a surface ionization detector. An additional enhancement of the signal to noise ratio by a factor of 10 of the KCN spectral lines was obtained by increasing the detection area of the detector. The effective aperture of the detector was 3×3 mm.

The source used in the present experiment (Fig 1) is essentially identical to the design of Glaser[19] The stainless steel oven consists of two chambers each indirectly heated by tantalum filaments The carrier gas enters the supply chamber and the mixture is expanded from the nozzle chamber. The temperature is monitored by two thermocouples located at the bottom of the supply chamber and at the nozzle chamber. The two temperatures can be varied to a large degree independently. The supply chamber was typically held at 1150 K corresponding to an estimated vapor pressure of KCN of about 10 mbar. The temperature of the noz-

zle chamber was usually 100 K higher. A skimmer (diameter 2.5 mm) at a distance of 25 mm from the nozzle was slightly heated by radiation from the source. No clogging occurred during a run of a full load of salt lasting for about two weeks.

We expanded through a 150 μm nozzle 1% to 2% KCN diluted in argon. The total backing pressure was 0.6 bar. A measurement of the velocity distribution[18] of a pure argon beam under identical conditions yielded a translational temperature $T_t = 30(5)$ K. From the intensities of a large number of $\Delta J = 0$ transitions in the KCN spectrum we estimated the rotational temperature of the KCN molecules in the beam $T_r = 40(10)$ K, which is within the error equal to T_t of the carrier gas argon. We conclude that the rotational relaxation of the KCN molecules in the beam is complete.

Much less can be said about the vibrational relaxation of the KCN molecules in the beam, since until now only a few transitions of excited vibrational states have tentatively been identified. However, since almost all of the strong and most of the weaker MBER transitions in the region between 8 and 26 GHz have been identified as belonging to the ground vibrational state it is felt that the vibrational relaxation of the low frequency vibrational modes is quite strong.

A first attempt was made to observe and analyze the rf spectrum (0–500 MHz) Although many strong well-resolved lines were observed in this region, we were not able to unravel the spectrum at that time From the previous microwave experiments[8] the $J = 1 \rightarrow 0$ transition was expected at 9.4 GHz. Searches have been made first between 9 and 10 GHz and subsequently over the complete frequency region between 1 and 26 GHz. To make scans over such wide frequency ranges feasible within a reasonable sweep time the instrumental linewidth (~20 kHz) was artificially broadened by frequency modulating the radiation sources [backward wave oscillators (BWO) or klystrons] with white noise.[20] In this way
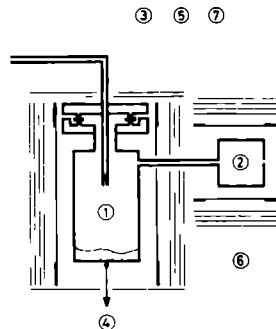
③ ⑤ ⑦

FIG 1 The supersonic beam source 1. Supply chamber, 2 Nozzle chamber, 3. Gas line, 4 Thermocouple, 5 Ta–Ni–Ta gasket, 6 Filaments, 7 Radiation shields

we could scan over a 1 GHz range in 45 min without loss of sensitivity of the spectrometer. Once a line was located roughly from a wide scan detailed measurements were made with the BWO or klystron phase locked to a stable frequency derived from a frequency synthesizer Many strong transitions were observed with this method. The typical signal to noise ratio was 40 at RC = 1 s. However, the density of transitions above 8 GHz was much lower than in the rf region.

When we started the analysis of the MBER spectrum no assumption on the structure of the KCN molecule was made. The initial identification of the MBER spectrum was based on a pattern recognition of two series of transitions that clearly showed a regularity in the frequency sequence and in their optimum voltages for the state selection fields. The two groups could be identified as transitions between K-doublet splittings in a slightly asymmetric prolate top molecule. In first order approximation these splittings are given[13] for $K_{-1} = 1$ and 2 by $\frac{1}{2}(B - C)J(J + 1)$ and $(B - C)^2(J - 1)J(J + 1)(J + 2)/(16(2A - B - C))$, respectively. After the initial J assignment of the K doublets all transitions in the observed region were predicted from an exact computer calculation of the MBER spectrum combined in a step by step calculation of the 100 GHz microwave data. The rotational transitions $1_{01} - 0_{00}$, $2_{02} - 1_{01}$, $3_{03} - 2_{02}$, $3_{13} - 4_{04}$, $7_{07} - 6_{16}$ and $16_{1,15} - 15_{2,14}$ could then also be identified, the first three and the K-doublet transitions are all a type, i.e., associated with μ_a, while the latter three transitions are b type In order to establish the identification of the above given b-type transitions and to increase the accuracy of some of the distortion constants we measured another five high J b-type transitions $12_{2,11} - 13_{1,12}$, $17_{1,16} - 16_{2,15}$, $22_{3,20} - 23_{2,21}$, $23_{3,21} - 24_{2,22}$, and $27_{3,25} - 26_{3,24}$. A total of 26 MBER transitions has been observed.

IV. FINAL FIT AND STRUCTURE OF KCN

The complementary information obtained from microwave absorption and MBER experiments has led to identical assignments. The observed transition frequencies from Table II were fitted to an asymmetric rotor model.[24] The best fit values for the determinable molecular parameters[21,28] are given in Table III. The a-type transitions determine mainly the B and C rotational constants, whereas the rotational constant A can accurately be obtained from the b-type lines. Two (H_{JK}, H_{KJ}) sextic distortion coefficients could be fitted from the spectra; the remaining five (H_J, H_K, h_J, h_K, h_{JK}) were set to zero. As can be seen from Table II the agreement between the observed and calculated transition frequencies is excellent. The planarity constraints for the τ's[13,14] were not imposed in the fit of the data which resulted in a rather large τ-planarity defect[14] for KCN: $\Delta\tau = -0.86(2)$ kHz. The derived constants assuming planarity are given in Table IV. Due to the large value of $\Delta\tau$ a rather large difference in the calculated centrifugal distortion constants τ_{aabb} and τ_{abab} is obtained if they are derived from $\{\tau_1, \tau_2\}$ or $\{\tau_1, \tau'_{cccc}\}$. The large value of the τ-planarity defect might be caused by the expected nonrigidity of the KCN molecule.

Although the quality of the fit of the data is very good, a precise determination of the structure is difficult. For a triatomic molecule spectroscopic information from at least two different isotopic species is necessary for a unique determination of the three structural parameters However, very reliable information on the CN distance is available from many molecules. Experimental values for HCN,[1] HNC,[2] and all the cyanogen halides[13] as well as the calculated values for LiNC and LiCN are all within $r_{CN} - 1$ $15 + 0$ 02 A The spread for the experimental values alone is even less r_{CN} (expt) $= 1.162 + 0.010$ A At the moment we have no reason to expect large deviations from these values for KCN.

A computer program was written to fit r_{KC} and $\angle$ KCN as a function of r_{CN} such that the three experimental rotational constants were calculated as well as possible. The values for A, B, and C were reproduced in this way to within 10 MHz. The calculations show that for r_{CN} $= 1.15$ A the K nucleus is located exactly on a line perpendicular to CN bond and through the center of mass of the CN group. In that case the CN moment of inertia determines entirely the rotational constant A, and there is no fit possible for smaller CN distances. For r_{CN} > 1.15 A two different possible structures are found the K nucleus is shifted either to the C nucleus (structure A) or to the N nucleus (structure B) From the present measurements no decision can be made which of these structures is the correct one. Figure 2 depicts the variation in the position of the K nucleus in r_{KC} and $\angle$ KCN, versus the CN distance. Both r_{KC} and $\angle$ KCN depend very critically on r_{CN}. In many cases zero point vibrations are another limiting factor for the accuracy in the determination of effective structural parameters. Although these effects are rather large in KCN, as follows from the inertial defect, they can completely be neglected compared to the uncertainties due to the r_{CN} variation The best structural parameters we can give for KCN from the present measurements are r_{CN} $= 1.162(10)$ Å, $r_{KC} = 2$ $6(1)$ Å, and $\angle$ KCN $- 76°(10)$. Isotopic substitution is necessary for a more precise structure determination.

Though accurate values for all the τ-distortion constants are obtained a reliable force field calculation has to await the more accurate structure. The lowest vibrational frequency of KCN can be estimated to within 10% to 20% from the inertial defect[13] $\omega_2 = h/2\pi^2\Delta I$. A value for $\omega_2 - 157$ cm^{-1} is obtained in this way, which is in good agreement with $\omega_2 = 139$ cm^{-1} from the matrix-isolation work.[6]

V. CONCLUSIONS AND DISCUSSION OF FURTHER ASPECTS

The present measurements have demonstrated for the first time that high temperature asymmetric molecules can be studied by MBER and microwave spectroscopy. It has been proved without doubt that KCN in the ground vibrational state behaves like an asymmetric rotor with a T-shaped structure. Structural parameters may be considerably improved by measuring isotopic species of KCN. This study will be done with the MBER technique in view of the simpler spectrum and the much lower ma-

TABLE II Frequencies (in MHz) of the observed and calculated rotational transitions of KCN in the ground vibrational state

J'	K'₁	K'₁	J	K₁	K₁	type	Observed frequency	Observed-calculated	Reference[a]
1	1	-	1	1	1	1	2 1 1 00(10)	0 03	MBER
1	1	1	1	1	1	a	1018 02(0)	0 03	MBER
1	1		1	1	0	a	8 178 2 1( )	0 01	MBER
7	1	0	7	1	7	1	11 102 87( )	0 17	MBER
8	1	7	8	1	8	a	11 29 1 1(0)	0 09	MBER
9	1	8	9	1	9	a	18 1 7 1 7(0)	- 0 07	MBER
10	1	9	10	1	10	1	21 149 1 1(0)	- 0 12	MBER
16	2	14	16	2	15	1	6 7 9 10(10)	- 0 01	MBER
17	2	15	17	2	16	a	8 100 59(10)	- 0 01	MBER
18	2	16	18	2	17	1	10 517 08(10)	0 01	MBER
19	2	17	19	2	18	1	12 803 17(10)	- 0 01	MBER
20	2	19	20	2	19	a	15 589 90(10)	0 01	MBER
21	2	19	21	2	20	a	18 1 15 64(10)	0 02	MBER
22		20	22	2	21	a	22 077 10(10)	- 0 01	MBER
23	2	21	23	2	22	a	25 899 58(10)	- 0 01	MBER
1	0	1	0	0	0	a	9 175 19(10)	0 01	MBER
2	0	-	1	0	1	a	18 318 5 3(30)	0	MBER
3	1	1	4	0	4	b	11 41 1 37(10)	0 03	MBER
7	0	7	6	1	6	b	16 795 78(30)	- 0 03	MBER
12	2	11	11	1	12	b	19 333 91(30)	0 04	MBER
16	1	15	15	2	11	b	17 648 11(10)	- 0 02	MBER
17	1	16	16	2	15	b	30 303 37(20)	0 01	MBER
22	3	20	23	2	-1	b	30 162 39(20)	0 01	MBER
23	3	21	24	2	22	b	17 6 15 59(20)	- 0 01	MBER
27	2	25	26	3	24	b	21 500 65(20)	0	MBER
1	1	0	2	1	2	a	27 816 57(25)	0 01	mw
3	0	3	2	0	2	a	28 416 80(10)	- 0 01	mw, MBER
3	2	1	2	2	0	a	28 123 85(30)	- 0 22	mw
3	1	2	2	1	1	a	29 027 89(30)	- 0 08	mw
4	1	4	3	1	3	a	37 085 61(10)	0 04	mw
4	0	4	3	0	3	a			
4	3	2	3	3	1	a	37 877 86(50)	0 03	mw
4	3	1	3	3	0	a			
4	2	3	3	2	2	a	37 886 97(20)	- 0 01	mw
4	2	2	3	2	1	a	37 909 69(20)	0	mw
4	1	3	3	1	2	a	38 700 59(15)	- 0 03	mw
9	6	3	8	6	2	a 1	85 034 2(5)	- 0 24	8
9	6	4	8	6	3	a 1			
9	5	5	8	5	4	a 1	85 111 4(3)	0 15	8
9	5	4	8	5	3	a 1			
9	4	5	8	4	4	a 1	85 178 3(3)	- 0 10	8
9	4	6	8	4	5	a 1			
9	2	8	8	2	7	a	85 196 7(3)	- 0 08	8
9	2	7	8	2	6	a	85 468 0(4)	- 0 11	8
9	1	8	8	1	7	a	87 005 4(2)	- 0 03	8
10	1	10	9	1	9	a	92 621 3(5)	0 18	8
10	0	10	9	0	9	a	94 360 1(3)	0 03	8
10	7	3	9	7	2	a 1	94 382 1(2)	- 0 01	8
10	7	4	9	7	3	a 1			
10	6	5	9	6	4	a 1	94 480 7(2)	0 11	8
10	6	4	9	6	3	a 1			
10	5	5	9	5	4	a 1	94 566 9(2)	- 0 06	8
10	5	6	9	5	5	a 1			
10	4	7	9	4	6	a 1	94 643 4(2)	- 0 02	8
10	4	6	9	4	5	a 1			
10	2	9	9	2	8	a	94 617 3(3)	0 10	8
10	3	8	9	3	7	a	94 714 8(4)	0	8
10	3	7	9	3	6	a	94 721 0(4)	- 0 07	8
10	2	8	9	2	7	a	95 019 3(2)	0 05	8
10	1	9	9	1	8	a	96 649 2(2)	0 07	8
11	1	11	10	1	10	a	101 858 4(3)	- 0 11	8
11	9	3	10	9	2	a 1	103 556 9(4)	- 0 17	8
11	9	2	10	9	1	a 1			
11	8	3	10	8	2	a 1	103 694 1(2)	0 06	8
11	8	4	10	8	3	a 1			

52

TABLE II *(Continued)*

J''	K''_{-1}	K''_1	J	K_{-1}	K_1	Type	Observed frequency	Observed-calculated	Reference[a]
11	0	11	10	0	10	a	103 705 8(2)	0, 01	8
11	7	5	10	7	4	a l	103 817 0(2)	0 02	8
11	7	4	10	7	3	a l			8
11	6	5	10	6	4	a l	103 926 0(3)	− 0 08	8
11	6	6	10	6	5	a l			8
11	5	7	10	5	6	a l	104 022, 3(2)	0	8
11	5	6	10	5	5	a l			8
11	2	10	10	2	9	a	104 092, 5(3)	− 0, 14	8
11	4	7	10	4	6	a l	104 108 6(2)	− 0, 04	8
11	4	8	10	4	7	a l			8
11	3	9	10	3	8	a	104 190 9(4)	0 15	8
11	3	8	10	3	7	a	104 200, 8(5)	− 0, 13	8
11	2	9	10	2	8	a	104 586 9(2)	0 03	8
11	1	10	10	1	9	a	106 284 9(4)	− 0 18	8

[a]MBER and mw stand for the results of the present MBER and microwave absorption studies, respectively.

terial consumption in comparison to microwave spectroscopy.

Detailed information about the electronic structure is highly desirable for a better understanding of the unusual bond. Some information may be obtained from measurements of the dipole moment components μ_a and μ_b and from the hyperfine structure. For the low J MBER transitions we were able to resolve the nuclear hyperfine structure associated with the K and N nuclei. However, in the present analysis which combines the MBER and microwave spectra the emphasis is on the determination of the structure of the KCN molecule. In this analysis

the hyperfine splittings were neglected while the errors in the frequencies are taken such that the uncertainties due to the hyperfine effects are well covered. MBER experiments to determine the electric dipole moment and the hyperfine structure are in progress.

Sixty-eight lines from the $J = 4 - 3$ transition have been observed in the microwave absorption experiment. Since only five of them belong to the ground vibrational state (one line is missing due to an accidental overlap) lines from at least 11, but most probably from many more excited states contribute to the observed spectrum. These states cover a considerable part of the expected
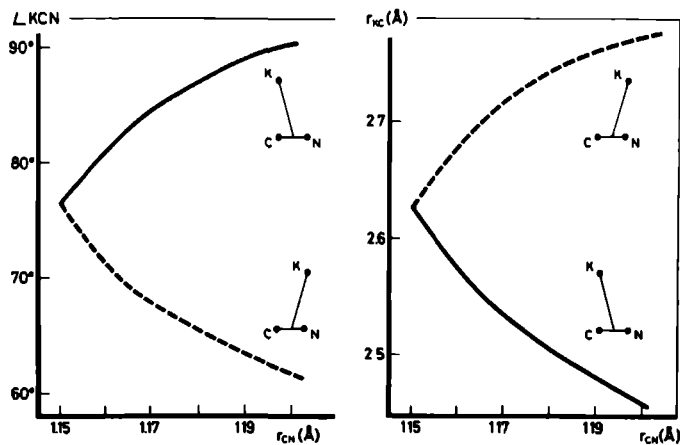

FIG. 2. The ∠KCN and the KC distance vs the CN distance as calculated from the rotational constants. The solid and broken lines correspond to structure A and B, respectively.

TABLE III. Rotational constants for the ground vibrational state of KCN.

Constant	Value (MHz)[a]
A''	58265.81(4)
B''	4940.055(2)
C''	4536.214(2)
τ'_{aaaa}	– 5.33(1)
τ'_{bbbb}	– 0.02703(3)
τ'_{cccc}	– 0.01871(3)
τ_1	– 1.5557(4)
τ_2	– 0.12063(3)
$H_{JK} \times 10^5$	– 5.4(2)
$H_{KJ} \times 10^5$	95(1)
$\Delta \tau \times 10^{3\,b}$	– 0.86(2)

[a] The uncertainties represent one standard deviation as determined by the least squares fit.[14] The quality of the fit can be judged from $\sigma = 0.25$ where $\sigma = [\chi^2/(n-m)]^{1/2}$ with χ^2 the as usual defined chi square value, n the number of lines and m the number of parameters in the fit.

[b] Reference 14.

TABLE IV. Derived molecular constants for KCN assuming planarity.[a] All entries are in MHz except ΔI which is in amu $Å^2$

	Parameters used for calculation			
	τ_1, τ_2		τ_1, τ'_{cccc}	
A^a	58265.35		58265.39	
B	4939.658		4939.661	
C	4536.07		4536.04	
τ_{aaaa}	– 5.33		– 5.33	
τ_{bbbb}	– 0.027 03		– 0.027 03	
τ_{aabb}	0.153		0.069	
τ_{abab}	– 0.891		– 0.814	
ΔI^b	0.4292		0.4298	

[a] A, B, and C are the τ-free rotational constants.

[b] $\Delta I = (h/8\pi^2) (1/C - 1/A - 1/B)$.

potential barrier height for the transition to polytopic bonding and therefore provide a test of the theoretical models describing the large amplitude motions.[9,11] The results of Bunker and Howe[9] show that their rigid bender model qualitatively describes the effective asymmetric top structure and the low bending vibrational frequency for a reasonable potential height. An analysis of the spectrum for excited states in KCN will therefore provide valuable information about the height and the shape of the potential. Lines from three excited states have been tentatively assigned, which show that the effect of vibrations on the rotational constants cannot be described by the usual linear τ dependence. However, the information from the spectrum is much less complete as compared to the ground vibrational state and more experimental and theoretical work has to be done. The interpretation of spectroscopic data will be complicated by the fact that $2\omega_2$ is nearly equal to ω_1.

The presently determined structure can be of help to remove discrepancies in the thermodynamic data of KCN as obtained from mass spectroscopic experiments and calculations based on the second and third law. This is not only of theoretical interest but also of some practical importance for the understanding of chemical problems arising in blast furnaces.[23]

Preliminary estimates can be made of the structure of the other alkali cyanides as a guideline for future work. The most satisfactory explanation for the trend in the vibrational frequencies ω_2 (Table I) is to assume that LiCN is linear as predicted by the *ab initio* cal-

culations and that a change to a T-shaped structure takes place for NaCN. Assuming approximately the same barrier height the slope of the potential function is much steeper for the T-shaped configuration which explains the increase of ω_2.

ACKNOWLEDGMENTS

[1] J. W. Simmons, W. F. Anderson, and W. Gordy, Phys. Rev. 77, 77 (1950).

[2] R. A. Creswell, E. F. Pearson, M. Winnewisser, and G. Winnewisser, Z. Naturforsch. Teil A 31, 221 (1976).

[3] B. Bak, E. Clementi, and R. N. Kortzeborn, J. Chem. Phys. 52, 764 (1970).

[4] E. Clementi, H. Kistenmacher, and H. Popkie, J. Chem. Phys. 58, 2460 (1973).

[5] B. Bak (private communication).

[6] Z. K. Ismail, R. H. Hauge, and J. L. Margrave, J. Chem. Phys. 57, 5137 (1972), J. Mol. Spectrosc. 54, 402 (1975).

[7] G. E. Leroi and W. Klemperer, J. Chem. Phys. 35, 774 (1961).

[8] P. Kuijpers, T. Torring, and A. Dymanus, Chem. Phys. Lett. 42, 423 (1976).

[9] P. R. Bunker and B. M. Landsberg, J. Mol. Spectrosc. 67, 374 (1977), P. R. Bunker and D. J. Howe (to be published).

[10]S. L. Holmgren, M. Waldman, and W. Klemperer, J. Chem. Phys. 67, 4414 (1977).

[11]B. I. Zhilinskii, V. A. Istomin, and N. F. Stepanov, Chem. Phys. 31, 413 (1978).

[12]J. Hoeft, F. J. Lovas, E. Tiemann, and T. Törring, Z. Angew. Phys. 31, 265 (1971).

[13]W. Gordy and R L. Cook, *Microwave Molecular Spectra* (Interscience, New York, 1970).

[14]W. H. Kirchhoff, J. Mol. Spectrosc. 41, 333 (1972).

[15]J. M. L. J. Reinartz, Thesis, Katholieke Universiteit, Nijmegen (1976).

[16]J. C. Zorn and T. C. English, Advances in Atomic and Molecular Physics, edited by D. Bates and I. Esterman (Academic, New York, 1973), Vol 9.

[17]R. van Wachem and A. Dymanus, J Chem. Phys. 46, 3749 (1967), R. van Wachem, Thesis, Katholieke Universiteit,

Nijmegen (1967).

[18]W. L. Meerts, G. ter Horst, J. M. L. J. Reinartz, and A. Dymanus, Chem. Phys. 35, 253 (1978).

[19]M. Gläser, Diplomarbeit, Göttingen (1972)

[20]W. L Meerts, J. P. Bekooy, and A. Dymanus, Mol. Phys. 37, 425 (1979).

[21]J. K. G. Watson, J. Chem. Phys. 46, 1935 (1967).

[22]J. K. G. Watson, J. Chem. Phys. 48, 4517 (1968).

[23]F. C. Ehlert (private communication).

[24]The results listed in Tables II–IV were obtained using a computer program written in Nijmegen based on Watson's reduced Hamiltonian [$s_{111} = -4R_6/(B-C)$] (Refs 21 and 22) The calculations were repeated with the NBS program (Ref 14) The best fit results from both computations agreed to within one standard deviation

55

HIGH-RESOLUTION LASER-RF SPECTROSCOPY ON
THE $A^2\Pi_{3/2}$-$X^2\Pi_{3/2}$ SYSTEM OF IODINE-OXIDE (IO)

J.P. Bekooy, W.Leo Meerts and A. Dymanus

Fysisch Laboratorium, Katholieke Universiteit, Toernooiveld,
6525 ED Nijmegen, The Netherlands

ABSTRACT

The rotational spectra of the vibrational bands 2-0, 2-1 and 2-2 of the $A^2\Pi_{3/2}$-$X^2\Pi_{3/2}$ system of the IO radical have been studied at high resolution by molecular-beam laser-excitation spectroscopy. The hyperfine structure could be resolved for the lowest rotational levels and the hyperfine constants eQq_1 and $a+\frac{1}{2}(b+c)$ have been determined for both the excited and ground states. Hyperfine splittings within rotational levels of the ground vibrational $X^2\Pi_{3/2}$ state have been studied by a new spectroscopic method: microwave optical double-resonance on an electrically state-selected beam. The hyperfine constants eQq_2 and $b-C_1(\lambda-2)$ of the $v=0$, $X^2\Pi_{3/2}$ state could be deduced as well. The widths of the rotational levels in the excited $v=2$, $A^2\Pi_{3/2}$ state have been determined. Apart from the vibrationally-dependent predissociation, a rotationally-dependent pre-dissociation has been observed.

Spectroscopy on the ground and first excited elecronic states of the halogen monoxides is hindered by instability of these radicals and extensive predissociation in the $A^2\Pi_i$ states. Their possible intermediate role in stratospheric (ClO and BrO) and tropospheric (IO) (1) photochemistry, which limits the atmospheric abundance of ozone, has raised interest in the past years. The spectra of ClO and BrO have been studied most extensively and the spectrum of FO in the gas phase has been observed only recently by laser magnetic resonance (2). The $A^2\Pi_{3/2}$-$X^2\Pi_{3/2}$ system of IO has been subject of several investigations. It was first observed in emission by Vaidya (3). Coleman *et al.* (4) extended the emission spectrum at low dispersion and analyzed the vibrational band system. Durie and Ramsay (5) observed the absorption spectrum, and Durie *et al.* (6) observed and analyzed the vibrational and rotational structure of the moderately resolved emission spectrum. Vibronic progressions of absorption and emission spectra of IO isolated in an argon matrix were observed by Loewenschuss *et al.* (7). The ground vibrational $X^2\Pi_{3/2}$ state of IO was studied by electron resonance spectroscopy in the J=3/2 rotational level by Carrington *et al.* (8) and in the J=5/2 level by Brown *et al.* (9). Saito (10) studied the two lowest rotational transitions in the ground vibrational $X^2\Pi_{3/2}$ state by microwave absorption spectroscopy.

In this paper we report a study on the $A^2\Pi_{3/2}$- $X^2\Pi_{3/2}$ system of the IO radical by high-resolution laser-RF spectroscopy. The hyperfine interaction in the excited state and the hyperfine Λ-doublet splittings in the ground state have been observed for the first time. Two distinct experimental methods have been used: molecular-beam laser-excitation (MBLE) and microwave optical double-resonance on an electrically state-selected beam (MODRES). The latter method is a new and powerful technique, that combines the high resolution of microwave spectroscopy on molecular beams with the high sensitivity of state-resolved detection by laser-induced fluorescence.

The rotational spectra of the vibrational bands 2-0, 2-1 and 2-2 of the $A^2\Pi_{3/2}$-$X^2\Pi_{3/2}$ transition have been studied using the MBLE method. Hyperfine structures could be resolved for the lowest rotational transitions. The effective rotational constant B, the centrifugal distortion constant D, the electric quadrupole coupling constant eQq_1 and the magnetic hyperfine constant $a+\frac{1}{2}(b+c)$ have been determined for the v=2 level of the $A^2\Pi_{3/2}$ state and the v=0, 1 and 2 levels of the $X^2\Pi_{3/2}$ state. For the ground state, vibrational constants and vib-

rational series expansion coefficients for the rotational constants have been derived.

The widths of the rotational levels in the excited v=2, $A^2\Pi_{3/2}$ state have been determined from the optical excitation spectra. Apart from the predissociation, which varies with vibrational level and is commonly observed for the $A^2\Pi_i$ states of the halogen monoxides, a rotationally-dependent predissociation has been observed as well, indicating additional gyroscopic interaction with un-bound states.

Hyperfine splittings within rotational levels of the ground vibrational $X^2\Pi_{3/2}$ state have been further studied by the MODRES method. From these measurements the non-axial electric quadrupole coupling constant eQq_2 and the effective magnetic hyperfine constant $b-C_I(\lambda-2)$ could be determined for the v=0 level of the $X^2\Pi_{3/2}$ ground state.

For the interpretation of the observed spectra, theory for $^2\Pi$ states has been employed. The final constants have been determined from a merged least-squares fit to all data from the present investigation, combined with flame emission data of Durie *et al*. (6) and microwave absorption data of Saito (10).

2. EXPERIMENTAL METHODS

The two configurations of the spectrometer used in the investigation of IO are shown in Fig. 1. In case of the MBLE experiments the laser beam intersects the molecular beam at position (A), while for the MODRES experiments it inter-sects at position (B). The MBLE method is well established. With this method, transitions to excited electronic states can be studied by means of detection of the subsequently emitted laser-induced fluorescence (LIF). The spectral resolution is usually limited (apart from the natural linewidth) by the residual Doppler broadening (in the order of 10 MHz) determined by the degree of molecular beam collimation.

The MODRES method is a new and powerful technique, which combines high resolution with high sensitivity. A microwave optical double-resonance arrangement is used, in which transitions induced by microwave radiation between certain levels in the electronic ground state are detected as a change in the LIF intensity. Since in case of microwave transitions both ground state levels involved are almost equally populated, state selection is required. This is achieved by an electrostatic quadrupole field, called A-field in analogy with
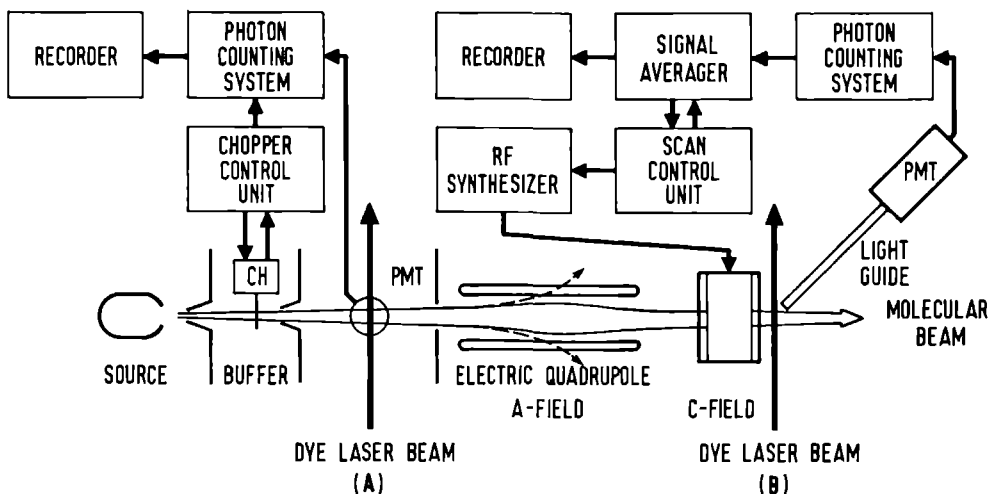
Fig. 1. Outline of the spectrometer. The dye laser beam intersects the molecular beam orthogonally either at position (A), in case of the molecular-beam la-ser-excitation (MBLE) configuration or at position (B), in case of the microwave optical double-resonance on an electrically state-selected beam (MODRES) con-figuration. CH: beam chopper and PMT: photomultiplier.

the molecular-beam electric-resonance (MBER) method. In the experimental set-up (Fig. 1) the molecular beam produced by the source is state selected by the A-field and detected by LIF. The microwave or radio-frequency (RF) transition is induced in the C-field located between the A-field and the intersection of the laser and molecular beam at position (B). The laser frequency is kept fixed at a specific optical excitation transition and the LIF intensity is monitored. In this way the laser monitors the number of molecules in a specific energy level of the ground electronic state. The A-field deflects molecules according to their quantum states, towards the molecular beam axis (positive Stark effect, trajectories indicated by solid lines in Fig. 1) or away from it (negative Stark effect, dashed line trajectories). If in the C-field a transition from a state transmitted to a state rejected by the A-field is induced by radio-frequency (RF) (or microwave) radiation, a decrease (flop-out) in the LIF intensity will occur if the initial state is probed by the laser (double-resonance condition). Alternatively, an increase (flop-in) will occur if the final state is probed by the laser. As illustration a schematic energy level diagram is given in Fig. 2, in which two of the double-resonance transitions observed are indicated. The Λ-doublet components of the hyperfine levels in the ground state with symmetry -
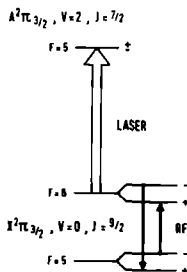
Fig. 2. Schematic energy level diagram, in which two of the double-resonance transitions observed are indicated.

and + exhibit mainly positive and negative Stark effects, respectively. The LIF detection was performed on the $A^2\Pi_{3/2}-X^2\Pi_{3/2}$, 2-0, P(9/2), F'=5←F''=6 (+←- and -←+) transition. The hyperfine RF transitions $6_-\to5_+$ (flop-out) and $6_+\gets5_-$ (flop-in) within the J=9/2 rotational level of the v=0, $X^2\Pi_{3/2}$ ground state have been observed.

The MODRES method furnishes a high spectral resolution (in the order of 10 kHz), because the linewidths are only determined by the transit time of the molecules through the C-field transition region. It should be noted that the linewidths in the double-resonance RF spectra do not depend on the much broader linewidths of the LIF transitions. The state-resolved LIF detection improves the sensitivity by several orders of magnitude compared to total beam detection, as applied in conventional molecular-beam electric-resonance (MBER) (for a review see e.g. Ref. (11)). Since the laser excitation is state selective, the signals and noise originate only from the molecular states of interest, aside from spurious background due to straylight and photodetector noise. Furthermore, the double-resonance condition facilitates identification of complicated optical spectra, which is an advantage with regard to the MBLE method. Another difference with MBER is the absence of the state analyzing B-field, which allows detection of both flop-in and flop-out signals. Inclusion of this B-field is only necessary in the (rare) case the laser excitation cannot accomplish full state analysis because the two states connected by the microwave radiation fall within its spectral resolution. The drawback of the MODRES method is its restriction to transitions between (ground) states complying with rather strict state-selection rules.

The present MODRES method resembles the molecular-beam magnetic-resonance with laser detection as introduced by Grundevik *et al.* (12) and the molecu-

lar-beam laser-induced fluorescence resonance as introduced by Rosner *et al.* (13). The first method employs inhomogeneous magnetic A- and B-fields and applies to atoms or molecules with magnetic dipole moments. In the method of Rosner *et al.* the A-field is replaced by the intersection with another beam from the same laser, which produces state labeling by depleting the population of a specific energy level in the ground electronic state by means of optical pumping. This method is not restricted to polar species, however it applies only if sufficient optical pumping can be achieved.

The IO radical was produced by the reaction of atomic oxygen with iodine molecules,

$$O(^3P)+I_2(^1\Sigma_g^+) \rightarrow IO(^2\Pi)+I(^2P). \tag{1}$$

This reaction was found to be twice as efficient in beam formation as the reaction of atomic oxygen with methyl-iodide (CH_3I) used by Saito (10). The molecular beam of IO radicals was produced in a reaction source analogous to the source used in the experiments on the hydroxyl (OH) radical (14). The optimized design is shown in Fig. 3. The source consists of pyrex tubes, with inner diameters of 4 and 10 mm, that are wrapped around with heating wires. The temperature was kept at 400 to 500 K to maintain the iodine molecules in vapour phase. Atomic oxygen is produced by a microwave discharge at 2.45 GHz, located off-axis to eliminate stray light along the beam direction. About 10% dissociation to atomic oxygen was obtained at a power dissipation of 75 to 150 W. The iodine molecules are injected into the reaction zone via an orifice of 2 mm diameter. The end of the source, in front of the skimmer, has been contracted to an optimized diameter of 6 mm. The efficiency of IO beam formation is strongly dependent on this diameter and increased by an order of magnitude compared to an uncontracted
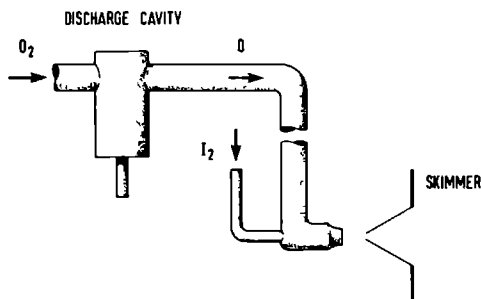

Fig. 3. Diagram of the reaction source for IO molecular beam production.

10 mm tube. The molecular beam is formed by a conical skimmer with an aperture of 2 mm located about 12 mm downstream from the source. Typical pressure in the source chamber (pumped by a 500 m^3/h Roots pump) was 4×10^{-2} mbar. The iodine consumption was about 2.5 g/h. Various compounds are deposited on the inner wall of the reaction tube and on the skimmer. This results in clogging and necessitates cleaning after about seven hours of measurement. Yellow-green chemiluminescence emanating from the reaction zone proved to be helpful to adjust the source conditions.

The laser radiation for the experiments has been produced by a tunable single-frequency c.w. dye laser (Coherent Radiation 599-21). The gain medium is a solution of Stilbene 3 (420) dye in ethylene glycol (0.75 g/l) and is pumped by the UV lines from an Ar-ion laser (Spectra Physics 171-UV). The dye laser has been equipped with Coumarin 102 (480) optics. The maximum single-frequency output power in the region 445 to 475 nm decreases from 100 to 35 mW, respectively, at a pumping power of 1.7 W. The dye laser power can be stabilized by an external feedback system. The effective spectral bandwidth due to residual jitter of the laser frequency is 3 MHz. An external scanning ramp generator provides a linear up or down going ramp to drive the scan controls of the dye laser.

A thermally stabilized confocal Fabry-Pérot interferometer (Burleigh CFT-500), with a free spectral range of 150 MHz, is used to monitor the dye laser frequency. The transmission peaks in the fixed mode of operation furnish relative frequency markers if the laser is scanned. In the MODRES experiments the interferometer is used in the scanning mode to monitor eventual drifts in the dye laser frequency, which are subsequently compensated by manual adjustment of the scan controls. Calibration of the free spectral range has been performed against known splittings in the IO ground state, with an accuracy of 1×10^{-4}. The dye laser was scanned across transitions terminating in the same hyperfine level of a rotational state in the excited v=2, $A^2\Pi_{3/2}$ state, but originating from different hyperfine levels in rotational states in the v=0, $X^2\Pi_{3/2}$ ground state whose energy separation is known from the data of Saito (10). The calibration scans spanned intervals of 50 and 70 GHz, covering hyperfine structures of the rotational transitions Q(3/2) to P(5/2) and Q(5/2) to P(7/2), respectively.

The absolute frequency of the dye laser is determined using a wavelength meter, which compares the dye laser wavelength with the accurately known wavelength of a reference laser. Its principle is based on a Michelson interferometer with electronic counting of interference fringes (15-17). The wavelength meter incorporates variation of the optical path length inside a vacuum chamber (eliminating elaborate dispersion corrections), phase-locked

100-fold fringe frequency multiplication (for fringe interpolation) and a single-frequency HeNe reference laser with thermal frequency stabilization (18,19). The wavelength of this reference HeNe laser was determined regularly by measuring the wavelength of the dye laser tuned to the Lamb-dip of the transition at 436 nm of the ^{198}Hg secondary standard. The absolute wavelength of this transition has been determined accurately relative to the ^{86}Kr primary standard (20). By this intrinsic method of calibration, any eventual systematic errors are eliminated. The absolute accuracy of the digital wavelength meter is 1.2×10^{-7}, throughout the visible region.

An outline of the spectrometer has been given in Fig. 1. In the MBLE experiments the dye laser beam intersects the molecular beam orthogonally at position (A) (distance from the source is 30 cm). The IO beam is modulated by a mechanical chopper to eliminate off-phase background signals. The LIF is collected by an optical system consisting of aspherical lenses and a concave spherical mirror, in a direction perpendicular to both beams, with an angular efficiency of 20-25%. The collected LIF is transmitted to the photocathode of a photomultiplier (EMI 9635) and monitored by a photon-counting system (ORTEC-Brookdeal 5C1). The vibrational bands of the optical spectra are located at 445 nm (2-0), 459 nm (2-1) and 473 nm (2-2). The collected light is passed through a spectral filter (Schott CG 495, thickness 3 mm) with cut-off wavelength at 495 nm, to discriminate against scattered laser light. The signal is registered on a dual-channel chart recorder, together with laser frequency marks provided by the Fabry-Pérot reference interferometer. The strongest lines in the IO spectrum amounted to 8000 count/s, yielding a signal to noise ratio of about 40 at a counting time of 1 s. The spectral resolution is determined by a convolution of the natural linewidth and the instrumental limitations imposed by residual Doppler broadening, laser frequency jitter, transit time broadening and wavefront curvature broadening (21,22). Under the experimental conditions (full angular divergence of the molecular beam is 20 mrad, laser frequency jittter is 3 MHz, diameter of the laser beam is 5 mm and full angular divergence of the laser beam is 0.5 mrad) the Gaussian profile from instrumental broadening is estimated to have a width (FWHM) of 10-20 MHz. The linewidths observed in the IO spectrum were always dominated by the natural linewidths. A typical spectral recording of the hyperfine structure of the Q(3/2) rotational transition of the 2-0 band is shown in Fig. 4.

For the MODRES experiment (Fig. 1) with laser intersection at position (B), the laser frequency is tuned to a specific optical excitation transition in the 2-0 band. In this case the LIF is collected by a light guide (Schott LST) at an
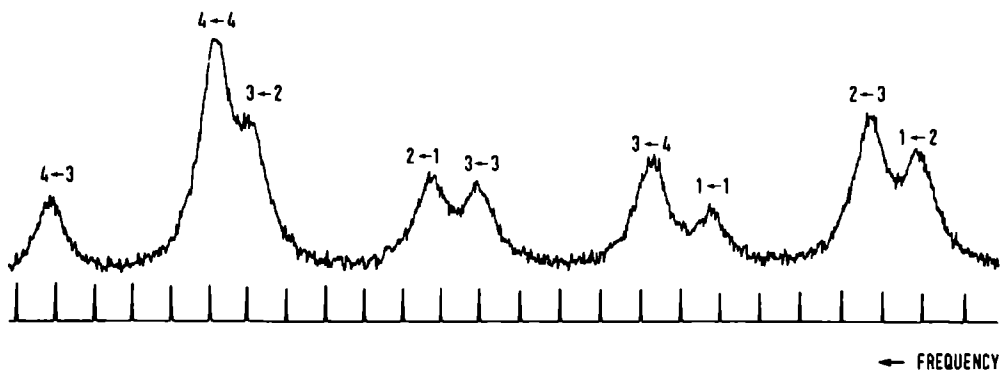
Fig. 4. Spectral recording of the Q(3/2) rotational transition in the 2-0 vibra-tional band of the $A^2\Pi_{3/2}$-$X^2\Pi_{3/2}$ system of IO (at 445.04175(5) nm), observed by MBLE. The hyperfine structure transitions are indicated as F'←F" (+←- and -←+). Frequency intervals between two subsequent transmission peaks of the interferometer given in the lower trace, are 149.605(15) MHz. The natural line-width is 148(12) MHz (FWHM).

angle of 45° with both the laser and molecular beam, with an angular efficiency of about 2%. The collected LIF is detected by a cooled photomultiplier (EMI 9863/350) connected to the photon-counting system. The double-resonance signal stimulated by the RF radiation in the C-field is observed by monitoring the LIF intensity versus the RF frequency. The RF is generated by a programmable RF syn-thesizer (Hewlett-Packard 8660 B). A signal averager (Hewlett-Packard 5480 B), interfaced with the scan control unit, has been employed. For searching over wide frequency regions, artificial line broadening by random frequency modu-lation of the RF synthesizer has been employed (14). After preliminary location of a transition, an accurate frequency determination is performed at normal re-solution. Several hyperfine transitions within rotational levels of the v=0, $X^2\Pi_{3/2}$ ground state of IO have been studied. The hyperfine levels are split into two closely spaced Λ-doublet states with different symmetry, which exhibit main-ly linear Stark effect. The large dipole moment of 2.5 D (23) allows state se-lection for the lower rotational levels at moderate voltages. The intensities of the double-resonance transitions were about 15 count/s. The main reason for the strong reduction of the signals is the larger distance from the source (145 cm). In most cases 32 RF scans (each scan took one minute at one second time constant) were averaged, yielding a final signal to noise ratio in the order of two. Al-though the obtainable linewidths are in principle 10 kHz (the length of the
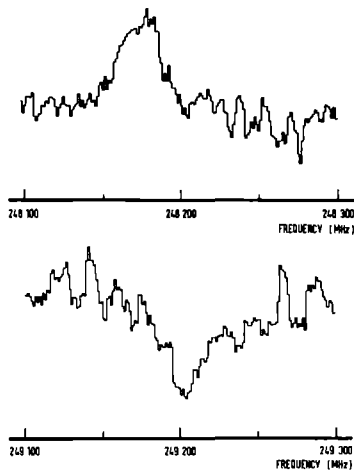
Fig. 5. *Spectral recording of the hyperfine transitions within the J=9/2 rotational level of the v=0, $X^2\Pi_{3/2}$ ground state of IO, observed by MODRES. The LIF detection was performed on the $A^2\Pi_{3/2}$-$X^2\Pi_{3/2}$, 2-0, P(9/2), F'=5←F"=6 (+←- and -←+) transition. The hyperfine RF transitions $6_+←5_-$ (flop-in signal) and $6_-→5_+$ (flop-out) have been observed.*

C-field is 5 cm), this limit is not reached for the low J states of IO. This is due to the residue of the compensated Earth's magnetic field, which causes broadening of transitions in the paramagnetic $X^2\Pi_{3/2}$ state. A typical spectral recording of hyperfine transitions within the J=9/2 rotational state is shown in Fig. 5. A schematic energy level diagram corresponding to these double-resonance transitions has been given in Fig. 2.

3. THEORY

Both the observed excited $A^2\Pi_{3/2}$ and ground $X^2\Pi_{3/2}$ state belong to $^2\Pi$ doublets. The ground $X^2\Pi$ doublet is known to be inverted with a large spin-orbit separation and can be described by a coupling scheme close to Hund's case (a). The Hamiltonian for a diatomic molecule in an electronic $^2\Pi$ state in absence of external fields may be written in a formal way as

$$H = H_{ev}+H_F+H_{hf}.\qquad (2)$$

Here H_{ev} represents the part concerning the purely electronic and vibronic term energies, H_F contains the rotational energy and the fine-structure inter-actions, and H_{hf} describes the hyperfine interactions. The theory to be used for the interpretation of the spectra incorporates two modifications of the theory derived in detail elsewhere (14,24,25). Firstly, for H_F the effective Hamiltoni-an for the rotational and spin structure of a given isolated vibronic state de-rived by Brown *et al.* (26) has been adopted. Their treatment is to be prefered since the resulting effective Hamiltonian is uncoupled from other electronic and vibronic states. The matrix elements are evaluated using an expansion of the Hamiltonian in $\underline{N}^2$ instead of $\underline{R}^2$ as previously. The second modification concerns the phase factors for the off-diagonal matrix elements between the $^2\Pi_{1/2}$ and $^2\Pi_{3/2}$ states. The phase convention now employed is in accordance with the direct tensor method of Brown and Howard (27).

A basis set of Hund's case (a) wavefunctions, symmetrized with respect to reflection in any plane through the molecular axis, is used (n=X,A labels the electronic states)

$$|n^2\Pi_\Omega^\pm vJ\rangle = (|nvJ\Lambda\Sigma\Omega\rangle \pm (-1)^{J-1/2}|nvJ-\Lambda-\Sigma-\Omega\rangle)/2^{\frac{1}{2}}. \tag{3}$$

The total wavefunctions $|n^2\Pi_\Omega^\pm vJIF\rangle$ including the nuclear spin are constructed as a product of the functions $|n^2\Pi_\Omega^\pm vJ\rangle$ and the nuclear spin functions $|IM_I\rangle$ ac-cording to the coupling scheme $\underline{F}=\underline{J}+\underline{I}$. The matrix elements for the part H_F of the effective Hamiltonian are given by

$$\langle n^2\Pi_{1/2}^\pm vJIF|H_F|n^2\Pi_{1/2}^\pm vJIF\rangle = -\tfrac{1}{2}A_{nv} - \tfrac{1}{2}A_{Dnv}(X+2) - \gamma_{SRnv}$$

$$+B_{nv}(X+2) - D_{nv}(X+1)(X+4) + H_{nv}(X+1)(X^2+8X+8)$$

$$\pm(-1)^{J-1/2}\tfrac{1}{2}p_{nv}(J+1/2) \pm (-1)^{J-1/2}q_{nv}(J+1/2), \tag{4}$$

$$\langle n^2\Pi_{3/2}^\pm vJIF|H_F|n^2\Pi_{3/2}^\pm vJIF\rangle = \tfrac{1}{2}A_{nv} + \tfrac{1}{2}A_{Dnv}X$$

$$+B_{nv}X - D_{nv}X(X+1) + H_{nv}X(X+1)(X+2), \tag{5}$$

$$\langle n^2\Pi_{1/2}^\pm vJIF|H_F|n^2\Pi_{3/2}^\pm vJIF\rangle = \tfrac{1}{2}\gamma_{SRnv}X^{\frac{1}{2}}$$

$$-B_{nv}X^{\frac{1}{2}} + 2D_{nv}X^{\frac{1}{2}}(X+1) - H_{nv}X^{\frac{1}{2}}(X+1)(3X+4)$$

$$\mp(-1)^{J-1/2}\tfrac{1}{2}q_{nv}X^{\tfrac{1}{2}}(J+1/2), \tag{6}$$

where $X=(J+1/2)^2-1=(J-1/2)(J+3/2)$. When two signs are given, the upper and lower sign is appropriate for the states with symmetry $(-1)^{J-1/2}$ and $(-1)^{J+1/2}$, respectively. Expressions for higher order terms can be found in a paper by Amiot *et al.* (28). The contributions included in the expressions above arise from the spin-orbit coupling (A) with centrifugal distortion (A_D), the spin-rotation interaction (γ_{SR}), the rotational energy (B) with centrifugal distortion to first (D) and second order (H) and the Λ-splitting (p and q). The matrix elements for the hyperfine part H_{hf} of the Hamiltonian are given by

$$\langle n^2\Pi^{\pm}_{1/2}vJIF|H_{hf}|n^2\Pi^{\pm}_{1/2}vJ'IF\rangle =$$

$$G(JJ'IF)\left\{(-1)^{J'-1/2}\begin{pmatrix}J & 1 & J' \\ -1/2 & 0 & 1/2\end{pmatrix}[a_{nv}-\tfrac{1}{2}(b_{nv}+c_{nv})+\delta_{JJ'}2C_{Inv}X]\right.$$

$$\left.\mp\begin{pmatrix}J & 1 & J' \\ -1/2 & 1 & -1/2\end{pmatrix}d_{nv}/2^{\tfrac{1}{2}}\right\}$$

$$+Q(JJ'IF)(-1)^{J'-1/2}\begin{pmatrix}J & 2 & J' \\ -1/2 & 0 & 1/2\end{pmatrix}\tfrac{1}{4}eQq_{1nv}, \tag{7}$$

$$\langle n^2\Pi^{\pm}_{3/2}vJIF|H_{hf}|n^2\Pi^{\pm}_{3/2}vJ'IF\rangle =$$

$$G(JJ'IF)(-1)^{J'-3/2}\begin{pmatrix}J & 1 & J' \\ -3/2 & 0 & 3/2\end{pmatrix}[a_{nv}+\tfrac{1}{2}(b_{nv}+c_{nv})+\delta_{JJ'}(2/3)C_{Inv}X]$$

$$+Q(JJ'IF)(-1)^{J'-3/2}\begin{pmatrix}J & 2 & J' \\ -3/2 & 0 & 3/2\end{pmatrix}\tfrac{1}{4}eQq_{1nv}, \tag{8}$$

$$\langle n^2\Pi^{\pm}_{1/2}vJIF|H_{hf}|n^2\Pi^{\pm}_{3/2}vJ'IF\rangle =$$

$$G(JJ'IF)(-1)^{J'-1/2}\begin{pmatrix}J & 1 & J' \\ -3/2 & 1 & 1/2\end{pmatrix}b_{nv}/2^{\tfrac{1}{2}}$$

$$\mp Q(JJ'IF)\begin{pmatrix}J & 2 & J' \\ -3/2 & 2 & -1/2\end{pmatrix}\tfrac{1}{4}eQq_{2nv}/6^{\tfrac{1}{2}}, \tag{9}$$

where $G(JJ'IF)=[(2J+1)(2J'+1)I(I+1)(2I+1)]^{\tfrac{1}{2}}(-1)^{J+I+F}\begin{Bmatrix}F & J & I \\ 1 & I & J'\end{Bmatrix}$ and

$$Q(JJ'IF)=\left[\frac{(2J+1)(2J'+1)(I+1)(2I+1)(2I+3)}{I(2I-1)}\right]^{\tfrac{1}{2}}(-1)^{J+I+F}\begin{Bmatrix}F & J & I \\ 2 & I & J'\end{Bmatrix}.$$

These expressions[1] contain the magnetic hyperfine (a, b, c and d), the nuclear spin-rotation (C_I) and the electric quadrupole $(eQq_1$ and $eQq_2)$ coupling constants. It should be noted that the sign in front of eQq_2 is opposite of that used before (24,25), so consequently the eQq_2 value reverses sign. In view of the confusion on the sign of eQq_2, a separate discussion on this topic is given in the appendix.

The presently available data on the IO spectrum do not allow for an independent determination of all the molecular constants occurring in the effective Hamiltonian. At first, the nearly total correlation among A_{Dnv} and γ_{SRnv} is removed, as usually, by a transformation of the Hamiltonian, which eliminates γ_{SRnv} and leads to the effective parameters (26)

$$(T_{ne}+G_{nv})^{eff} = T_{ne}+G_{nv}-\tfrac{1}{2}\gamma_{SRnv}\lambda_{nv}/(\lambda_{nv}-2), \tag{10}$$

$$A_{nv}^{eff} = A_{nv}+\gamma_{SRnv}\lambda_{nv}/(\lambda_{nv}-2), \tag{11}$$

$$A_{Dnv}^{eff} = A_{Dnv}-2\gamma_{SRnv}/(\lambda_{nv}-2), \tag{12}$$

where $\lambda_{nv}=A_{nv}/B_{nv}$.

The spin-orbit coupling constant A of the $X^2\Pi$ ground state has been estimated by Brown et al. (9) as $-2\,330$ cm^{-1}. In view of the close agreement (within a few percent) of their estimates for BrO and ClO with recent experimental values (29,30), this value appears to be quite reliable. Although the value of A for the excited $A^2\Pi$ state is unknown, it is reasonable to assume it is large as well, like in ClO (31). As the B values are in the order of 0.3 cm^{-1}, the values of λ are large. The spin-rotation coupling constant γ_{SR} may be estimated from A (32) to be smaller than 1 GHz in case of the $X^2\Pi$ ground state, corresponding to a contribution to A_D^{eff} of less than 0.3 MHz. If the spin-orbit separation is not negligible compared with the vibrational interval, an additional correction must be added to A_D (33). However, this correction is in the order of 10 kHz for the $X^2\Pi$ ground state and can be neglected.

All the spectroscopic data on IO belong to the $A^2\Pi_{3/2}-X^2\Pi_{3/2}$ system only, which imposes further limitations on the determination of molecular constants

---

[1] Eq. (8) corrects an unfortunate misprint in the sign factor of the magnetic hyperfine term in Eq. (4) of Ref. (14).

and only allows the evaluation of effective parameters. For G_{nv} and A_{nv} the usual expansions as a series in $v+\frac{1}{2}$ are applied

$$G_{nv} = \omega_{en}(v+\tfrac{1}{2}) - \omega_e x_{en}(v+\tfrac{1}{2})^2, \tag{13}$$

$$A_{nv} = A_{en} - \alpha_{An}(v+\tfrac{1}{2}) + \gamma_{An}(v+\tfrac{1}{2})^2. \tag{14}$$

For the $^2\Pi_{3/2}$ state (see Eq. (5)) the contributions from γ_{SRnv} in Eq. (10) and (11) cancel and the term $\frac{1}{2}A_{en}$ may be absorbed into an effective $T_{ne}^{eff}(^2\Pi_{3/2})$. The following effective vibrational parameters are obtained for $G_{nv}^{eff}(^2\Pi_{3/2})$

$$\omega_{en}^{eff}(^2\Pi_{3/2}) = \omega_{en} - \tfrac{1}{2}\alpha_{An}, \tag{15}$$

$$\omega_e x_{en}^{eff}(^2\Pi_{3/2}) = \omega_e x_{en} - \tfrac{1}{2}\gamma_{An}. \tag{16}$$

Similar the term A_{Dnv}^{eff} can be absorbed into an effective rotational constant, to a good approximation given by

$$B_{nv}^{eff}(^2\Pi_{3/2}) = B_{nv} + \tfrac{1}{2}A_{Dnv}^{eff}. \tag{17}$$

The value of $B_{nv}^{eff}(^2\Pi_{3/2})$ determined from the spectra depends only slightly on A_{nv}, because the off-diagonal term (see Eq. (6)) contributes after diagonalization by $B_{nv}/(\lambda_{nv}-2)$, which is only -1.5 MHz for the $X^2\Pi$ ground state. Again, the usually applied vibrational expansion for B_{nv} has to be modified into an effective formulation,

$$B_{nv}^{eff}(^2\Pi_{3/2}) = B_{en}^{eff}(^2\Pi_{3/2}) - \alpha_{en}^{eff}(^2\Pi_{3/2})(v+\tfrac{1}{2}) + \gamma_{en}^{eff}(^2\Pi_{3/2})(v+\tfrac{1}{2})^2, \tag{18}$$

where

$$B_{en}^{eff}(^2\Pi_{3/2}) = B_{en} + \tfrac{1}{2}A_{Den}^{eff}, \tag{19}$$

and $\alpha_{en}^{eff}(^2\Pi_{3/2})$ and $\gamma_{en}^{eff}(^2\Pi_{3/2})$ contain relatively small contributions from the vibrational dependence of A_{Dnv}^{eff} through Eq. (17). For the first-order centrifugal distortion parameter D_{nv}, the expansion

$$D_{nv} = D_{en} + \beta_{en}(v+\tfrac{1}{2}) \tag{20}$$

has been applied. The Λ-doubling for the $^2\Pi_{3/2}$ state arises purely via mixing with the $^2\Pi_{1/2}$ state. Its energy contributions can be approximated by $\pm(-1)^{J-1/2}(J-1/2)(J+1/2)(J+3/2)q_{nv}^{eff}/(\lambda_{nv}-2)$, where

$$q_{nv}^{eff} = q_{nv}+(\tfrac{1}{2}p_{nv}+q_{nv})/(\lambda_{nv}-2), \tag{21}$$

giving rise to a very small splitting of the energy levels. In the pure precession approximation (34) the second term in Eq. (21) amounts half the magnitude of q_{nv} (since then $p_{nv}=\lambda_{nv}q_{nv}$). The main features of the hyperfine structure are governed by the contributions from $a_{nv}+\tfrac{1}{2}(b_{nv}+c_{nv})$ and eQq_{1nv}. Smaller contributions arise from C_{Inv} and the off-diagonal term from b_{nv}. The latter two terms are totally correlated and do not allow an independent determination of C_{Inv} and b_{nv}. To a good approximation the contribution from C_{Inv} can be absorbed into the effective parameter

$$b_{nv}^{eff} = b_{nv}-C_{Inv}(\lambda_{nv}-2). \tag{22}$$

The value of C_{Inv} may be roughly estimated as 50 kHz, thus both terms in the above equation give comparable contributions to b_{nv}^{eff} for IO. The small hyperfine Λ-doublet splittings depend mainly on the off-diagonal term eQq_{2nv}. Since the energy contributions of q_{nv}^{eff}, b_{nv}^{eff} and eQq_{2nv} all arise purely from mixing with the $^2\Pi_{1/2}$ state, the values of these parameters determined from the spectra are proportional to $\lambda_{nv}-2$ and thus depend strongly on the value of A_{nv}.

The excited $A^2\Pi_i$ states of the halogen monoxides exhibit extensive predissociation. The predissociation causes an additional decay path for the excited $A^2\Pi$ state, via interaction with unbound excited states. The total decay rate is then given by

$$\Gamma_{tot} = \Gamma_{rad}+\Gamma_{pred}, \tag{23}$$

where Γ_{rad} and Γ_{pred} denotes the radiative and predissociative decay rate, respectively. Due to predissociation the lifetime of the excited state is shortened, which broadenes the energy levels (to a width $\Delta v=\Gamma_{tot}/2\pi$) and diminishes the yield of spontaneous fluorescence emission (to a fraction $\Gamma_{rad}/\Gamma_{tot}$) in case of predissociation into non-fluorescent products (like ground state atoms). A survey on the nature of the coupling Hamiltonians with selection rules and dependence on the molecular quantum numbers in case of weak predissociation of a discrete excited level coupled to a continuum level, has been given by Vigué *et*

70

al. (35). The radiative decay rate of the excited $A^2\Pi$ state of IO may be esti-
mated from extrapolation of the corresponding electronic transition moment of
ClO (36), giving $\Gamma_{rad} \sim 10^7 - 10^8$ s^{-1} and $\Delta\nu_{rad} \sim 1-10$ MHz Durie *et al.* (6) studied
the $A^2\Pi_{3/2} - X^2\Pi_{3/2}$ transition of IO from flame emission spectra They found that
vibrational bands with v'=1, 4 and 5 are completely diffuse, bands with v'=3 are
distinctly diffuse and bands with v'=0 and 2 have rotational lines which are
sharp The widths of rotational levels in the excited v=2, $A^2\Pi_{3/2}$ state have
been observed in the present experiment

4 RESULTS AND ANALYSIS

The spectral line profile in the MBLE experiments is a convolution of a Lor-
entzian profile (natural linewidth, homogeneous line broadening) and a Gaussian
profile (instrumental resolution, inhomogeneous line broadening), which results
in a Voigt profile with a total linewidth $\Delta\nu_V$ The Gaussian contribution has an
estimated linewidth (FWHM) $\Delta\nu_G$ of 10-20 MHz (Sect 2) The Lorentzian contrib-
ution with a linewidth $\Delta\nu_L$ arises from the finite lifetime of the excited state,
which is determined by the radiative and the predissociative decay times The
transitions studied terminate in the less predissociative vibrational level
(v=2) of the $A^2\Pi_{3/2}$ state, and the observed natural linewidths increase from 148
MHz (J=3/2) up to about 2 GHz (J=49/2) Since there is no analytical expression
for the Voigt profile, numerical evaluation is required Fortunately, for IO the
Lorentzian contribution dominates Because evaluation of Lorentzian profiles
consumes much less computer time, a Lorentzian rather than a Voigt profile has
been fitted by a least-squares method to the experimentally observed line shape
For the most unfavourable case (with the smallest linewidth of 148 MHz) its ade-
quacy in describing the Voigt profile has been checked, by fitting it to the
corresponding Voigt profile, generated by a computational method (37) The over-
all agreement is good (within 0 1% of the central line intensity) and fully le-
gitimates the use of Lorentzian profiles for data reduction from the IO spectra
The linewidth $\Delta\nu_L$ of the Lorentzian contribution can be extracted from the ob-
served total linewidth $\Delta\nu_V$, with an accuracy better than 0 5%, by the approxi-
mated composition rule (38)

$$\Delta\nu_L = \Delta\nu_V [1 - (\Delta\nu_G / \Delta\nu_V)^2].$$
(24)

The spectral recordings have been digitized in order to facilitate data reduction by a computer program. The resolved hyperfine structures of the lowest rotational transitions have been identified and analyzed first. The individual line centres and intensities of the hyperfine components of a given rotational transition, were varied in the fitting procedure, together with a single linewidth for all the components. When the hyperfine components were allowed to have individually different linewidths, no significant variation was found within the experimental uncertainty.

The hyperfine structure could not be resolved for the higher rotational transitions and these spectra have been analyzed in a different way. The hyperfine pattern of a given rotational transition was fully calculated, using the diagonal hyperfine constants eQq_1 and $a+\frac{1}{2}(b+c)$ determined from the lowest rotational transitions and calculated relative intensities (39). Then, only the frequency of the hyperfine-free origin and the single linewidth of the hyperfine components were varied in the fit. In this procedure the Λ-doubling effects were neglected, as no indication of Λ-doubling splittings was noticed in the spectra. This is not unexpected, since the Λ-doubling splitting in the $X^2\Pi_{3/2}$ state for the highest observed rotational level (J=51/2) is calculated to be less than 0.5 MHz and it is reasonable to assume the Λ-doubling splitting in the $A^2\Pi_{3/2}$ to be in the same order of magnitude.

In principle the Lorentzian linewidth contains homogeneous broadening contributions caused by collisions and saturation. Collision broadening can be excluded in view of the collision-free condition in the molecular beam. Saturation broadening increases the linewidth by the factor $(1+S)^{\frac{1}{2}}$, wherein the saturation parameter S is the ratio of the induced emission rate to the total relaxation rate. By reducing the applied laser power it was experimentally verified that saturation effects can also be excluded. It was found that the fluorescence intensity decreased proportional and the observed linewidths remained unchanged within the experimental uncertainty. Moreover, at the applied laser intensities of less than 1.5 mW/mm^2, the value of S can be estimated to be smaller than 10^{-3}.

The accuracy of the frequency interval measurements is in the order of 10 MHz, within a single laser scan. The absolute accuracy and thus the relative accuracy of different scans, is in the order of 70 MHz. The accuracy of the linewidth measurements is about 10%. The measurements of the RF transition frequencies in the MODRES experiments have an accuracy in the order of 10 kHz.

The frequencies of transitions from the $A^2\Pi_{3/2}$-$X^2\Pi_{3/2}$ system of IO, observed in the present study, are given in Table I, II and III. The MBLE spectra are arranged in three groups corresponding to the 2-0, 2-1 and 2-2 vibrational bands,

TABLE I

Observed and calculated frequency intervals (MHz) between hyperfine transitions and between hyperfine-free origins of rotational transitions in vibrational bands of the $A^2\Pi_{3/2}-X^2\Pi_{3/2}$ spectrum of IO.

Vib. band	F'	F"	Rot. trans.		F'	F"	Rot. trans.	Observed value	Obs. error	Obs. - calc.
2-0	4	3	Q(1.5)	-	4	4	Q(1.5)	637.2	4.8	-3.5
	3	2	Q(1.5)	-	4	4	Q(1.5)	-147.3	4.6	2.5
	2	1	Q(1.5)	-	4	4	Q(1.5)	-835.8	5.8	4.2
	3	3	Q(1.5)	-	4	4	Q(1.5)	-1 022.8	6.4	1.2
	3	4	Q(1.5)	-	4	4	Q(1.5)	-1 665.6	4.8	-1.0
	1	1	Q(1.5)	-	4	4	Q(1.5)	-1 898.0	11.7	2.1
	2	3	Q(1.5)	-	4	4	Q(1.5)	-2 476.0	3.9	1.3
	1	2	Q(1.5)	-	4	4	Q(1.5)	-2 662.9	5.6	0.4
	4	4	P(2.5)	-	4	5	P(2.5)	584.0	9.9	-0.9
	3	3	P(2.5)	-	4	5	P(2.5)	-696.4	6.7	-2.1
	3	4	P(2.5)	-	4	5	P(2.5)	-1 081.6	3.1	-1.9
	2	1	P(2.5)	-	4	5	P(2.5)	-1 752.5	30.8	-0.4
	2	2	P(2.5)	-	4	5	P(2.5)	-1 898.5	8.4	3.0
	2	3	P(2.5)	-	4	5	P(2.5)	-2 145.5	5.4	2.2
	1	1	P(2.5)	-	4	5	P(2.5)	-2 806.5	18.2	5.6
	1	2	P(2.5)	-	4	5	P(2.5)	-2 957.5	16.6	4.0
	5	5	P(3.5)	-	5	6	P(3.5)	526.1	19.4	-3.1
	4	4	P(3.5)	-	5	6	P(3.5)	-186.9	11.7	-2.2
	4	5	P(3.5)	-	5	6	P(3.5)	-472.3	3.2	0.1
	3	3	P(3.5)	-	5	6	P(3.5)	-806.2	11.5	-2.7
	3	4	P(3.5)	-	5	6	P(3.5)	-947.4	4.6	-6.2
	2	2	P(3.5)	-	5	6	P(3.5)	-1 323.7	16.7	-6.1
	2	3	P(3.5)	-	5	6	P(3.5)	-1 366.0	7.7	-3.9
	1	1	P(3.5)	-	5	6	P(3.5)	-1 688.4	10.1	-8.3
	1	2	P(3.5)	-	5	6	P(3.5)	-1 688.4	10.1	-3.8
	0	1	P(3.5)	-	5	6	P(3.5)	-1 871.8	30.1	-7.7
			R(1.5)	-			R(5.5)	1 560.3	20.0	-5.7
			R(4.5)	-			R(5.5)	6 600.0	18.0	-4.2
			R(2.5)	-			R(5.5)	7 381.0	20.0	-6.0
			R(3.5)	-			R(5.5)	9 063.6	17.0	-2.9
			Q(2.5)	-			R(8.5)	-4 571.4	14.0	-19.8
			Q(1.5)	-			R(8.5)	5 781.4	14.0	-18.5
			Q(3.5)	-			R(9.5)	4 136.5	23.0	5.3
			P(2.5)	-			R(10.5)	5 486.8	14.0	-21.3
			P(3.5)	-			R(11.5)	6 310.9	16.0	5.6
			P(4.5)	-			R(12.5)	7 120.4	13.0	13.8
			P(5.5)	-			R(13.5)	7 901.1	16.0	-11.4
			P(6.5)	-			R(14.5)	8 722.2	14.0	-1.4
			P(7.5)	-			R(15.5)	9 557.2	16.0	17.0

TABLE I - Continued

Vib. band	F'	F"	Rot. trans.		F'	F"	Rot. trans.	Observed value	Obs. error	Obs. - calc.
			P(8.5)	-			R(16.5)	10 362.7	19.0	-0.4
			P(9.5)	-			R(17.5)	11 193.0	23.0	0.4
			P(10.5)	-			R(18.5)	12 031.0	19.0	1.8
			P(11.5)	-			R(19.5)	12 883.8	21.0	10.4
			P(12.5)	-			R(20.5)	13 754.2	19.0	28.4
			P(13.5)	-			R(21.5)	14 536.9	42.0	-49.9
			P(14.5)	-			R(22.5)	15 414.0	53.0	-43.0
			P(15.5)	-			R(23.5)	16 330.1	29.0	-6.6
2-1	4	3	Q(1.5)	-	3	4	Q(1.5)	2 286.1	7.9	-1.7
	1	1	Q(1.5)	-	3	4	Q(1.5)	-258.1	10.2	-0.2
	2	3	Q(1.5)	-	3	4	Q(1.5)	-830.5	5.3	-0.5
	1	2	Q(1.5)	-	3	4	Q(1.5)	-1 021.8	7.6	-0.8
	4	4	P(2.5)	-	4	5	P(2.5)	579.0	9.3	-0.8
	3	3	P(2.5)	-	4	5	P(2.5)	-705.0	7.9	-0.1
	3	4	P(2.5)	-	4	5	P(2.5)	-1 086.9	3.7	-2.1
	2	1	P(2.5)	-	4	5	P(2.5)	-1 757.9	34.0	13.0
	2	2	P(2.5)	-	4	5	P(2.5)	-1 915.4	11.6	1.3
	2	3	P(2.5)	-	4	5	P(2.5)	-2 154.8	7.4	3.3
	1	1	P(2.5)	-	4	5	P(2.5)	-2 819.7	31.4	10.9
	1	2	P(2.5)	-	4	5	P(2.5)	-2 972.4	21.0	4.1
	5	5	P(3.5)	-	4	5	P(3.5)	1 001.1	19.7	-0.3
	5	6	P(3.5)	-	4	5	P(3.5)	471.5	3.8	-1.0
	4	4	P(3.5)	-	4	5	P(3.5)	282.6	15.9	-1.6
	3	3	P(3.5)	-	4	5	P(3.5)	-346.1	11.7	-1.1
	3	4	P(3.5)	-	4	5	P(3.5)	-474.8	5.6	-2.3
	2	2	P(3.5)	-	4	5	P(3.5)	-850.0	22.6	8.9
	2	3	P(3.5)	-	4	5	P(3.5)	-899.5	9.7	-1.2
	1	1	P(3.5)	-	4	5	P(3.5)	-1 223.0	9.2	2.3
	1	2	P(3.5)	-	4	5	P(3.5)	-1 223.0	9.2	2.9
	0	1	P(3.5)	-	4	5	P(3.5)	-1 409.5	20.7	-0.1
			R(1.5)	-			R(6.5)	8 646.8	19.0	1.9
			R(5.5)	-			R(6.5)	9 695.5	14.0	8.5
			R(2.5)	-			R(6.5)	14 886.9	18.0	13.5
			R(4.5)	-			R(6.5)	15 408.2	16.0	13.5
			R(3.5)	-			R(6.5)	17 135.6	16.0	12.1
			Q(1.5)	-			Q(2.5)	9 935.6	25.0	-8.4
			R(8.5)	-			Q(2.5)	10 423.5	42.0	4.0
			Q(3.5)	-			R(9.5)	-2 693.3	27.0	21.2
			P(2.5)	-			R(10.5)	-3 645.2	21.0	-25.8
			P(3.5)	-			R(11.5)	-4 133.4	17.0	-7.5
			P(4.5)	-			R(12.5)	-4 629.0	20.0	-0.7
			P(5.5)	-			R(13.5)	-5 131.4	19.0	-5.2
			R(14.5)	-			P(6.5)	5 615.1	14.0	-4.1
			R(15.5)	-			P(7.5)	6 109.9	13.0	3.0

TABLE I - Concluded

Vib. band	F'	F"	Rot. trans.		F'	F"	Rot. trans.	Observed value	Obs. error	Obs. - calc.
			R(16.5)	-			P(8.5)	6 588.7	17.0	-0.2
			R(17.5)	-			P(9.5)	7 032.3	24.0	-32.7
			R(18.5)	-			P(10.5)	7 547.1	18.0	12.3
2-2	4	3	Q(1.5)	-	4	4	Q(1.5)	628.9	12.5	16.7
	3	2	Q(1.5)	-	4	4	Q(1.5)	-196.4	12.0	-1.9
	2	1	Q(1.5)	-	4	4	Q(1.5)	-894.2	16.3	-1.7
	3	3	Q(1.5)	-	4	4	Q(1.5)	-1 068.3	19.6	-15.5
	3	4	Q(1.5)	-	4	4	Q(1.5)	-1 671.8	14.1	-6.8
	1	1	Q(1.5)	-	4	4	Q(1.5)	-1 965.7	35.6	-13.4
	2	3	Q(1.5)	-	4	4	Q(1.5)	-2 518.5	14.4	-12.5
	1	2	Q(1.5)	-	4	4	Q(1.5)	-2 706.0	22.0	1.4
	4	4	P(2.5)	-	4	5	P(2.5)	579.8	19.0	7.1
	3	3	P(2.5)	-	4	5	P(2.5)	-714.5	15.8	3.1
	3	4	P(2.5)	-	4	5	P(2.5)	-1 085.1	12.7	7.3
	2	2	P(2.5)	-	4	5	P(2.5)	-1 925.5	14.4	7.7
	2	3	P(2.5)	-	4	5	P(2.5)	-2 179.3	13.6	-8.5
			R(1.5)	-			R(5.5)	-3 688.1	24.0	-26.9
			R(2.5)	-			R(5.5)	2 967.0	19.0	-9.5
			R(4.5)	-			R(5.5)	4 800.8	17.0	-6.5
			R(3.5)	-			R(5.5)	5 791.7	16.0	-7.7
			Q(1.5)	-			R(8.5)	-6 804.3	19.0	-25.2
			Q(2.5)	-			R(9.5)	3 734.5	24.0	-22.0
			P(2.5)	-			R(10.5)	-12 824.7	19.0	-34.6
			P(3.5)	-			R(11.5)	-14 612.6	21.0	-4.5

TABLE II

Observed and calculated absolute frequencies (cm^{-1}) of hyperfine-free origins of rotational transitions in vibrational bands of the $A^2\Pi_{3/2}$-$X^2\Pi_{3/2}$ spectrum of IO.

Vib. band	Rot. trans.	Observed value	Obs. error	Obs. - calc.
2-0	R(5.5)	22 471.0987	0.0027	-0.0010
	R(6.5)	22 470.7411	0.0025	-0.0002
	R(7.5)	22 470.2432	0.0025	-0.0014
	R(8.5)	22 469.6091	0.0025	-0.0007
	R(9.5)	22 468.8348	0.0025	-0.0019
	R(10.5)	22 467.9245	0.0025	-0.0010
	R(11.5)	22 466.8751	0.0025	-0.0010
	P(4.5)	22 465.9255	0.0025	0.0001
	P(5.5)	22 464.6279	0.0025	0.0015
	P(6.5)	22 463.1910	0.0025	0.0017
	P(7.5)	22 461.6168	0.0025	0.0027
	P(8.5)	22 459.9013	0.0025	0.0004
	P(9.5)	22 458.0501	0.0025	0.0005
	P(10.5)	22 456.0593	0.0025	-0.0010
	P(11.5)	22 453.9334	0.0025	0.0004
	P(12.5)	22 451.6671	0.0025	-0.0005
	P(13.5)	22 449.2640	0.0025	-0.0002
	P(14.5)	22 446.7244	0.0025	0.0016
	P(15.5)	22 444.0426	0.0025	-0.0008
	P(16.5)	22 441.2267	0.0025	0.0007
	P(17.5)	22 438.2707	0.0025	0.0001
	P(18.5)	22 435.1759	0.0025	-0.0014
	P(19.5)	22 431.9444	0.0029	-0.0015
	P(20.5)	22 428.5783	0.0030	0.0017
	P(21.5)	22 425.0681	0.0029	-0.0013
	P(22.5)	22 421.4239	0.0031	-0.0003
	P(23.5)	22 417.6421	0.0028	0.0011
	P(24.5)	22 413.7195	0.0029	-0.0004
	P(25.5)	22 409.6603	0.0029	-0.0007
2-1	R(6.5)	21 798.0112	0.0024	0.0001
	R(7.5)	21 797.5568	0.0024	0.0016
	Q(2.5)	21 796.6189	0.0025	-0.0001
	R(9.5)	21 796.2448	0.0024	-0.0004
	R(10.5)	21 795.3899	0.0024	-0.0011
	R(11.5)	21 794.4030	0.0024	-0.0011
	R(12.5)	21 793.2843	0.0024	-0.0001
	R(13.5)	21 792.0302	0.0025	-0.0017
	P(6.5)	21 790.4583	0.0024	-0.0008

TABLE II - Concluded

Vib. band	Rot. trans.	Observed value	Obs. error	Obs. - calc.
	P(7.5)	21 788.9249	0.0024	0.0002
	P(8.5)	21 787.2573	0.0024	-0.0004
	P(9.5)	21 785.4584	0.0025	0.0003
	P(10.5)	21 783.5281	0.0024	0.0022
	P(11.5)	21 781.4613	0.0024	0.0002
	P(12.5)	21 779.2637	0.0024	0.0000
	P(13.5)	21 776.9345	0.0024	0.0008
	P(14.5)	21 774.4718	0.0024	0.0006
	P(15.5)	21 771.8764	0.0026	0.0002
	P(16.5)	21 769.1486	0.0024	0.0000
	P(17.5)	21 766.2885	0.0024	-0.0000
	P(18.5)	21 763.2954	0.0024	-0.0005
2-2	R(5.5)	21 134.3115	0.0024	0.0027
	R(6.5)	21 134.0236	0.0024	0.0025
	R(7.5)	21 133.6101	0.0024	0.0039
	R(8.5)	21 133.0650	0.0024	0.0010
	R(9.5)	21 132.3960	0.0024	0.0014
	R(10.5)	21 131.5989	0.0024	0.0011
	R(11.5)	21 130.6744	0.0024	0.0007
	R(12.5)	21 129.6228	0.0024	0.0005
	P(4.5)	21 129.0727	0.0024	-0.0018
	R(13.5)	21 128.4423	0.0024	-0.0013
	P(5.5)	21 127.8340	0.0024	-0.0014
	R(14.5)	21 127.1344	0.0024	-0.0031
	P(6.5)	21 126.4680	0.0024	-0.0011
	P(7.5)	21 124.9753	0.0024	-0.0003
	P(8.5)	21 123.3533	0.0024	-0.0017
	P(9.5)	21 121.6057	0.0024	-0.0015
	P(10.5)	21 119.7322	0.0024	-0.0001
	P(11.5)	21 117.7303	0.0024	0.0001
	P(12.5)	21 115.6013	0.0024	0.0003
	P(13.5)	21 113.3443	0.0024	-0.0004

TABLE III

Observed and calculated frequencies (MHz) of hyperfine transitions in the $v=0$, $X^2\Pi_{3/2}$ ground state of IO.

F'	F"	Rot. trans.	Observed value	Obs. error	Obs. - calc.	
4_-	3_+	Q(1.5)	640.767	0.030	-0.004	
4_-	3_+	Q(2.5)	385.716	0.015	0.004	
5_+	4_-	Q(3.5)	288.129	0.010	-0.002	
5_-	4_+	Q(3.5)	287.294	0.010	-0.000	
6_-	5_+	Q(4.5)	249.211	0.006	0.000	
6_+	5_-	Q(4.5)	248.179	0.008	0.000	

and are given in Table I and II   Table I contains frequency intervals between hyperfine transitions, with unresolved Λ-doublet splittings, ($|\Delta F| = 0,1$ and -←+, +←-) and frequency intervals between hyperfine-free origins of rotational transitions ($|\Delta J| = 0,1$ and -←+, +←-)   In Table II absolute frequencies of rotational transitions are given   The RF transitions in the $X^2\Pi_{3/2}$, v=0 ground state observed by the MODRES method are listed in Table III   These hyperfine transitions are of the type $\Delta J=0$, $|\Delta F|=1$ and symmetry -←→+ or +←→-

It should be noted that the data set allows an unambiguous assignment of the quantum numbers involved and electronic state characterizations, with the exception of the vibrational quantum number v=2 in the excited $A^2\Pi_{3/2}$ state that has been given in accordance with earlier investigations (see e g Ref (6))   The spectral line intensities are governed by the transition moments, the degree of predissociation and the population of energy levels in the ground state   Using the Franck-Condon factors calculated by Rao *et al.* (40), the vibrational temperature in the IO beam was roughly estimated from relative intensity measurements to be 600 K

The molecular parameters of IO have been determined in a least-squares fit of the calculated to the observed spectra, merging the results of the present study with those already existing in the literature   The present data on the 2-0 vibrational band of the $A^2\Pi_{3/2}$-$X^2\Pi_{3/2}$ spectrum and the $X^2\Pi_{3/2}$, v=0 ground state were fitted, combined with the $X^2\Pi_{3/2}$, v=0 microwave absorption data of Saito (10) and the 2-0, $A^2\Pi_{3/2}$-$X^2\Pi_{3/2}$ flame emission data of Durie *et al.* (6)   In view of small internal inconsistencies in the microwave absorption data, as can be judged from discrepancies in sum and difference intercombination rules, the quoted errors had to be enlarged three times. The data of Durie *et al.* are consistent within an accuracy of 0 02 cm^{-1}, with the exception of two lines (P(39 5) and R(58 5)) which deviate more than three times this error and were consequently rejected from the fit   The results of this fit determine the molecular parameters in the $A^2\Pi_{3/2}$, v=2 and $X^2\Pi_{3/2}$, v=0 states   The present data on the 2-1 vibrational band of the $A^2\Pi_{3/2}$-$X^2\Pi_{3/2}$ spectrum were fitted with the excited state parameters constrained within their uncertainty to their values obtained from the 2-0 band   This is done as the 2-0 band yields the most accurate parameters for the $A^2\Pi_{3/2}$, v=2 state. The present data on the 2-2 vibrational band of the $A^2\Pi_{3/2}$-$X^2\Pi_{3/2}$ spectrum were fitted, combined with the 2-2, $A^2\Pi_{3/2}$-$X^2\Pi_{3/2}$ emission data of Durie *et al.* and with the excited state parameters again constrained to the results from the 2-0 band   Again, some lines from the data of Durie *et al.* had to be rejected (R(66 5), R(68 5), R(75 5), R(77 5), P(64.5), P(65 5), P(67 5), P(68 5) and P(69 5)), while the consistency was

TABLE IV

Molecular parameters of IO. All values are in MHz, unless otherwise indicated. The errors correspond to three standard deviations.

	$X^2\Pi_{3/2}$ state			$A^2\Pi_{3/2}$ state
	$v = 0$	$v = 1$	$v = 2$	$v = 2$
A_{nv}^{eff} $(cm^{-1})^a$	-2 330	-2 330	-2 330	-2 330
$B_{nv}^{eff}(^2\Pi_{3/2})$	10 158.586(35)	10 077.05(29)	9 995.25(25)	8 087.76(12)
D_{nv}	0.01021(75)	0.0101(20)	0.00943(72)	0.00945(69)
H_{nv}	$-0.09(31)\times10^{-6}$	$-1.2(4.8)\times10^{-6}$	$-0.21(15)\times10^{-6}$	$-0.19(13)\times10^{-6}$
q_{nv}^{eff}	0.3(1.2)			
$a_{nv}+\frac{1}{2}(b_{nv}+c_{nv})$	583.832(95)	576.7(1.8)	568.8(5.5)	1 138.2(1.5)
b_{nv}^{eff}	660(68)			
eQq_{1nv}	-1 894.75(91)	-1 932(24)	-1 921(115)	-1 078(23)
eQq_{2nv}	-3 808(298)			
$\nu_0 \, {}^{A-X}_{2-v} \, (cm^{-1})^b$	22 470.0104(25)	21 797.1497(24)	21 133.0288(26)	

^{a} Parameter constrained at this value (see text).

^{b} Band origins of the 2-v vibrational bands of the $A^2\Pi_{3/2}$-$X^2\Pi_{3/2}$ spectrum.

greatly improved by lowering their absolute frequencies for the 2-2 band by 0.03 cm^{-1}. The final molecular parameters of IO are given in Table IV. Since the present results are more accurate and contain additional information and since data from previous studies have been included, a comparison with former results is not meaningful.

The observed natural widths $\Delta\nu$ of the rotational states in the v=2 vibrational level of the excited $A^2\Pi_{3/2}$ state are presented as a function of $J(J+1)$ in Fig. 6. The widths consist of inseparable radiative and predissociative parts (Eq. (23)). As the radiative width was estimated as 1-10 MHz (Sect. 3), the predissociation rate exceeds the radiation rate by several orders of magnitude. The variation of the lifetime τ in the v=2 level of the excited state can be described well by

$$1/\tau = 1/\tau_0 + kJ(J+1), \qquad (25)$$

where τ_0 denotes the extrapolated lifetime of the rotation-free state. The following values have been determined: τ_0=1.21(12) ns (corresponding to the width $\Delta\nu_0$=132(13) MHz) and k=1.72(16)×10^7 s^{-1}.

Attempts to observe MBLE spectra to other vibrational levels in the excited $A^2\Pi_{3/2}$ state (concentrated on the 0-0 and 3-0 vibrational bands) were not suc-
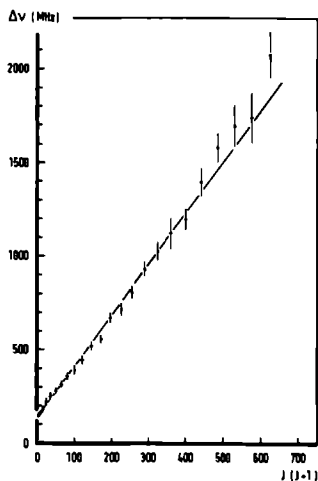

Fig. 6. Observed natural widths (FWHM) $\Delta\nu$ of the rotational states in the v=2 vibrational level of the excited $A^2\Pi_{3/2}$ state of IO, plotted as a function of J(J+1).

cessful. The stronger predissociation in the excited v=3 level (6) and the low Franck-Condon factor of the 0-0 band (40) most probably account for this. Attempts to observe RF transitions in the v=0, $X^2\Pi_{3/2}$ ground state by conventional MBER spectroscopy or to observe laser excitation spectra through the subsequent (photo) dissociation, both by means of beam detection with a mass spectrometer, failed as well. This demonstrates the higher sensitivity of laser-induced fluorescence detection.

5. DISCUSSION

All the spin-orbit coupling constants A have been constrained at the estimation of -2 330 cm^{-1} (9). The indicated errors do not reflect uncertainty in these A values. The dependence of the determined parameters on the A values has been discussed in Sect. 3. Vibrational effects in A_{Xv} can be expected to be negligible compared to the accuracy of the $B_{Xv}^{eff}(^2\Pi_{3/2})$ values. However, the unknown spin-orbit coupling constant A_{Av} in the excited $A^2\Pi_{3/2}$ state has a relatively large impact on the uncertainty of the $B_{A2}^{eff}(^2\Pi_{3/2})$ value. If $|A_{A2}|$ is assumed to be larger than 233 cm^{-1}, this corresponds to an uncertainty in $B_{A2}^{eff}(^2\Pi_{3/2})$ of 14 MHz. The following effective internuclear distances are obtained from the corresponding $B_{nv}^{eff}(^2\Pi_{3/2})$ values: $r_{X0}^{eff}(^2\Pi_{3/2})$=0.1871448(19) nm, $r_{X1}^{eff}(^2\Pi_{3/2})$=0.1879004(32) nm, $r_{X2}^{eff}(^2\Pi_{3/2})$=0.1886677(30) nm and $r_{A2}^{eff}(^2\Pi_{3/2})$=0.20974(18) nm. The stated errors in $r_{nv}^{eff}(^2\Pi_{3/2})$ also reflect the estimated uncertainty in the A_{nv} values.

The present data cover the lowest three vibrational levels of the ground state and allow vibrational expansion of the molecular constants. The results for the $X^2\Pi_{3/2}$ state are given in Table V. It should be noted that the values of $\omega_{eX}^{eff}(^2\Pi_{3/2})$ and $\omega_e x_{eX}^{eff}(^2\Pi_{3/2})$ in Table V have been derived from an expansion up to second order in v+½, because the present data are limited to two vibrational intervals. If the third order coefficient $\omega_e y_{eX}^{eff}(^2\Pi_{3/2})$ determined as -0.01$_3$ MHz by Durie et al. (6) is included, the values of $\omega_{eX}^{eff}(^2\Pi_{3/2})$ and $\omega_e x_{eX}^{eff}(^2\Pi_{3/2})$ have to be corrected by +5.75$\omega_e y_{eX}^{eff}(^2\Pi_{3/2})$ (=-0.08 cm^{-1}) and +4.5$\omega_e y_{eX}^{eff}(^2\Pi_{3/2})$ (=-0.06 cm^{-1}), respectively. The equilibrium values for ω, B and r have been deduced from the effective constants in the following way. If it is assumed that the vibrational effect in A_{Xv} in ClO (1.02% (30)) and IO are equal to within 20%, the coefficient α_{AX} of IO can be estimated to be -23.8(4.8) cm^{-1}. The vibrational frequency ω_{eX} is then obtained from Eq. (15). Assuming the ratio A_{DX}/A_X in IO to be equal to within 20% to these ratios in ClO (30) and

TABLE V

Derived molecular constants for the $X^2\Pi$ ground state of IO. The errors correspond to three standard deviations.

Constant	Value	Unit
$\omega_{eX}^{eff}(^2\Pi_{3/2})^a$	681.6004(91)	cm^{-1}
$\omega_e x_{eX}^{eff}(^2\Pi_{3/2})^a$	4.3699(30)	cm^{-1}
$B_{eX}^{eff}(^2\Pi_{3/2})$	10 199.25(46)	MHz
$\alpha_{eX}^{eff}(^2\Pi_{3/2})$	81.27(91)	MHz
$\gamma_{eX}^{eff}(^2\Pi_{3/2})$	-0.13(32)	MHz
D_{eX}	0.01042(66)	MHz
β_{eX}	-0.00038(51)	MHz
$r_{eX}^{eff}(^2\Pi_{3/2})$	0.1867713(46)	nm
ω_{eX}^b	669.7(2.4)	cm^{-1}
B_{eX}^c	10 083(24)	MHz
r_{eX}^c	0.18784(22)	nm

^{a} Derived from an expansion up to second order in $v+\frac{1}{2}$.

^{b} Derived using the estimated α_{AX}=-23.8(4.8) cm^{-1} (see text).

^{c} Derived using the estimated A_{DeX}=233(47) cm^{-1} (see text).

BrO (29), the A_{DeX} value for IO can be estimated as 233(47) MHz. Eq. (19) yields the equilibrium rotational constant B_{eX} and the corresponding equilibrium internuclear distance r_{eX}. The results are given in Table V. Alternatively, the well-known relation (valid for a Morse potential)

$$\omega_{en}^{\ 2} = 4B_{en}^{\ 3}/D_{en} \tag{26}$$

may be applied. This yields ω_{eX}=662(21) cm^{-1}, where the error mainly results from the limited accuracy of D_{eX}. This value shows gratifying agreement with the corresponding value in Table V. Besides, by substituting effective constants in Eq. (26) and using Eq. (15) and (19), the following relation between α_{An} and A_{Den} is obtained

$$\alpha_{An} = -(4/D_{en}^{\frac{1}{2}})\{[B_{en}^{eff}(^2\Pi_{3/2})]^{3/2}-[B_{en}^{eff}(^2\Pi_{3/2})-\tfrac{1}{2}A_{Den}]^{3/2}\}. \tag{27}$$

The values of $B_{eX}^{eff}(^2\Pi_{3/2})$ and D_{eX} have been determined from the spectra. With the estimated A_{DeX} value, Eq. (27) yields α_{AX}=-23.0(4.8) cm^{-1}, which agrees very well with the estimate of α_{AX} made above.

The lack of data on the $A^2\Pi_{1/2}$-$X^2\Pi_{1/2}$ system seriously limits the determination of all the molecular parameters. Especially, only an upper limit can be given for the Λ-doubling parameter q^{eff}. Determination of a complete set of magnetic hyperfine constants is also impeded.

The hyperfine constants are related to expectation values of electronic operators (24). The hyperfine constants in the $X^2\Pi$ ground state of ClO (30) and BrO (29,41) show that the electron distribution in the outer shell of both molecules is nearly identical with the unpaired π electron mainly located at the halogen atom. Particularly, the expectation values of $<\sin^2\theta/r^3>_U$ derived from the d constant and the eQq_2 constant, show a good agreement: (in units of 10^{24} cm^{-3}) 14.9 and 15.3, respectively, in case of ClO and 28.0 and 27.4, respectively, in case of BrO (see Appendix). The electron distribution in the outer shell of IO is essentially identical to the ClO and BrO distributions. The d constant of IO can be estimated from the presently determined eQq_2 constant (-3 808(298) MHz). This value yields $<\sin^2\theta/r^3>_U$=46.1(3.6)×10^{24} cm^{-3}, which gives d=1 099(110) MHz.

The vibrational effects in the $X^2\Pi_{3/2}$ ground state are about 1%. The excitation to the $A^2\Pi_{3/2}$ state involves a considerable change in the electron distribution, as can be noticed by large effects on the hyperfine constants, accompanied by an increase in the internuclear distance.

The predissociation rate of the $A^2\Pi_{3/2}$, v=2 state has been found to be proportional to J(J+1). No significant dependence on the quantum number F was noticed and both the + and - parity levels are predissociative to an equal extent (as can be deduced from the double-resonance condition). Until now, only vibrational dependence of the predissociation rate in the $A^2\Pi_i$ states has been reported for IO (6), BrO (42) and ClO (43). The nature of the interacting unbound state(s) is still subject to discussion. Recent calculations (44) have shown that presumably more than one interacting repulsive state is involved in case of ClO. The presently observed rotational dependence of the predissociation rate could in principle be due to a rotational variation of the Franck-Condon density for predissociation (centrifugal effect). However, this is not very likely in view of the rather strong variation observed. It seems more plausible that this variation originates from an additional gyroscopic interaction with unbound states. Accurate and complete measurements on the variation of the widths in the excited $A^2\Pi_i$ states of the halogen monoxides are desirable for understanding the predissociation.

6. CONCLUSIONS

The present study presents the first high-resolution investigation of the $A^2\Pi_{3/2}$-$X^2\Pi_{3/2}$ system of IO by means of laser-induced fluorescence. More accurate and new information about the molecular constants of IO has been obtained, summarized in Table IV and V. The hyperfine interaction in the excited state and the hyperfine Λ-doublet splittings in the ground state have been observed for the first time.

Spectroscopic techniques based on laser-induced fluorescence, are probably not suitable for application to the lighter halogen-monoxides, which exhibit more extensive predissociation. Observation of the $A^2\Pi_{1/2}$-$X^2\Pi_{1/2}$ system of IO will also be hindered by low degree of population in the $X^2\Pi_{1/2}$ state as a consequence of the large fine-structure interval.

The new technique of microwave optical double-resonance on an electrically state-selected beam (MODRES) presented in this paper has promising prospects for observations on the ground state spectra of polar molecules. Its high resolution and high sensitivity have been demonstrated in the experiments on the thermally populated and low concentration beam of the predissociative IO radical.

ACKNOWLEDGEMENTS

APPENDIX

The question of the sign of the non-axial electric quadrupole coupling constant eQq_2 (see Eq. (9)) is connected to the problem of the choice of the phase factors for the off-diagonal matrix elements between the $^2\Pi_{1/2}$ and $^2\Pi_{3/2}$ states. The three major off-diagonal contributions arise from B, b and eQq_2. The phase convention we used before (24) was introduced by Van Vleck (34) and is based on the reversed angular momentum method (45,46). It resulted, however, in contradictory results for the value of $<\sin^2\theta/r^3>_U$ derived from d and eQq_2 (see below). Recently Brown and Howard (27) established a consistent phase convention from the direct tensor method. When the off-diagonal matrix elements obtained from the direct tensor and reversed angular momentum methods are compared, the signs in front of B and b are to be reversed, while the sign in front of eQq_2 remains unaffected. Because the contributions of the off-diagonal matrix elements to the energy depend only on the relative signs, the sign of the eQq_2 value is consequently to be reversed. The phase convention employed presently is in accordance with the direct tensor method. The present sign of eQq_2 is also in agreement with the physical interpretation of the hyperfine coupling constants, considering the mutual relations for d and q_2 (24)

$$d = (3/2)gg_I\mu_0\mu_N<\sin^2\theta/r^3>_U, \quad (A1)$$

$$q_2 = -3<\sin^2\theta/r^3>_T. \quad (A2)$$

Here U and T denote averaging over the unpaired electron and the total electron density, respectively. Eq. (A2) can be rewritten in an effective average for the unpaired electron: in the case of a single π electron in the outer shell by

$$q_2[(n\pi)] = -3<\sin^2\theta/r^3>_U \quad (A3)$$

and in the case of three equivalent π electrons by

$$q_2[(n\pi^+)^2(n\pi^-)] = 3<\sin^2\theta/r^3>_U. \tag{A4}$$

The signs of $<\sin^2\theta/r^3>_U$ derived from the values of d and eQq_2, now agree (being both positive) in case of, for example, OD and SD (24), NO (25), CCl and ClO (47). For the halogen monoxides (three π electrons) ClO (30,48) and BrO (29,41)[2], both with positive d values, the corrected and consistent eQq_2 values are negative and positive, respectively. The d value of IO will be positive as well and consequently the eQq_2 value for IO is expected to be negative.

---

[2] Cohen *et al.* (41) obtained a positive value of eQq_2 for BrO due to an erroneous sign in their Eq. (15).

REFERENCES

1. W. L. Chameides and D. D. Davis, J. Geophys. Res. 85, 7383-7398 (1980).

2. A. R. W. McKellar, Canad. J. Phys. 57, 2106-2113 (1979).

3. W. M. Vaidya, Proc. Indian Acad. Sci. A 6, 122-128 (1937).

4. E. H. Coleman, A. G. Gaydon, and W. M. Vaidya, Nature 162, 108-109 (1948).

5. R. A. Durie and D. A. Ramsay, Canad. J. Phys. 36, 35-53 (1958).

6. R. A. Durie, F. Legay, and D. A. Ramsay, Canad. J. Phys. 38, 444-452 (1960).

7. A. Loewenschuss, J. C. Miller, and L. Andrews, J. Mol. Spectrosc. 80, 351-362 (1980).

8. A. Carrington, P. N. Dyer, and D. H. Levy, J. Chem. Phys. 52, 309-314 (1970).

9. J. M. Brown, C. R. Byfleet, B. J. Howard, and D. K. Russell, Mol. Phys. 23, 457-468 (1972).

10. S. Saito, J. Mol. Spectrosc. 48, 530-535 (1973).

11. J. C. Zorn and T. C. English, Advances in Atomic and Molecular Physics, D. Bates and I. Estermann (eds.), Vol. 9, Academic Press, New York, 1973.

12. P. Grundevik, M. Gustavsson, I. Lindgren, G. Olsson, L. Robertsson, A. Rosén, and S. Svanberg, Phys. Rev. Lett. 42, 1528-1531 (1979).

13. S. D. Rosner, R. A. Holt, and T. D. Gaily, Phys. Rev. Lett. 35, 785-789 (1975).

14. W. L. Meerts, J. P. Bekooy, and A. Dymanus, Mol. Phys. 37, 425-439 (1979).

15. J. L. Hall and S. A. Lee, Appl. Phys. Lett. 29, 367-369 (1976).

16. F. V. Kowalski, R. T. Hawkins, and A. L. Schawlow, J. Opt. Soc. Amer. 66, 965-966 (1976).

17. F. V. Kowalski, R. E. Teets, W. Demtröder, and A. L. Schawlow, J. Opt. Soc. Amer. 68, 1611-1613 (1978).

18. R. Balhorn, H. Kunzmann, and F. Lebowsky, Appl. Opt. 11, 742-744 (1972).

19. S. J. Bennett, R. E. Ward, and D. C. Wilson, Appl. Opt. 12, 1406 (1973).

20. V. Kaufman, J. Opt. Soc. Amer. 52, 866-870 (1962).

21. K. Shimoda (ed.), High-Resolution Laser Spectroscopy, Topics in Applied Physics, Vol. 13, Springer-Verlag, Berlin, Heidelberg, New York, 1976.

22. W. Demtröder, Laser Spectroscopy, Springer Series in Chemical Physics, Vol. 5, Springer-Verlag, Berlin, Heidelberg, New York, 1981.

23. C. R. Byfleet, A. Carrington, and D. K. Russell, Mol. Phys. 20, 271-277 (1971).

24. W. L. Meerts and A. Dymanus, Canad. J. Phys. 53, 2123-2141 (1975).

25. W. L. Meerts, Chem. Phys. 14, 421-425 (1976).

26. J. M. Brown, E. A. Colbourn, J. K. G. Watson, and F. D. Wayne, J. Mol. Spectrosc. 74, 294-318 (1979).

27. J. M. Brown and B. J. Howard, Mol. Phys. 31, 1517-1525 (1976).

28. C. Amiot, J.-P. Maillard, and J. Chauville, J. Mol. Spectrosc. 87, 196-218 (1981).

29. A. R. W. McKellar, J. Mol. Spectrosc. 86, 43-54 (1981).

30. J. A. Coxon, Canad. J. Phys. 57, 1538-1552 (1979).

31. J. A. Coxon, W. E. Jones, and E. G. Skolnik, Canad. J. Phys. 54, 1043-1052 (1976).

32. S. Green and R. N. Zare, J. Mol. Spectrosc. 64, 217-222 (1977).

33. J. M. Brown and J. E. Schubert, J. Mol. Spectrosc. 95, 194-212 (1982).

34. J. H. Van Vleck, Phys. Rev. 33, 467-506 (1929).

35. J. Vigué, M. Broyer, and J. C. Lehmann, J. Physique 42, 937-947 (1981), J. Physique 42, 949-959 (1981).

36. M. Mandelman and R. W. Nicholls, J. Quant. Spectrosc. Radiat. Transfer 17, 483-491 (1977).

37. B. H. Armstrong, J. Quant. Spectrosc. Radiat. Transfer 7, 61-88 (1967).

38. S. N. Dobryakov and Ya. S. Lebedev, Sov. Phys. Dokl. 13, 873-875 (1969).

39. W. Gordy and R. L. Cook, Microwave Molecular Spectra, Interscience, New York, 1970.

40. M. L. P. Rao, D. V. K. Rao, and P. T. Rao, Phys. Lett. A 50, 341-342 (1974).

41. E. A. Cohen, H. M. Pickett, and M. Geller, J. Mol. Spectrosc. 87, 459-470 (1981).

42. M. Barnett, E. A. Cohen, and D. A. Ramsay, Canad. J. Phys. 59, 1908-1916 (1981).

43. J. A. Coxon and D. A. Ramsay, Canad. J. Phys. 54, 1034-1042 (1976).

44. P. R. Bunker and P. C. Klein, Chem. Phys. Lett. 78, 552-554 (1981).

45. J. H. Van Vleck, Rev. Mod. Phys. 23, 213-227 (1951).

46. K. F. Freed, J. Chem. Phys. 45, 4214-4241 (1966).

47. Y. Endo, S. Saito, and E. Hirota, J. Mol. Spectrosc. 92, 443-450 (1982), J. Mol. Spectrosc. 94, 199-207 (1982).

48. R. K. Kakar, E. A. Cohen, and M. Geller, J. Mol. Spectrosc. 70, 243-256 (1978).

BAK 70   B. Bak, E. Clementi and R.N. Kortzeborn, J. Chem. Phys. 52 (1970) 764

BAL 72   R. Balhorn, H. Kunzmann and F. Lebowsky, Appl. Opt. 11 (1972) 742

BEN 73   S.J. Bennett, R.E. Ward and D.C. Wilson, Appl. Opt. 12 (1973) 1406

BRO 72   J.M. Brown, C.R. Byfleet, B.J. Howard and D.K. Russell, Mol. Phys. 23 (1972) 457

BYF 71   C.R. Byfleet, A. Carrington and D.K. Russell, Mol. Phys. 20 (1971) 271

CAR 70   A. Carrington, P.N. Dyer and D.H. Levy, J. Chem. Phys. 52 (1970) 309

CHA 80   W.L. Chameides and D.D. Davis, J. Geophys. Res. 85 (1980) 7383

CHU 70   A. Churg and D.H. Levy, Astrophys. J. 162 (1970) L161

CLE 73   E. Clementi, H. Kistenmacher and H. Popkie, J. Chem. Phys. 58 (1973) 2460

CLO 71   P.N. Clough, A.H. Curran and B.A. Thrush, Proc. Roy. Soc. London A 323 (1971) 541

DEM 81   W. Demtröder, Laser Spectroscopy, Springer Series in Chemical Physics, Vol. 5 (Springer-Verlag, Berlin, Heidelberg, New York 1981)

DUR 60   R.A. Durie, F. Legay and D.A. Ramsay, Can. J. Phys. 38 (1960) 444

EDL 66   B. Edlén, Metrologia 2 (1966) 12

GRU 79   P. Grundevik, M. Gustavsson, I. Lindgren, G. Olsson, L. Robertsson, A. Rosén and S. Svanberg, Phys. Rev. Lett. 42 (1979) 1528

HAL 76   J.L. Hall and S.A. Lee, Appl. Phys. Lett. 29 (1976) 367

HER 68   M. Hercher, Appl. Opt. 7 (1968) 951

KAU 62   V. Kaufman, J. Opt. Soc. Am. 52 (1962) 866

KOW 76   F.V. Kowalski, R.T. Hawkins and A.L. Schawlow, J. Opt. Soc. Am. 66 (1976) 965

KOW 78   F.V. Kowalski, R.E. Teets, W. Demtröder and A.L. Schawlow, J. Opt. Soc. Am. 68 (1978) 1611

KUI 76   P. Kuijpers, T. Törring and A. Dymanus, Chem. Phys. Lett. 42 (1976) 423

LEE 71   K.P. Lee, W.G. Tam, R. Larouche and G.A. Woonton, Can. J. Phys. 49 (1971) 2207

LEE 73   F.H. de Leeuw and A. Dymanus, J. Mol. Spectrosc. 48 (1973) 427

LEE 74   K.P. Lee and W.G. Tam, Chem. Phys. 4 (1974) 434

LET 77   V.S. Letokhov and V.P. Chebotayev, Nonlinear Laser Spectroscopy, Springer Series in Optical Sciences, Vol. 4 (Springer-Verlag, Berlin, Heidelberg, New York 1977)

MCK 79   A.R.W. McKellar, Can. J. Phys. 57 (1979) 2106

MEE 72   W.L. Meerts and A. Dymanus, J. Mol. Spectrosc. 44 (1972) 320

MEE 75   W.L. Meerts and A. Dymanus, Can. J. Phys. 53 (1975) 2123

MEE 79   W.L. Meerts, J.P. Bekooy and A. Dymanus, Mol. Phys. 37 (1979) 425

MIE 68   K.D. Mielenz, K.F. Nefflen, W.R.C. Rowley, D.C. Wilson and E. Engelhard, Appl. Opt. 7 (1968) 289

OWE 67   J.C. Owens, Appl. Opt. 6 (1967) 51

RAN 60   D.H. Rank, G. Skorinko, D.P. Eastman, G.D. Saksena, T.K. McCubbin Jr. and T.A. Wiggins, J. Opt. Soc. Am. 50 (1960) 1045

RAO 74   M.L.P. Rao, D.V.K. Rao and P.T. Rao, Phys. Lett. A 50 (1974) 341

ROS 75   S.D. Rosner, R.A. Holt and T.D. Gaily, Phys. Rev. Lett. 35 (1975) 785

SAI 73   S. Saito, J. Mol. Spectrosc. 48 (1973) 530

SHI 76   K. Shimoda (ed.), High-Resolution Laser Spectroscopy, Topics in Applied Physics, Vol. 13 (Springer-Verlag, Berlin, Heidelberg, New York 1976)

ZOR 73   J.C. Zorn and T.C. English, Advances in Atomic and Molecular Physics, D. Bates and I. Estermann (eds.), Vol. 9 (Academic Press, New York 1973) 243

Hoge-resolutie moleculaire bundel spectroscopie
bij microgolf en optische frequenties

Molecuul spectroscopie is de belangrijkste bron van informatie over structuren en eigenschappen van moleculen. Spectra kunnen worden beschreven in termen van bepaalde parameters, vaak moleculaire constanten genoemd, die verband houden met electronische en geometrische structuren, met vibraties en rotaties van het moleculaire frame, met eigenschappen van electronen en kernen en met electrische en magnetische moleculaire eigenschappen. Deze constanten zijn van belang om de fysische en chemische eigenschappen van stoffen te begrijpen en om theoretische berekeningen te toetsen. Moleculaire spectra zelf zijn bruikbaar voor het identificeren van moleculen en het bepalen van de concentratie en om de fysische condities in een gegeven (verafgelegen) systeem te kakarteriseren.

Moleculaire bundel spectroscopie biedt de mogelijkheid om spectra waar te nemen met een hoog oplosssend vermogen. Reductie van Doppler verbreding van spectraal lijnen wordt verkregen door het loodrecht op een gecollimeerde moleculaire bundel instralen van microgolf en optische straling. In de experimenten werden drie verschillende spectroscopische methoden toegepast: moleculaire-bundel electrische-resonantie (MBER), moleculaire-bundel laser-excitatie (MBLE) en microgolf optische dubbel-resonantie aan een electrisch toestands geselecteerde bundel (MODRES). In de MBER methode worden bepaalde moleculaire toestanden geselecteerd door middel van inhomogene electrische velden, waarna door microgolf straling geïnduceerde overgangen worden waargenomen als afname van de moleculaire bundel intensiteit. Met MBER wordt een hoge resolutie (~10 kHz) behaald. In de MBLE methode worden moleculen in de bundel door een laser geëxciteerd. Deze overgangen worden waargenomen door middel van detectie van de laser-geïnduceerde fluorescentie. De MBLE heeft een hoge gevoeligheid en een resolutie van ~10 MHz, afgezien van natuurlijke lijnbreedtes. De MODRES methode is een nieuw ontwikkelde techniek, die de hoge resolutie en gevoeligheid van de bovenstaande methodes combineert in een dubbel-resonantie configuratie. In een door een inhomogeen electrisch veld toestands geselecteerde bundel worden door microgolf straling geïnduceerde overgangen waargenomen door de resulterende veranderingen in de laser-geïnduceerde fluorescentie. Een beschrijving is gegeven van de spectrometer in de MBLE en MODRES configuraties.

Bestudeerd zijn spectra van het hydroxyl (OH) radicaal, het kalium-cyanide (KCN) molecuul en het jodium-oxide (IO) radicaal. De hyperfijn lambda-splitsingen in de laagste rotatie toestanden van het vibrationeel aange-slagen OH radicaal werden gemeten met de MBER methode. Moleculaire constanten voor zowel de $^2\Pi_{1/2}$ als de $^2\Pi_{3/2}$ grond toestand konden worden bepaald. Voor-spellingen zijn gegeven van constanten en astrofysisch interessante overgangs frequenties in vibrationeel hoger aangeslagen toestanden. Vergelijking van de resultaten met theoretische berekeningen leverde een goede overeenstemming op.

Het rotatie spectrum van het KCN molecuul in de grond vibratie toestand werd eveneens met MBER gemeten. Door een KCN bundel te produceren met een supersone expansie van een mengsel van KCN verdund in Ar, werd een sterke rotatie en vibratie koeling bereikt. Hierdoor konden goed opgeloste en interpreteerbare spectra worden waargenomen. De resultaten zijn gecombineerd met rotatie over-gangen uit microgolf absorptie experimenten. Uit de rotatie constanten is de on-verwacht T-vormige structuur van KCN bepaald.

De rotatie spectra van de vibratie banden 2-0, 2-1 en 2-2 van de $A^2\Pi_{3/2}$-$X^2\Pi_{3/2}$ overgang van het IO radicaal werden bestudeerd met MBLE. De af-stembare optische straling werd geproduceerd door een kleurstof laser. De hyperfijn structuur kon worden opgelost voor de laagste rotatie niveaus. Tevens werden met MODRES opsplitsingen in de hyperfijn structuur van de $X^2\Pi_{3/2}$, v=0 grond toestand gemeten. Voor de electronisch aangeslagen toestand zijn hyperfijn en rotatie constanten bepaald en voor de grond toestand hyperfijn, ro-tatie en vibratie constanten. Naast vibratie afhankelijke predissociatie werd een rotatie afhankelijke verbreding van niveaus in de aangeslagen toestand ten gevolge van predissociatie waargenomen.

Op 6 februari 1955 ben ik geboren te Leiden. De middelbare schoolopleiding volgde ik aan de Rembrandt Scholengemeenschap te Leiden en behaalde in 1972 het diploma HBS-B. Aansluitend begon ik de studie natuurkunde aan de Rijksuniversiteit Leiden. Het kandidaatsexamen natuurkunde en wiskunde met bijvak sterrenkunde werd behaald in januari 1975, het doctoraal examen experimentele natuurkunde met bijvak wiskunde in september 1977. Tijdens mijn afstudeerperiode was ik werkzaam in de werkgroep Molecuulfysica. Van november 1977 tot augustus 1982 was ik als wetenschappelijk medewerker in dienst van de Katholieke Universiteit te Nijmegen. Mijn promotieonderzoek verrichtte ik op de afdeling Atoom- en Molecuulfysica onder leiding van Prof. dr. A. Dymanus en Dr. W.L. Meerts. De resultaten van dit onderzoek staan beschreven in het proefschrift.

1. De teken verandering van de electrische quadrupool koppeling term eQq_2 in de Hamiltoniaan, die Brown en Schubert introduceren bij de analyse van het EPR spectrum van het OD radicaal om overeenstemming met oudere literatuur te verkrijgen, leidt tot een tegenspraak met de fysische interpretatie van deze koppelings constante.

   J.M. Brown and J.E. Schubert, J. Mol. Spectrosc. 95 (1982) 194.

2. De emissie doorsneden voor magnetische dipool overgangen van het OH^+ ion, berekend door Singh en de Almeida, zijn een factor 10^4 te groot.

   P.D. Singh and A.A. de Almeida, Astron. Astrophys. 84 (1980) 177.

3. In de analyse van het laser-geïnduceerde fluorescentie spectrum van sym-triazine verwaarlozen Heaven et al. ten onrechte het energie verschil tussen de A_1'' en A_2'' toestanden.

   M. Heaven, T. Sears, V.E. Bondybey and T.A. Miller, J. Chem. Phys. 75 (1981) 5271.

4. In de interpretatie van de translatie energie afhankelijkheid van de chemiluminescente doorsnede van de $Ba + N_2O$ reactie verwaarlozen Wren en Menzinger ten onrechte relaxatie van de knik-vibratie ν_2 van N_2O tijdens de supersone expansie.

   D.J. Wren and M. Menzinger, Disc. Faraday Soc. 67 (1979) 97.

5. De bewering van Hudgens en McDonald dat de verschuiving van de ν_1 vibratie lijn in het Raman spectrum van SF_6 het meest gevoelig is voor excitatie van de ν_1 vibratie is onjuist.

   J.W. Hudgens and J.D. McDonald, J. Chem. Phys. 76 (1982) 173.

6. De door Baldacchini et al. gevonden a-thermische rotatie verdeling in een supersone expansie van NH_3 kan verklaard worden uit het niet corrigeren voor absorptie tengevolge van achtergronds gas.

   G. Baldacchini, S. Marchetti and V. Montelatici, Chem. Phys. Lett. 91 (1982) 423.

7. In een laser wordt niet zelden geavanceerde technologie gecombineerd met inferieure constructies.

8. De grondwet dient zodanig gewijzigd te worden, dat bij verkiezingen voor de zetelverdeling van de Tweede Kamer ook een lijst wordt opgenomen, die resulteert in lege zetels.